QUANTITATIVE MODELING OF THE REACTION/DIFFUSION KINETICS OF TWO-CHEMISTRY PHOTOPOLYMERS

by

JAMIE ELIZABETH KOWALSKI

B.A., Kenyon College, 2003

A thesis submitted to the

Faculty of the Graduate School of the

University of Colorado in partial fulfillment

of the requirement for the degree of

Doctor of Philosophy

Department of Electrical, Computer, and Energy Engineering

2014

This thesis entitled:

Quantitative modeling of the reaction/diffusion kinetics of two-chemistry photopolymers

written by Jamie E. Kowalski

has been approved for the Department of Electrical, Computer, and Energy Engineering

_____

Robert R. McLeod

_____

Fredric R. Askham

*Date*_____

The final copy of this thesis has been examined by the signatories, and we

Find that both the content and the form meet acceptable presentation standards

Of scholarly work in the above mentioned discipline.

Kowalski, Jamie Elizabeth (Ph.D., Electrical, Computer, and Energy Engineering)

Quantitative modeling of the reaction/diffusion kinetics of two-chemistry photopolymers

Thesis directed by Associate Professor Robert R. McLeod

Optically driven diffusion in photopolymers is an appealing material platform for a broad range of applications, in which the recorded refractive index patterns serve either as images (e.g. data storage, display holography) or as optical elements (e.g. custom GRIN components, integrated optical devices). A quantitative understanding of the reaction/diffusion kinetics is difficult to obtain directly, but is nevertheless necessary in order to fully exploit the wide array of design freedoms in these materials.

A general strategy for characterizing these kinetics is proposed, in which key processes are decoupled and independently measured. This strategy enables prediction of a material's potential refractive index change, solely on the basis of its chemical components. The degree to which a material does not reach this potential reveals the fraction of monomer that has participated in unwanted reactions, reducing spatial resolution and dynamic range.

This approach is demonstrated for a model material similar to commercial media, achieving quantitative predictions of index response over three orders of exposure dose (~1 to ~10^3 mJ cm^{-2}) and three orders of feature size (0.35 to 500 microns). The resulting insights enable guided, rational design of new material formulations with demonstrated performance improvement.

CONTENTS

CHAPTER

TABLES

Table

FIGURES

Figure

CHAPTER I

INTRODUCTION

1.1 Holographic media requirements

Problem space

Optically driven diffusion in photopolymers is an appealing material platform for a broad range of applications, in which the recorded index features serve either as images (e.g. data storage, display holography) or as optical elements (e.g. custom GRIN components, integrated optical devices). All of these applications are characterized by simultaneous stringent requirements on both optical properties (achievable index modulation, sensitivity) and mechanical and process properties (cheap, rugged, mechanically stable). We begin by describing these requirements, with respect to various particular applications, and using them to evaluate the performance of diffusive photopolymers relative to other material platforms. Then we review work that has been done to model the reaction/diffusion kinetics of these materials, with a particular emphasis on the unique challenges of modeling two-chemistry media.

Optical specifications

For nearly all applications, the total achievable refractive index modulation Δn (often expressed in the holography literature as M/# per thickness) is of critical importance. For integrated optical components, Δn determines critical specs such as achievable optical power of a gradient-index lens, or mode size of a waveguide. For display holograms, Δn determines the diffraction efficiency achievable in a thin media layer. Likewise, for holographic data storage, Δn

determines the number of holograms of a given diffraction efficiency that can be recorded in a given volume of media, and therefore the achievable storage density.

In diffusive photopolymers, this achievable index modulation depends on the loading (i.e. the doping concentration) of writing monomer. So increasing the monomer loading will increase the "signal" term (diffraction from the intended hologram) but also increase the dominant "noise" term, which is optical scatter due to phase separation. Making matters worse, it will also increase the recording-induced volume shrinkage, which in thick samples acts to significantly distort the recorded features. In general, then, a good signal-to-noise ratio requires careful tuning of the concentration of writing monomer, to balance these opposing requirements.[1]

Next, high sensitivity (i.e. eventual refractive index modulation produced per unit exposure dose) is crucial for commercial applications that demand high throughput and inexpensive, low-power lasers. This motivates the use of processes with chemical gain, in which one photon absorption event can trigger many polymerization events. Sensitivity can be further improved by increasing the photoinitiator concentration, but only up to the point at which the corresponding increase in absorptivity leads to significantly non-uniform recording throughout the depth of thick samples.

Next, it is desirable that index response be linear in exposure dose and intensity, since any deviations from linear response imply a loss in recording fidelity and therefore wasted dynamic range. For radical chain-growth writing chemistries, these deviations can arise from depletion of photoinitiator and from bimolecular radical termination, both of which lead to an effectively sublinear material response. In some special cases, such as direct-write by a raster-scanning focused beam, the exposure dose can be pre-compensated to correct these deviations.[2] Oxygen inhibition of radical polymerization can also cause a thresholding effect that leads to significant nonlinearities. This thresholding effect can be eliminated with a uniform pre-exposure to

consume oxygen, but only in applications where the media layer can be sealed off from atmospheric oxygen during recording.

Next, the media spatial resolution, or more generally the index response as a function of spatial frequency, must be considered. In diffusive photopolymers, the response at high spatial frequencies is typically limited by some sort of diffusional blurring: either the diffusion of small mobile radicals, or the reaction-diffusion of the radical tips of immobilized growing chains. This determines a media resolution limit. The highest spatial frequencies, and therefore the most demanding requirements on media resolution, occur in the reflection hologram geometry, which includes display holograms and microholographic data storage. A low spatial frequency cutoff sometimes also exists, either in the case where photopolymerization vitrifies the media and interrupts diffusion over long time scales, or in the case where the coupled timescales of diffusion and reaction lead to nonlinearities such as the classic Zhao and Mouroulis "rabbit ears" profile.

Next, the material must be sensitive to the desired recording wavelengths. Data storage applications, for example, are limited to laser diode sources, and thus the recording wavelength can be no lower than ~405 nm, whereas display holography applications require sensitivity to three colors spanning the visible spectrum.

Finally, in addition to the recording-induced optical properties discussed so far, the passive/bulk optical properties must also be considered, especially for thick media layers. These include optical clarity (i.e. low intrinsic scatter), transparency, and phase uniformity.

Process specifications

Commercial applications demand material platforms that can be produced at low cost and with arbitrary form factors, with thicknesses up to ~1 mm. This is typically achieved with a thermo-setting polymer media that can be mold-cast.

Many conventional techniques for patterning photopolymers rely on a solvent wash; e.g. photoresists and micro-stereolithography. But any such wet chemical processing step is unsuitable for applications with millimeter-thick media layers, including holographic data storage and some integrated optical devices. Therefore media must be self-processing. A heat processing step may be tolerable in some cases.

It is required that commercial media remain stable for some "shelf life" prior to exposure. For polymerization-based writing chemistries, this may require the addition of inhibiting species (or ambient oxygen may be sufficient to inhibit radical processes). After exposure, the media must remain stable over long times (as much as decades in the case of data storage), in the presence of humidity, heat, and ambient light including both UV and long wave. Stability concerns are not limited to degradation of recorded features, but also include delamination, yellowing, and out-diffusion of volatile organic compounds.

Mechanical specifications

Thick holographic elements are extraordinarily sensitive to the recording-induced volume shrinkage that is characteristic of radical polymerization writing chemistries. Not only does this shrinkage distort the holographic fringes, but, even worse, the shrinkage is typically anisotropic and amplified by the Poisson ratio, due to the mechanical constraints imposed by the packaging of the media layer. This anisotropy means that shrinkage can only partially be compensated by

tuning the readout angle or wavelength. Thus, tolerances on recording-induced volume shrinkage are as stringent as 0.05% for typical holographic data storage architectures.

Similarly, holographic elements in the Bragg diffraction regime are very sensitive to thermal expansion, and so it is desirable that the coefficient of thermal expansion be as low as possible. For this reason a high glass transition temperature is favorable. But this must be carefully balanced against other design considerations which favor a low glass transition temperature. First, a low glass transition temperature yields faster diffusion, and thus diffusion-driven index development mechanisms will be faster and have greater sensitivity. Second, a lower glass transition temperature generally corresponds to a lower matrix bulk refractive index and thus a greater index contrast with the high-index writing monomer.

Finally, additional requirements on mechanical properties arise in cases where protective packaging is impractical and instead the media must be exposed directly to the environment, as is especially common for integrated optical devices. In these cases, elastic modulus (rigidity) and scratch hardness become especially important. Given this set of optical, process, and mechanical specifications, diffusive photopolymers compare favorably to other material platforms, as follows.

1.2 Candidate material platforms

Non-mass-transport mechanisms

First we consider mechanisms for index modulation that are not driven by mass transport. These have the advantage that they can readily be implemented in a glassy host matrix, which affords good optical clarity, bulk mechanical ruggedness, and negligible volume shrinkage.

The photorefractive effect provides one such mechanism. Photorefractive polymers[3] are easily fabricated by casting, in contrast to the expensive process of crystal growth, cutting, and polishing required for photorefractive crystals[4]. The dynamic range of these polymer media is typically low ($\Delta n \sim 3\times10^{-4}$), but can be greatly enhanced by using polar chromophores that are reoriented by a strong applied electric field[5]. Sensitivity is low (order 10^{-6} cm^2/J) and thermal processing is required in order to achieve long lifetimes of recorded features.

Another mechanism not driven by mass transport is photochromism. Here a glassy host matrix such as PMMA is doped with a photochromic dye: traditionally an azobenzene derivative, but other chemistries have been explored, including ortho-nitrostilbene[6] and Dewar benzene derivatives.[7] Again, bulk optical properties are good and recording does not induce any volume shrinkage. However, thermal stability is an issue, and the sensitivity is still poor (0.05 cm^2/J in the above reference), as is the dynamic range (Δn of roughly 3×10^{-5}). The addition of mesogenic side groups can stabilize the reorientation and give resonance enhancement to the index change, up to a remarkable $\Delta n \sim 0.5$,[8] but does not address the problem of sensitivity.

Finally, chalcogenide glasses exhibit a complex and not thoroughly understood range of photoinduced effects, including photodarkening, photorefractive effects, structural changes such as crystallization, and dissolution of metals followed by mass transport.[9] Photoinduced structural changes can yield a dynamic range as high as order $\Delta n \sim 0.1$, with fair sensitivity, of order 0.1 cm^2/J.[10]

Diffusion in gelatins

Next we turn to diffusive mechanisms for index change. These mechanisms modulate the actual composition of the media, potentially affording high dynamic range, but also introducing complications with respect to mechanical, bulk optical, and process properties.

Dichromated gelatins, for example, afford a very high dynamic range,[11] of the order $\Delta n \sim 0.1$. However, they have limited sensitivity, require cumbersome wet chemical processing and suffer from significant recording-induced shrinkage. The historically important silver halide gelatins[12] boast comparably high dynamic range and an astonishingly good sensitivity, order 10^3 cm^2/J, but all the same wet processing issues remain.

Diffusion in glassy media (via post-baking)

Diffusion of chromophores is noteworthy in that it is suitable for implementation in glassy host matrices. Upon photo-exposure, an initially mobile chromophore is selectively attached to the matrix, as in the classic system PQ/PMMA[13] or the more recently developed NQ/PMMA[14]; or, conversely, an initially attached chromophore is selectively released[15]. Diffusion through the glassy matrix is normally negligibly slow, but a post-baking step speeds it up dramatically, so that the mobile chromophores diffuse to equilibrium, thereby generating a moderately strong index modulation. It should be emphasized that each photon absorption event produces at most a single index-modulation event – that is, there is no chemical amplification. This characteristic leads to low shrinkage, as compared to radical photopolymerization, which forms long polymer chains with fewer degrees of freedom. But it also leads to low sensitivity (~ 0.3 cm^2/J).

Diffusive photopolymers (chemical amplification)

Greater sensitivity, comparable to that of silver halide, can be achieved by using recording mechanisms with chemical amplification, such as radical chain-growth in which a single photon-

absorption event can initiate a long chain of polymerization events. In general, this approach carries a penalty of correspondingly greater recording-induced shrinkage, due to the greater reduction of molecular degrees of freedom. Typical components of such a system are as follows:

1.3 Diffusive photopolymers: components and applications

Host matrix or binder

Two general design strategies exist for these media. In the single-chemistry strategy[16], the system is initially a resin containing monomer, photoinitiator, and high molecular weight binder. The same photopolymerization chemistry is used both to record patterned features and to crosslink the entire media layer. Typically this is realized with a partial uniform flood-cure either before or after a patterned recording exposure.

This strategy has been applied to several commercially important media. DuPont's Omnidex[17] films use high-index acrylate writing monomers and cellulose-based binders; they achieve good dynamic range ($\Delta n \sim 0.06$) upon thermal post-processing to facilitate diffusion. Polaroid's DMP-128 films use acrylate writing monomers and a polyethylene imine binder. Subsequent solvent processing leads to the formation of micropores in the exposed regions[18]. Since the pores are filled with air or with some highly index-contrasting solvent,[19] the resulting index modulation can be quite high, $\Delta n \sim 0.08$, with good sensitivity (~ 5 cm^2/J).

In the two-chemistry strategy, a solid host matrix is formed by a first (typically thermoset) polymer, followed by recording into a second (typically radical) photopolymer. This two-chemistry approach is increasingly preferred in commercial holographic media[20] due to its additional design freedoms: the matrix polymer that dominates passive properties (e.g. modulus

and phase flatness) can be engineered independently from the writing polymer that dominates the recording properties (e.g. index contrast and scatter).

Commercial media utilizing this strategy include Bayer's Bayfol HX[21] which achieves $\Delta n \sim 0.04$ with self-processing and good sensitivity of ~2 cm^2/J. But the form factor is limited to thin films (~20 μm), a regime with more forgiving tolerances on recording-induced scatter and volume shrinkage. Lucent spinoff InPhase developed media that could be cast in much thicker layers (~1 mm) while maintaining excellent scatter and shrinkage properties. In order to meet these additional requirements, dynamic range was scaled back to $\Delta n \sim 3\times10^{-3}$, with sensitivity of 4.5×10^{-3} cm^2/J. More recently, InPhase's successor Akonia has demonstrated dramatic improvements in usable dynamic range, reaching $\Delta n > 0.1$.[22]

Finally, it has also been shown that the polymer host matrix can be replaced by nanoporous glass, into which a photopolymer resin is infiltrated, simultaneously achieving fast diffusion and negligible volume shrinkage. In addition, the glass can be polished and affords excellent bulk mechanical rigidity.[23] Fabrication of nanoporous glass remains prohibitively expensive, but a promising alternative is hybrid inorganic-organic sol-gel glasses.[24]

Writing monomer

Radical chain-growth polymerization is the most commercially interesting writing chemistry, due in large part simply to its versatility, with a large toolbox of well-understood chemical components. However, this approach fundamentally requires compromise between opposing material requirements: for example, the matrix crosslink density must be low enough to enable fast diffusion of mobile species, but also high enough to maintain desired bulk mechanical properties like rigidity and low thermal expansion. Similarly, the concentration of writing

monomer must be high enough to achieve the required dynamic range, but also low enough to keep recording-induced shrinkage and scatter within stringent limits.

A major focus of materials development efforts has been the synthesis of writing monomers with good index contrast and solubility. Typically the matrix is chosen to have low index (consistent with low T_G), and the writing monomer is chosen to have high index through the addition of, for example, aromatic groups or heavy atoms. These additions are heavily constrained by solubility considerations.

Furthermore, volume shrinkage can be ameliorated by increasing the number of high-index groups per functional groups. Taking this approach to its extreme, highly dendronized macro-monomers have been shown[25] to reduce volume shrinkage to as low as 0.04% while maintaining a moderate index contrast of $\Delta n \sim 2\times10^{-3}$. Further increases in macro-monomer size are ultimately limited by solubility and diffusivity.

Radical chain-growth is not the only possible writing chemistry. Cationic ring-opening opening polymerization affords the unique advantage that the ring opening mechanism creates a volume increase that can be engineered to compensate for polymerization-induced volume shrinkage.[16] The use of a cationic rather than a radical polymerization also means that recording is not inhibited by oxygen, and that it continues to exhibit a linear response even at high exposure intensities, enabling architectures in which a moving media layer is addressed by a pulsed laser or a laser with nanosecond-scale external modulation. Commercial media Aprilis[26] achieves $\Delta n \sim 0.1$ with negligibly small (~0.04%) shrinkage. However, this approach suffers from unwanted dark polymerization.

Free radical ring-opening polymerization[27] has the potential to achieve the best of both worlds: compensation of volume shrinkage to within a remarkable 0.02%, and also suppression of dark polymerization. But with only a limited toolkit of available chemical components, this approach has not yet achieved competitive performance in other respects, with Δn of only 1×10^{-3} and a sensitivity of 1.1×10^{-3} cm^2/J.

Photoinitiator

A further advantage of radical polymerizations is that a large set of well-understood photoinitiators (sometimes in conjunction with co-initiators and sensitizers[28]) are available, covering exposure wavelengths from UV to near IR. Of more recent interest[29] are macro-photoinitiators, which are slower to undergo unwanted diffusion into unexposed regions, and can even be fully tethered to the matrix.[30] Additionally, macro-photoinitiators can be less susceptible to cage recombination reactions, which often produce unwanted volatile organic photoproducts.

Two-photon initiation processes are of increasing interest, since they afford a sharp reduction in unwanted out-of-focus material response. The two-photon absorption cross-sections are very small, requiring high exposure intensities that are only possible in an exposure geometry in which a focused (and often pulsed) writing beam is rastered through the media. This exposure geometry significantly constrains the achievable throughput, and additionally renders impractical any bulk post-cure step to remove active and volatile writing chemistry. Although the two-photon cross-sections of many standard photoinitiators have been well characterized,[31] little attempt has been made to model the subsequent reaction/diffusion kinetics.

Retarders and inhibitors

Often the media is also doped with polymerization retarders, which have been shown to reduce recording-induced scatter.[32] This can be understood in terms of the formation of parasitic gratings, which are typically the dominant physical mechanism for recording-induced scatter.[33] When recording a signal grating into any media, some small but finite amount of material scatter is present and leads to the formation of a manifold of weak noise gratings. But if the recorded index develops on the same time scale as the recording exposure, the developing noise gratings self-amplify by coupling more and more light away from the signal grating. However, if a retarder is introduced, most of the index development can be delayed until after the exposure, thereby reducing the self-amplification effect. This benefit must, of course, be balanced against the ensuing loss in sensitivity.

Matrix-attachment sites

Relatively little academic work has addressed the processes by which initially mobile radical chains become immobilized (which may include chain-length-dependent slowing, topological entanglement, and transfer of radicals to the matrix). But, as will be shown in Chapter 2, these processes have a critical impact on the fidelity of recording, since the media spatial resolution is governed by the competition between two processes: on the one hand, diffusion of mobile radicals from exposed regions to dark regions, and, on the other hand, immobilization of those radicals.

The importance of radical immobilization is dramatically illustrated by recent work reported by Akonia[34]. Here protected-radical groups are incorporated into the matrix to provide a new and highly favorable pathway for immobilization: growing radical chains react with these matrix-attached groups and thereby become bonded to the matrix. This new reaction pathway increases the rate of matrix attachment, and is shown to yield as much as a six-fold improvement in usable

dynamic range. Even greater control of matrix attachment can in principle be achieved using, for example, thiol-click chemistry[35] although further materials development is still necessary here.

Chemically inert counter-diffusants

Another general strategy for enhancing dynamic range is to dope the media with some freely diffusing but chemically inert species that will be displaced into the unexposed regions as writing polymer accumulates in the exposed regions. Either the writing polymer or the counter-diffusant can have high refractive index, as long as these two components are strongly index-contrasting. Media with low-index counter-diffusant has been incorporated into Dupont commercial media,[36] while high-index counter-diffusant has been demonstrated by Soviet groups.[37,38]

Nanoparticles are appealing candidates for high-index counter-diffusants. However, minimizing scatter in such media is a significant challenge, especially since scatter is highly sensitive to small variations in nanoparticle size and degree of aggregation. A dynamic range of up to $\Delta n \sim 5\times10^{-3}$ has been achieved while still keeping scatter to low levels.[39]

Polymer-dispersed liquid crystals, which are an important class of materials due to their capacity for dynamic electrically switchable diffractive elements,[40] have many of the same properties since the non-reactive liquid crystals.are similarly displaced into unexposed regions. Optical scatter from the nematic microdomains remains a problem[41], especially since reducing the microdomain size involves a fundamental tradeoff against the electric field strength required for switching. Therefore understanding the kinetics, and specifically the relation between exposure timescales and development timescales, is essential[42].

A more detailed treatment of nanoparticle and liquid crystal additives is outside the scope of this work, but since their distribution is governed by the distribution of writing polymer, the design strategies put forward here will be directly applicable to these cases as well.

Applications

Commercial development of holographic photopolymers has in large part been motivated by holographic data storage (HDS), which exploits volumetric rather than surface patterning to achieve high storage densities and throughputs. This concept can be realized through various page based architectures[43] (i.e. many large overlapping weak holograms); or through bitwise microholographic architectures[44]. The achievable storage density depends on the dynamic range Δn (with a scaling that is fundamentally the same for all architectures[45]). But the tolerances for recording-induced shrinkage and optical scatter are extraordinary rigorous, and thus these tolerances must be traded off against high Δn in a highly constrained materials design problem.

Another commercially important area is display holograms in thin films, with applications including diffusers for LED backlighting[46], transparent heads-up displays[47], concentrators for solar panels,[48] and security holograms. These applications require not only large index modulation, but also good spatial resolution in order to record reflection holograms, and good ruggedness in order to withstand challenging environmental conditions (e.g. abrasion in the case of security holograms, or ultraviolet exposure from sunlight in the case of solar concentrators). Other holographic optical elements, either single-layer or stratified, find applications in shear interferometry[49], spatial filtering (either external [50] or intracavity[51]), and signal processing (e.g. optical correlator[52])

A more exotic application is diffraction gratings for cold neutrons, first realized in deuterated PMMA[53] and more recently in photopolymer/nanoparticle composites[54]. High fringe visibility is important here, since it enables thinner gratings and therefore eases the exacting tolerances on angular alignment. Also, short lifetimes of recorded features are attributed to continued dark polymerization, so a fuller understanding of reaction kinetics is important.

The photopolymer material platform also supports non-holographic features, most notably direct-written waveguides.[55] This concept was demonstrated shortly after first realization of photopolymer media but is still of current interest[56] since it holds the promise of complete optical devices integrated into a single polymer layer without the need for mechanical alignment of individual components. Waveguides can be recorded via rastering a focused beam, via mask exposure, or via self-writing[57].

Furthermore, this material platform supports not only individual waveguides, but also couplers,[58] optical interconnects,[59] and coherent waveguide arrays[60]. Finally, it can also write other optical components enabling complete integrated optical devices. In particular, holographic exposure lends itself to the fabrication of Bragg gratings, which can serve as filters for WDM,[61] as resonators for polymer lasers[62], and as mechanical sensors. Chemical sensors are also possible, for applications including vapor detection[63] and tear glucose monitoring in contact lenses[64]. These can be further integrated with microfluidics within a single material platform[65] for lab-on-a-chip applications.

Finally, this material platform enables low-cost customizable recording of arbitrarily patterned gradient-index features[66], for applications including endoscopic probes, contact lenses and intra-ocular lenses (including UV recording of custom index profiles *in vivo* after implantation[67]).

1.4 Understanding kinetics in two-chemistry photopolymers

1.4.1 Unique measurement challenges

Conventional instruments for characterizing reaction/diffusion kinetics, such as FTIR spectroscopy or differential scanning calorimetry, face signal-to-noise challenges when attempting to characterize two-chemistry media, since in this case the writing chemistry of interest comprises only a small fraction of the material. For this reason an appealing alternative is to record a holographic grating and monitor its growth using Bragg diffraction of a probe beam. This technique affords high signal from small/weak material response. The measured diffraction efficiency can readily be converted to an index modulation via the Kogelnik equation or, more rigorously, via rigorous coupled-wave analysis (RCWA). (See [68] for an early use of Bragg growth curves to understand reaction kinetics.)

It should be remembered, however, that this Bragg measurement only gives information about a particular spatial frequency (typically the fundamental). It gives no direct information about higher spatial harmonics, or about the spatially uniform component. As we will show below, the latter in particular is far from negligible and can even account for most of the total dynamic range. Lastly, the straightforward relationship between diffraction efficiency and index modulation, as established by the Kogelnik equation, assumes a low scatter grating with uniform phase, amplitude, and spatial frequency throughout its depth. Thus it can only be applied quantitatively to media that already have relatively high performance, and is of limited utility in optimizing media with e.g. high volume shrinkage.

1.4.2 Establishing a diffusional mechanism for index modulation

Historically, the first step in understanding reaction/diffusion kinetics was simply identifying that the mechanism for index response was diffusional. Photopolymer holographic media were first realized in a liquid resin system with metal acrylates in acrylamide,[69] for which a diffusional mechanism was later proposed. Hologram growth times were found to be consistent with independently measured diffusivities[70].

Other early photopolymer media were not liquid resins, but instead formed a glassy host matrix, either polyester[71] or PMMA[72,73] The index formation mechanism was initially speculated to be photocrosslinking, but eventually found to be diffusion of residual free monomer[74]. Long development times (up to 200 hours in the latter case) were consistent with the low diffusivity of the PMMA matrix.

A final important class of early diffusion-driven media is systems which are initially liquid but which begin to crosslink upon photo-exposure. In this approach, first explored by Tomlinson et al[75] and further developed in early Lucent media,[76] the same photochemistry initiates both matrix formation and polymerization of high-index writing monomer. But matrix formation is much more reactive, so that a uniform pre-cure preferentially initiates matrix-forming reactions, leaving most of the writing monomer unreacted until a later patterned exposure. However, these processes fall short of being perfectly orthogonal: some writing monomer is incorporated into the matrix, thereby reducing the available index modulation. In these quasi-orthogonal systems, diffusivity typically decreases by orders of magnitude as conversion runs from 0 to 100%, so that small variations in the initial matrix-forming step can lead to undesirable large variations in recording kinetics.

1.4.3 Effects of strongly coupled reaction and diffusion

The next step in understanding reaction/diffusion kinetics is a treatment of the nonlinear effects arising from the coupling of reaction and diffusion. Todorov et al[77] empirically observe qualitatively different regimes depending on whether or not reaction and diffusion timescales are coupled. These two regimes are rigorously formalized in the foundational Zhao and Mouroulis[78] paper, which writes a generalized differential equation describing polymerization-driven diffusion, using a set of dimensionless, normalized space and time variables.

The key insight in all of this work is that when reaction and diffusion occur over similar timescales, and when individual exposures are sufficiently strong to locally deplete writing monomer in the bright regions, a strong coupling between reaction and diffusion arises, as follows. New writing monomer, in-diffusing from the dark regions, will tend to be polymerized on the edges of bright regions, before it can reach the center. This leads to a nonlinearity in index response, with characteristic "horns" at the edges of bright regions.

Even worse, this nonlinear regime often cannot be avoided in practical applications. Strong individual exposures, leading to local depletion of monomer, are necessary for e.g. Bragg filters or waveguides. High speeds of both reaction and diffusion are generally desirable, in order to achieve high sensitivity and development speed; thus, both processes must take place on similarly short timescales.

The Zhao and Mouroulis model is extended by Lougnot et al[79] to incorporate a local slowing of diffusion with increasing conversion of writing monomer. They conclude: "with a few exceptions, the response of [systems with coupled timescales of reaction and diffusion] cannot be linear." Similarly, Kovalenko et al[80] include not only a conversion-dependent diffusivity, but also a finite exposure time, with some amount of continued "dark" polymerization post-exposure. All of these extensions are expressed in terms of additional unitless parameters.

A fully quantitative and experimentally validated kinetic model is put forward by Colvin et al[81]. This model includes a simple formula, based on free volume theory, for the dependence of both reaction and diffusion rates on local degree of conversion, and this simple formula is experimentally shown to be surprisingly accurate. The general experimental strategy here is one we will follow – rate coefficients are measured independently in the weak-signal regime, then combined into a full reaction/diffusion model with no adjustable parameters that is tested in the strong-signal regime at both fundamental and higher spatial harmonics.

The design implications of this insight are explored in more depth by Schilling et al,[82] who argue that control of the reaction/diffusion kinetics is critical to realizing high performance. In particular, "The optimal material would strike a fine balance between the opposing material requirements of dimensional rigidity and fast diffusion time scales." In order to explore this trade-off, media are formulated with varying ratios of several co-polymerizing monomer components of different functionality and molecular weight – and therefore with a smoothly varying range of crosslink densities. High crosslink densities yield appealing bulk mechanical properties, but because of the low diffusivity, the photopolymerization cannot proceed to completion. This effect is confirmed by FTIR, but diffusion time scales are not directly measured.

1.4.4 NPDD approach: many simultaneous adjustable parameters

The Nonlinear Polymerization-Driven Diffusion (NPDD) model, developed in an influential series of papers[83] by Sheridan, Gleeson, et al working in acrylamide media, puts forward a new strategy for extracting reaction/diffusion rate coefficients. A fundamental difficulty in measuring these coefficients directly is that the relevant processes can be simultaneous and highly coupled. The NPDD strategy is to leave all of these rate coefficients as simultaneous free parameters in a

fit to Bragg-monitored grating growth curves. In order to produce a tractably simple set of equations for fitting, the reaction/diffusion equations are expanded as a spatial harmonic series, retaining only the first few terms. This corresponds neatly to the successive spatial harmonics probed by measurements of successive Bragg orders. Thus, this technique leverages the high SNR of Bragg measurements into precise values for fit parameters.

At the heart of the model is a proposed set of reaction/diffusion physics for the material in question, in this case PVA/AA. Most notably, the model proposes that growing chains promptly become entangled, but that the radical tips of these still-growing chains then undergo reaction-diffusion over relatively large distances, characterized by a "nonlocal parameter" $\sigma^{1/2} \sim 60$ nm. This mechanism generates diffusional blurring and gives rise to the spatial resolution limit of the media.[84] This set of reaction paths is extended in later work, to capture a wide range of additional physics, including: bimolecular termination[85] and primary termination; inhibiting species such as oxygen;[86] depletion of initiator during long exposures;[87] chain transfer agents;[88] and continued dark polymerization. Recent versions of the model also incorporate local slowing of diffusion with increasing degree of conversion.[89]

This approach is extended by Wu and Glytsis[90] working in DuPont media. Here, the harmonic expansion is replaced by full FDTD modeling, and the Kogelnik equation for diffraction efficiency is replaced by rigorous coupled-wave analysis (RCWA), but the results are qualitatively similar.

One fundamental challenge of this approach is that even a good fit to experimental data cannot in general be taken as validation of the underlying physical assumptions and set of reaction paths. To illustrate this challenge, we consider the work of Toal et al, working in an almost identical PVA/AA media formulation and using the same general modeling strategy of simultaneous

fitting.[91] The Toal model contains a somewhat different description of the underlying physics that produces diffusional blurring of small-pitch gratings. Where the Sheridan model assumes that growing chains promptly become entangled, but that the chain ends then undergo significant reaction diffusion, the Toal model instead assumes that growing chains undergo significant diffusion before becoming entangled. Further evidence for the Toal interpretation is adduced in Babeya et al.[92]

Because the two models contain different physics, they produce different values for fit parameters such as monomer diffusivity. Even more seriously, both models yield acceptable fits to Bragg data; in other words, this data does not decisively resolve the question of what is the fundamental physical mechanism behind the media resolution limit.

Recent work in the NPDD framework has addressed this concern by turning toward independent measurements of some parameter values. For example, Gallego et al[93] note the difficulty of disentangling reaction and diffusion effects with overlapping timescales, and so they separate timescales by increasing the pitch to 80 microns, so that diffusion is slower than reaction.

Much of the recent work from Sheridan et al also focuses on independent measurements. They demonstrate diffusivity measurements that are either decoupled from reaction (via the same approach of increasing the grating pitch),[94] or entirely non-holographic (via gravimetry).[95] Similarly, photoinitiator properties such as quantum efficiency have been studied independently in non-holographic experiments.[96]

Another important step toward independent measurements is an extension of the NPDD model to a material, the Trentler epoxy-resin formulation, for which the component refractive indices have already been reported elsewhere.[97] Using these reported values (as opposed to leaving

component refractive indices as adjustable parameters), the model achieves good agreement with grating growth experiments.[98] However, these reported index values are not corroborated directly, and the volume mixing rule for the components is assumed, rather than measured.

A more recent application of the NPDD model to Bayer two-chemistry media[99] represents a further extension of this trend toward independent measurements. The starting values for the iterative fit procedure are, wherever possible, set to the values determined by independent experiments. This is the case not only for the component refractive indices but also for the polymerization rate coefficient K_p (from pulsed-laser polymerization in combination with size-exclusion chromatography[100]) and the conversion-induced slowing coefficient α (from shear modulus measurements). Finally, the set of parameters obtained from an iterative fit is further validated against experimental results at different grating pitches.

1.4.5 Mechanism of index formation in two-chemistry photopolymers

A basic difficulty in extending kinetic models to treat the special case of two-chemistry media is that the mechanism of index modulation in such media is generally not as well understood as in the case of single-chemistry media with non-crosslinked binder. In particular, it is not clear in general whether a highly crosslinked matrix remains stationary as new writing monomer in-diffuses, leading to net densification of the media, or whether the matrix undergoes volume displacement toward the unexposed regions.

In media with non-crosslinked, high-molecular-weight binders, it has been understood since Smothers[101] (1990) that displacement of binder can play a key role in index modulation. Tomlinson et al[102] show that counter-diffusion, whether of binder or of weakly-reactive index-contrasting monomer, enables much greater Δn, compared to single-component systems that rely

only on densification. Likewise Karpov et al[103] demonstrate 10 to 20 times greater Δn in formulations with inert high-index counter-diffusers, compared to single-component systems.

But binder is not always displaced – a notable counterexample is the foundational work of Colburn and Haines[104] in early DuPont media. They argue that, for these open films, any displacement of binder would give rise to surface relief gratings which are not in fact observed, and thus instead densification must be the dominant index change mechanism. They also note that the available free volume of the gelled media might impose limits on how much in-diffusing writing monomer can be packed into the exposed regions.

In media with crosslinked matrix rather than a binder, a variety of displacement behaviors are again observed. Colvin et al[81] (1997) establish a quantitative model of index modulation in Lucent media. This model assumes 1:1 volume displacement of matrix (that is, zero net densification, analogous to ideal mixing of liquids) and achieves good agreement with experiment. It is noted that, under this assumption, the media dynamic range Δn should be proportional to the index difference of the components, ($n_{\text{writing polymer}} - n_{\text{matrix}}$), rather than $n_{\text{writing polymer}}$ alone. Later work by Dhar et al[1] (1999) offers a more compelling demonstration that dynamic range is exactly proportional to ($n_{\text{writing polymer}} - n_{\text{matrix}}$), but the connection to mixing rules is not discussed explicitly.

A novel technique for direct and quantitative observation of this matrix displacement is demonstrated by Kagan et al.[105] Working in a broadly similar two-chemistry media, they record gratings of several μm pitch and then use confocal Raman microspectroscopy to map out the concentration profiles of both writing monomer and matrix. These profiles reveal that matrix displacement occurs, but falls slightly short of 1:1 volume displacement, leaving some residual

density modulation. This suggests that no universal mixing rule can *a priori* be applied to all two-chemistry media; rather, the mixing behavior of any particular formulation must be investigated experimentally.

1.4.6 Conclusion

Two-component diffusive photopolymers afford excellent optical and mechanical properties within a cheap and flexible material platform. Understanding the coupled reaction/diffusion kinetics of such media poses unique challenges, but is crucial in order to optimize material performance, as will be shown below.

CHAPTER 2

FUNDAMENTAL CONCEPTS: MATRIX DISPLACEMENT AND FORMULA LIMIT

2.1 Introduction

2.1.1 Outline of "divide-and-conquer" approach

This work proposes a methodical "divide-and-conquer" strategy for characterizing the reaction/diffusion kinetics of two-chemistry media, by decoupling and independently measuring all key processes. This strategy takes its inspiration from the recent work in decoupled measurements described above, but extends it to realize a fully predictive model that invokes no additional adjustable fit parameters. This approach is demonstrated in model materials similar to commercial holographic media.

The first key step is to experimentally establish the mechanism for index modulation, including the degree of volume displacement of the matrix. This yields a quantitative, analytical relationship between index and writing polymer concentration, derived from the Lorentz-Lorenz relation. From this we readily obtain an expression for the "formula limit" or maximum achievable holographic index modulation, based solely on the properties and formulated concentrations of the material components. This is to be contrasted with traditional modeling approaches, in which the magnitude of index modulation is treated as an adjustable fit parameter, to be determined empirically from holographic experiments.

Next, the degree to which a material does not reach this formula limit reveals the fraction of writing polymer that is generated in a spatially uniform distribution instead of the desired patterned distribution. While this wasted uniform fraction does not contribute to usable dynamic

range, it still incurs the same recording-induced shrinkage penalty, and we will show that it also sets the media resolution limit. Comparing the usable dynamic range to the formula limit affords important insights into the relevant reaction paths. In particular, it will be shown that many standard assumptions do not hold for this representative model material, as follows.

First, it is typically assumed that the dominant termination mechanism is bimolecular, as expected for radical polymerizations, leading to a sublinear index response. Instead we find a very nearly linear index response, indicating that the dominant termination mechanism is unimolecular.

Next, it is often assumed (e.g. [98]) that the mechanism by which growing oligomer chains are immobilized is chain-length-dependent slowing of diffusion via entanglement. Furthermore, it is usually assumed (with some notable exceptions[91]) that this immobilization is so fast that diffusion of live mobile oligomer chains can be mostly neglected, and that the dominant mechanism for diffusional blurring is reaction-diffusion on long oligomer chains.

But in fact, it will be seen that immobilization must occur chiefly by attachment of radicals to the matrix, via chain transfer reactions. Furthermore, diffusional blurring is dominated by diffusion of relatively short mobile oligomers, rather than reaction-diffusion of long growing chains. Thus, it is crucial that any reaction/diffusion model of this system must track both mobile and immobile live and dead chains, and it must account for not only polymerization and termination reactions, but also chain transfer reactions.

Having established a set of reaction paths, next each rate coefficient in turn is measured independently, either non-holographically or in the weak-grating regime. The combined set of rate coefficients is then used to make quantitative predictions of index response in the highly-

coupled strong-grating regime, without any additional adjustable parameters. Accurate predictions serve to validate the particular parameter values, but even more importantly, confirm that the proposed set of reaction/diffusion equations does indeed capture all of the relevant reaction paths.

Finally, the resulting insights into the underlying physics suggests a set of new strategies for material design. A variety of techniques for enhanced spatial confinement of recording are demonstrated, achieving index modulation near the formula limit, and recording of microholograms below the diffraction limit.

2.1.2 Model material

The model material (Table 1) is designed to capture the same basic chemistry as commercial two-chemistry media[20] while using only off-the-shelf components. It comprises a thermosetting urethane host matrix and acrylate writing chemistry. The total usable peak-to-mean index modulation is measured to be $\Delta n = 1.5\times10^{-3}$ (corresponding to an M/# of 2.4 per 200 μm) using the standard technique of angular multiplexing of many weak gratings.[106] The recording-induced volume shrinkage is measured to be 0.5% using the standard slanted-grating technique,[107] in good agreement with previous results in the same material obtained from phase imaging of large recorded features.[108]

The glass transition temperature T_G is measured by dynamic mechanical analysis (DMA) to be ~18 °C. As shown in Figure 1, the consumption of writing chemistry is found to have little effect on T_G, with even total polymerization of writing monomer producing only a ~4°C increase in T_G. This supports the assumption, in the modeling section below, that all rate constants are approximately independent of the degree of polymerization of writing monomer.

Component	Name	Source	wt%
Urethane matrix			
1. Polyol	polyester block polyether diol, alpha-, omega-diol, (eq wt 234, from Aldrich)	Aldrich	55.61
2. Isocyanate	Desmodur 3900 (eq wt 179, Bayer)	Bayer	37.81
3. Plasticizer	Dibutyl phthalate	Aldrich	0.50
4. Catalyst	Dibutyltin dilaurate	Aldrich	0.01
Writing chemistry			
5. Photoinitiator	TPO: (2,4,6-trimethylbenzoyl)diphenylphosphine oxide	Aldrich	0.04
6. Writing monomer	TBPA: (2,4,6) tribromophenyl acrylate	Huyang Puicheng	6.00

Table 1: Model material formulation. Components are used as received, except TBPA which is purified by dissolving in methylene dichloride and filtering with a Millipore 0.5 micron pore membrane filter. Components 3-6 are mixed into the polyol at 60C, degassed, then mixed with isocyanate and cast between glass slides. For Figure 1, initial concentration of writing monomer is varied from 0% to 6%, and writing monomer is later added or removed from the gelled matrix via bulk diffusion.

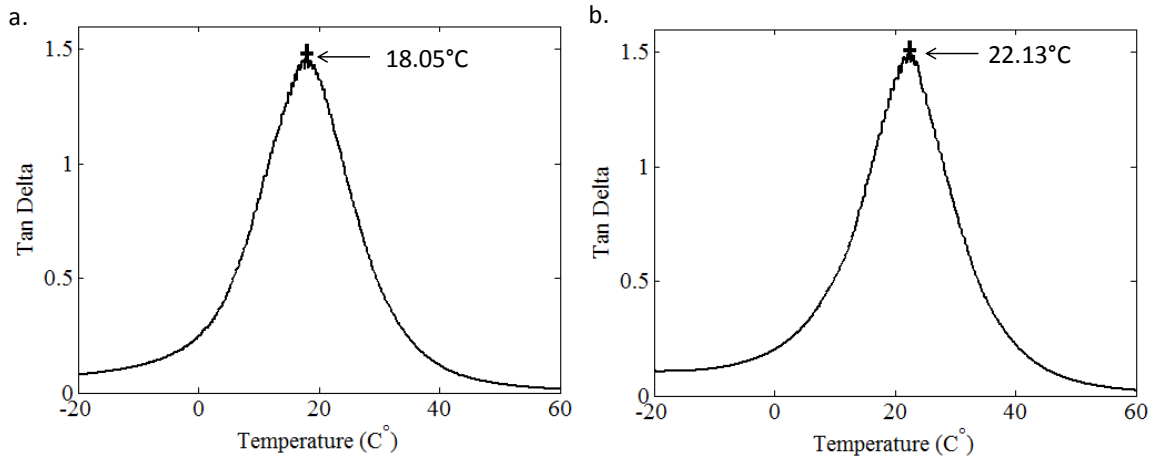

Figure 1. Dynamic mechanical analysis of the model material, showing that the glass transition temperature, T_G, is nearly unaffected by writing monomer conversion. (a) Measured T_G of the photopolymer formulation prior to exposure. (b) Measured T_G after flood exposure sufficient to reach 100% conversion of writing monomer. All measurements are at 1 Hz, and T_G is defined as the tan(δ) peak.

2.1.3 Analytical relation between index and monomer concentration

Traditional reaction/diffusion models only infer the relationship between refractive index modulation and writing polymer concentration indirectly, as an adjustable fit parameter to holographic experiments. This provides no direct understanding of the mechanism of index modulation, which in turn limits material design. Here, the relationship between refractive index and writing polymer concentration is instead established analytically, prior to holographic measurements. This approach reveals that displacement of the host matrix by in-diffusing writing monomer plays a crucial role in index modulation.

This analytical relationship is derived by using a prism coupler to measure the bulk index of a series of calibration samples, into which a range of different concentrations of writing monomer have been introduced. Writing monomer is introduced in one of two ways: either by mixing it with the liquid matrix precursor before thermoset (which ensures nearly perfect volume displacement of precursor), or by bulk diffusion into an already thermoset matrix (which closely matches the diffusive process of hologram recording, where the degree of volume displacement is not known *a priori*).

In the latter case, a diffusion gradient is produced independently of any photo-process, simply by laminating together two thin media samples with different initial writing monomer concentrations, so that writing monomer diffuses from one into the other (Figure 2). This diffusion process is monitored gravimetrically (by periodically delaminating and weighing the samples). Between measurements, the samples are held at a constant 60C and packaged with silica gel to minimize fluctuations in moisture content.

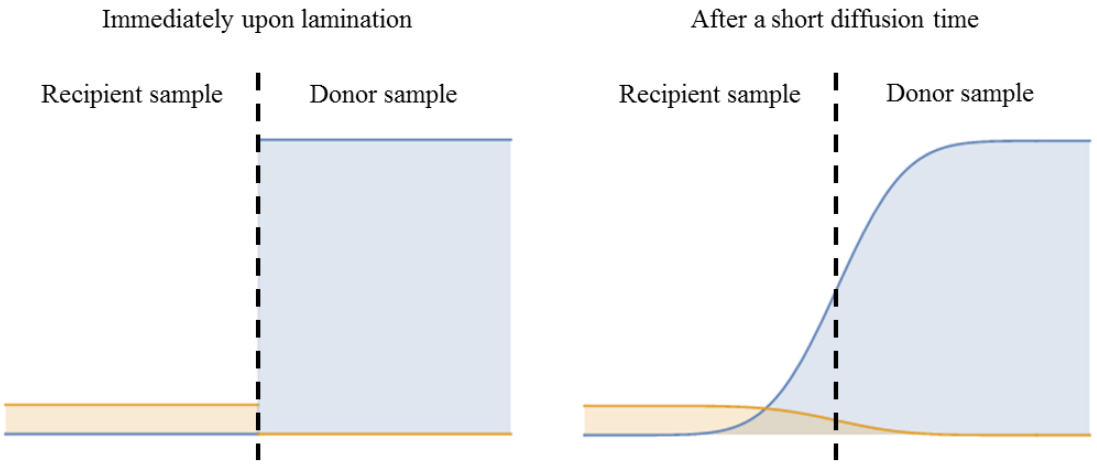

Figure 2. Schematic for uniform diffusion of writing monomer into an already crosslinked matrix. A diffusion gradient is created independently of any photo-process, simply by laminating together two thin samples of media. The concentration of mobile species near the interface quickly approaches the mean of the two initial concentrations, even if diffusion fronts are slow to penetrate deeper into the samples. Then the samples are peeled apart and the formerly joined faces are measured with a prism coupler, which only detects the refractive index very near the surface (within a fraction of a micron), where the mean concentration has already been reached.

In both cases, the introduced writing monomer is then uniformly flood-cured to consume all of the writing chemistry. After a period of at least 24 hours to ensure that the photopolymerization has run to completion, the bulk index is measured via prism coupler. We find, in Figure 3, that the measured relationship between bulk index and writing polymer concentration is the same in both cases, and thus the covalently cross-linked gelled matrix must be exhibiting the same 1:1 volume displacement as the liquid matrix components.

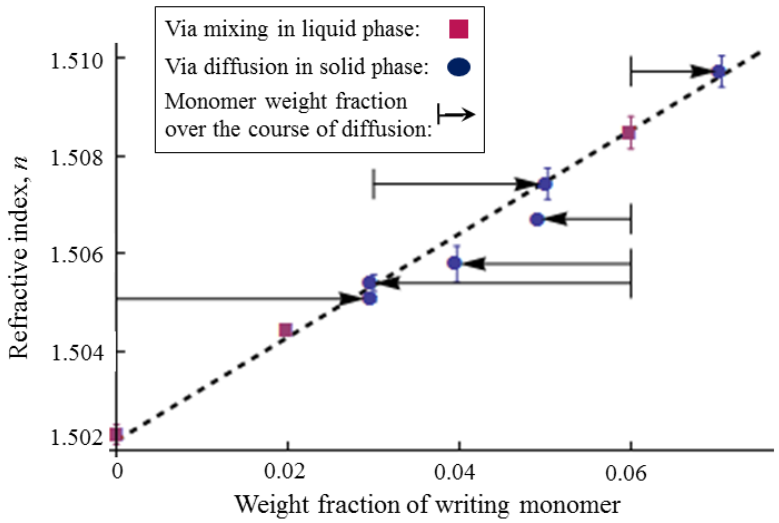

Figure 3. Bulk refractive index as a function of concentration of polymerized writing monomer, TBPA. Writing monomer is either dissolved into the liquid resin, or diffused into the thermoset matrix, with the in-diffusion process monitored gravimetrically. In either case, the sample is then flood-exposed and allowed to rest for >3 days to ensure complete polymerization; then bulk index is measured via Metricon 2010 prism coupler. The same refractive index relation holds in both cases: dashed line is a good (R^2 = 0.992) linear fit to all data points. Therefore the solid matrix must be exhibiting nearly perfect volume displacement, just as the liquid resin is.

Having established the mixing rule for matrix and writing polymer, it now becomes possible to express the analytical relationship between polymer concentration and index in terms of more physically fundamental quantities such as bulk indices. In general, this is given by the Lorentz-Lorenz relation:

$$\frac{n(\varphi)^2 - 1}{n(\varphi)^2 + 2} = \varphi\left(\frac{{n_{writing\ polymer}}^2 - 1}{{n_{writing\ polymer}}^2 + 2}\right) + (1 - \varphi)\left(\frac{{n_{matrix}}^2 - 1}{{n_{matrix}}^2 + 2}\right)$$

Equation 1

where φ is the volume fraction of writing polymer, and $n_{writing\ polymer}$ is the refractive index of solute writing polymer. In the limit where writing polymer is dilute (here <10 wt%) and low

index contrast with the matrix (here <10% fractional contrast), this reduces to a simple linear relationship:[109]

$$n(\varphi) = n_{matrix} + \varphi(n_{writing\ polymer} - n_{matrix}) \quad \textbf{Equation 2}$$

The volume fraction of writing polymer, φ, can be rewritten in terms of the more readily measurable weight fraction $p_{writing\ polymer}$ and the densities $\rho_{writing\ polymer}$ and ρ_{total}, yielding[109]:

$$n(p_{writ.\ pol.}) = n_{matrix} + (n_{writing\ polymer} - n_{matrix}) \frac{\rho_{total}}{\rho_{writing\ polymer}} p_{writing\ polymer}$$
$$= n_{matrix} + \kappa\, p_{writing\ polymer} \quad \textbf{(Equation 3)}$$

where κ can be measured most precisely by treating it as a single phenomenological quantity: the slope of the line in Figure 3. A linear fit (R^2 = 0.992, shown as dashed line) yields $n_{matrix} = 1.5023$ and $\kappa = 0.085$.

While this empirical fit provides the most precise measurement of κ, it is also of interest to analyze the more physically fundamental quantities that are lumped into it. Most of these can be measured independently, and thus we can find the remaining unknown quantity $n_{writing\ polymer}$, the index of solute polymerized writing monomer. It should be emphasized that this quantity is distinct from the index of solute or crystalline writing monomer, and is not readily measurable by more conventional means.

All the other terms in κ are measured as follows. The refractive index of pure matrix n_{matrix} = 1.5023 is found from the linear fit in Figure 1. The density of solute writing polymer $\rho_{writing\ polymer}$ = 2.5 g/mL is estimated by dissolving a known mass of writing monomer in a known volume of cyclohexanone and measuring the increase in volume. The density of the

material as a whole ρ_{total} = 1.1 g/mL is estimated from the manufacturer's reported densities for the matrix components, neglecting the volume shrinkage of order 10% upon thermally induced crosslinking. This set of values fully determines $n_{writing\ polymer}$ = 1.70, where the uncertainty in this value is dominated by these relatively crude estimates of density.

As further validation of this calculation, it can be repeated for a different host matrix (with T_G ~ -20 ºC, as introduced below) but the same writing monomer. The refractive index of this second matrix is notably different, and so the fit parameters to Equation 3 are different as well: $n_{matrix} = 1.4623$ and $\kappa = 0.1028$ (from a linear fit with R^2 = 0.999). However, these fit parameters yield $n_{writing\ polymer}$ = 1.70, which is in good agreement with the previous value, thereby confirming that this calculation arrives at the refractive index of solute polymerized writing monomer, independent of the matrix.

Finally, we can now show that these refractive index measurements are capable of resolving even small deviations from ideal mixing (i.e. small amounts of densification). The Lorentz-Lorenz relation can be rewritten in a form that does not assume ideal mixing, but rather a more general mixing rule:

$$\frac{n(\varphi)^2 - 1}{n(\varphi)^2 + 2} = \varphi\left(\frac{{n_{writing\ polymer}}^2 - 1}{{n_{writing\ polymer}}^2 + 2}\right) + (1 - X\varphi)\left(\frac{{n_{matrix}}^2 - 1}{{n_{matrix}}^2 + 2}\right)$$

where $0 \leq X \leq 1$, with $X = 1$ for 1:1 volume displacement of matrix and $X = 0$ for the case of no matrix displacement, only densification. The component refractive indices are calculated as before (using data from the case where writing monomer is mixed into the liquid matrix precursor, since the same 1:1 mixing rule can still be assumed to apply in that case). As shown in Figure 3, values of X even slightly less than unity can be seen to yield an obviously poorer fit to the remaining data.

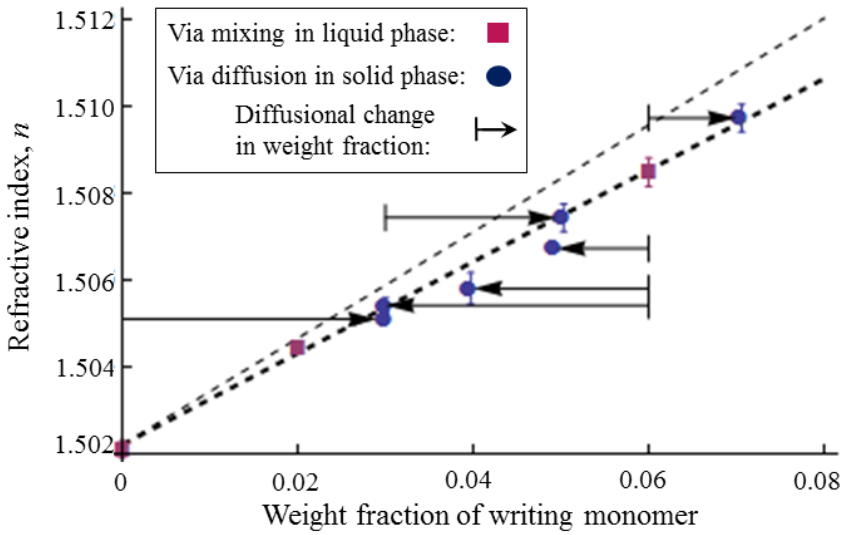

Figure 4. Two slightly different mixing rules are clearly distinguished via prism coupler data. Lower dashed line shows 100% volume displacement of matrix, as in the previous figure. Upper dashed line shows 90% volume displacement of matrix. The latter is calculated using the Lorentz-Lorenz relation and the component refractive indices extracted from the liquid-phase data (for which 100% volume displacement can always be assumed).

2.2 Confocal Raman microspectroscopy as further evidence of matrix counter-diffusion

2.2.1 Summary

The 1:1 volume displacement of the crosslinked matrix, inferred above from prism coupler experiments, can also confirmed more directly by scanning confocal Raman microspectroscopy. This technique provides an absolute, quantitative map of the spatial distribution of both writing polymer and matrix polymer. To observe displacement, a large (500 μm) feature is exposed with a dose sufficient to polymerize 100% of the writing monomer at the peak. After sufficient diffusion time and a final uniform flood exposure, the concentration profiles of both writing polymer and matrix are measured. As shown in Figure 5 (a) and (b) the matrix profile is a nearly perfect mirror image of the writing polymer profile, indicating that the matrix undergoes effectively 1:1 volume displacement by in-diffusing writing monomer, even for features as large as 500 μm.

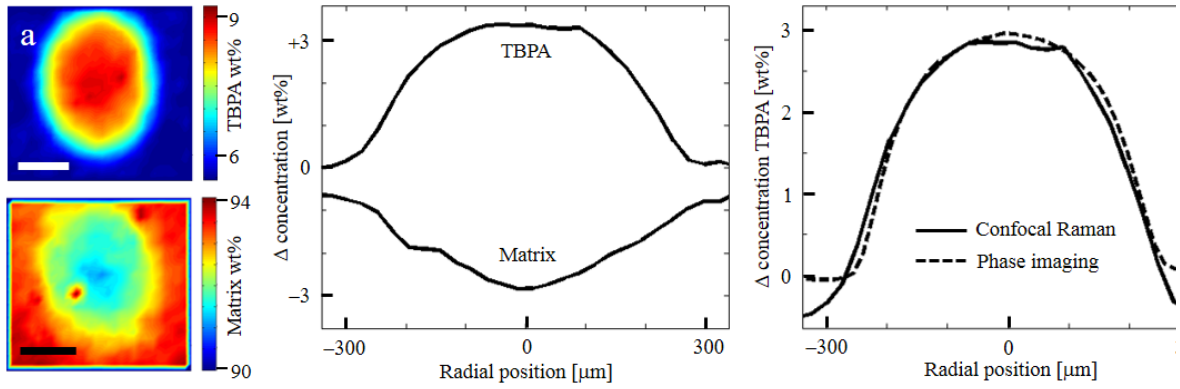

Figure 5. (a) Confocal Raman microspectroscopy yields concentration profiles of TBPA writing polymer, top, and urethane matrix polymer, bottom, within a gradient-index feature. The local densification of writing polymer causes a corresponding displacement of the host matrix, even over large scales (scale bars = 200 μm). Image courtesy of Adam Urness. (b) Spatial averages of those concentration profiles. (c) Writing polymer profile measured as a refractive index via phase-sensitive imaging and converted via Fig. 1 to concentration. This is compared to the confocal Raman result from (b), and to the prediction of the reaction/diffusion model discussed below.

2.2.2 Experimental details

The crucial first step in the confocal Raman measurement is identifying and calibrating distinctive Raman peaks for both writing polymer and matrix. This step uses a series of seven different spatially uniform samples, formulated with writing monomer concentrations ranging from 0 wt% to 12 wt%. These formulations are cast in 1mm thick layers between glass microscope slides, then completely and uniformly photopolymerized via flood cure. Finally they are measured with the scanning confocal Raman microscope and their spectra are compared.

A distinctive peak for the writing polymer is found at 237 cm^{-1}, as shown in Figure 6 (a). From these peak heights, a calibration is readily constructed, as shown in Figure 6 b.

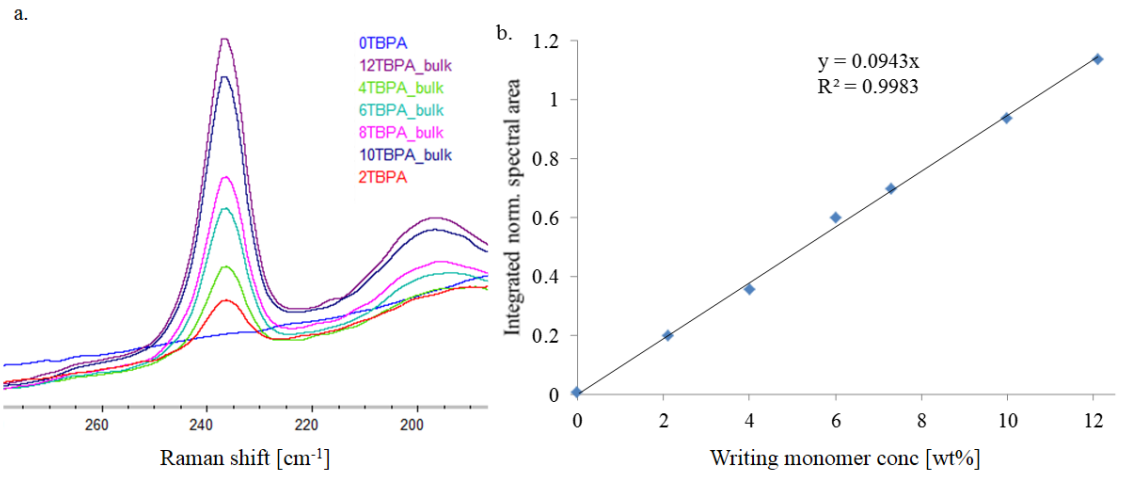

Figure 6. Confocal Raman calibration. (a) Raman spectra centered at 237 (cm^{-1}) of uniform calibration samples with varying amounts of writing monomer. (b) The relationship between the writing monomer concentration and the integrated normalized spectra of the 237 (cm^{-1}) spectral line. Images courtesy of Adam Urness.

A distinctive signal for the matrix also exists, between 2800 and 3000 cm^{-1}. This signal is not as well resolved into a single peak; therefore, instead of using the peak height, the signal is

integrated from 2810 to 3020 cm^{-1} and then normalized with respect to an unexposed area of the sample.

Once these calibrations have been obtained, large gradient-index features are recorded into new samples. Again, the media is cast in a 1 mm thick layer between two glass microscope slides. The index features are recorded with an exposure dose of 4000 mJ/cm^2 at the peak, which is empirically found to be sufficient to achieve 100% reaction of the writing monomer. The sample is then heated to 60 ºC, to speed up diffusion across the large (~500 μm) feature. After being held at 60 ºC for 10 days, the sample is uniformly photocured, so that no further polymerization takes place. Images of the distribution of writing monomer and matrix, shown in Figure 5a, are built by collecting a 29×27 grid of Raman spectra, spaced 26 and 21 μm respectively, where each spectrum is integrated for 60 seconds.

Finally, the writing polymer profile is also measured using a second, independent technique. Shack-Hartmann imaging of the recorded feature yields a phase profile; since the sample thickness is known, this is readily converted to a refractive index profile. Finally, this refractive index profile is converted to a writing polymer concentration profile using the results of the prism coupler experiments expressed as Equation 2.

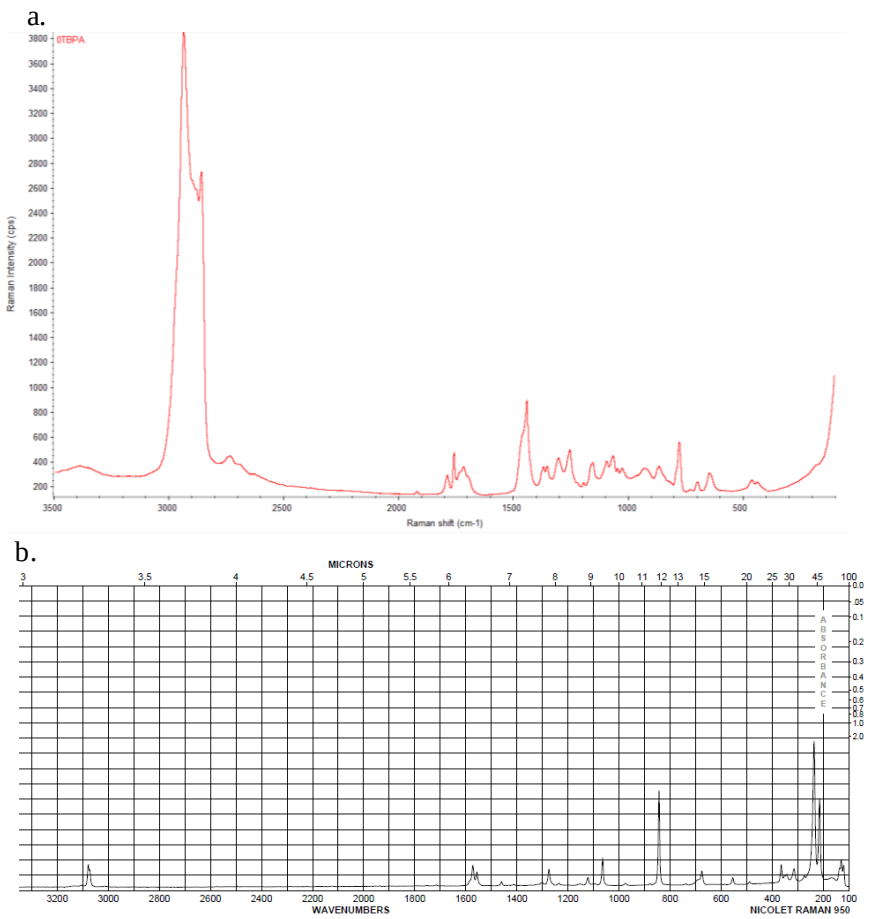

Figure 7. Orthogonal peaks in the measured confocal Raman spectra of (a) the urethane matrix and (b) tribromophenol, which enable independent measurement of the two concentration profiles. Images courtesy of Adam Urness.

2.2.3 Discussion

The curves in Figure 5 (b) are not perfect mirror images; this is attributed to the fact that the matrix distribution has smaller relative changes and therefore is more challenging to accurately quantify. Considering only the writing polymer distribution, however, we find excellent agreement between the directly measured writing polymer concentration and concentration inferred from refractive index (c) on the assumption of 1:1 matrix exclusion. (This is in contrast

to, for example, the results of Kagan et al in a different two-chemistry material,[105] which showed slightly less than 1:1 matrix exclusion, corresponding to a small residual density modulation.) The agreement between these two independent measurements of concentration profile establishes a rigorous validation of the analytical relationship obtained in Equation 2.

2.3 Materials design implications for matrix counter-diffusion

2.3.1 Matrix swellability is an important design parameter

This analytical approach has revealed that matrix displacement is a key mechanism in the formation of index modulations. This explains an empirical observation of Dhar et al[1] working in similar media, that media dynamic range is governed not simply by the refractive index of the writing polymer, but instead by the contrast between components. The fact that observed dynamic range scales almost exactly as $(n_{writing\ polymer} - n_{matrix})$ shows that volume displacement must be nearly 1:1 in the Dhar et al media.

This result also suggests that the ability of the matrix to fully swell or counter-diffuse is an important design constraint. For example, Trentler et al[97] working in epoxy/amide matrices show that if a matrix is so rigid that it can no longer swell to compensate for the influx of new writing monomer, the result is not that the material begins to undergo net densification, but rather that further in-diffusion of writing monomer is simply prevented, leading to a correspondingly lower dynamic range. They note that the degree of swellability depends in general both on the crosslink density and on the flexibility of the chains between crosslinks.

In our model material, it can be seen from Figure 3 that the swelling limit is not reached for concentrations of writing polymer up to 12 wt%, double the standard initial concentration of writing monomer. Other experiments[110] have shown that the swelling limit is still not reached

for even greater localized concentrations of writing polymer, up to as much as 60 wt%, or a factor of 10 more than the initial concentration of writing monomer. This is far in excess of the 10-15 wt% solubility limit of writing monomer in the liquid matrix precursor, thus further illustrating that the properties of writing polymer in-matrix cannot be straightforwardly extrapolated from those of writing monomer in crystalline form or in liquid solution.

2.3.2 Bulk mechanical effects on thick volume holograms

Matrix displacement also has significant implications for the bulk mechanical distortions suffered by thick volume holograms. It is well understood[111] that the fringes of a volume hologram in photopolymer media suffer bending and distortion due to the interplay of continuum-mechanical effects including recording-induced shrinkage, mechanical pinning at interfaces, and pre-stresses built in during sample formation. These effects in general produce a broadened and asymmetric angular spectrum, as can be shown via RCWA analysis[112]. In some cases, matrix displacement introduces an additional continuum-mechanical effect that produces similar broadening and asymmetry.

This is demonstrated in the following experiment, in which two different continuum-mechanical effects are observed over different timescales: first recording-induced shrinkage and then matrix displacement. First, a single weak grating in recorded in a sample of the model material, cast as before in a 1mm thick layer between glass microscope slides. The exposure region is roughly 4mm in diameter. Since this is a weak grating, all continuum-mechanical effects should be small, and Figure 8 (a) confirms that the angular spectrum is clean and symmetric.

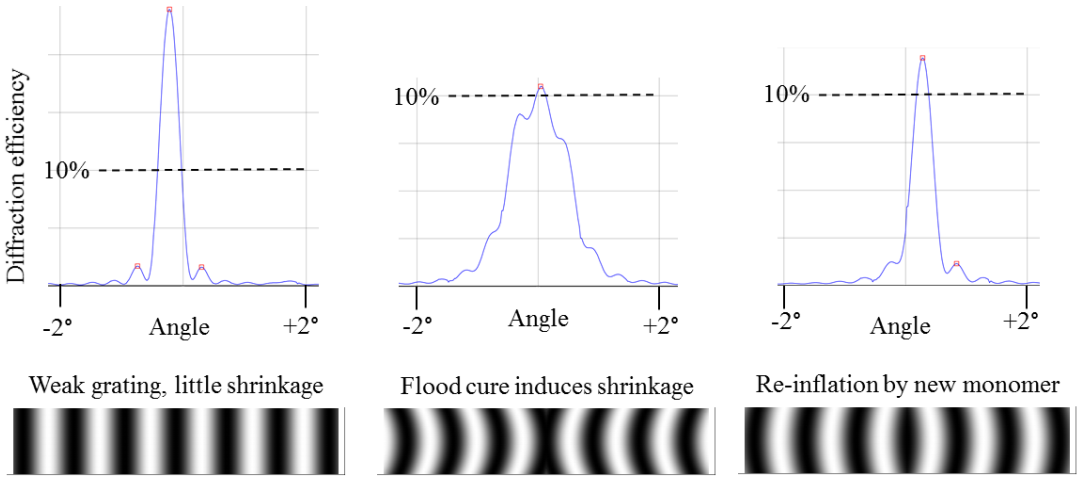

Figure 8. Fringe bending can be caused not only by polymerization-induced shrinkage, but also by matrix counterdiffusion effects. Angular spectra of a single weak grating, measured (a) immediately after exposure, showing negligible polymerization-induced shrinkage since this is a weak grating. (b) after many other gratings have been written in the same location but different angles, so that polymerization-induced shrinkage is much more pronounced. This shrinkage creates fringe bending, which in turn leads to the asymmetric and broadened angular spectrum. (c) Same grating, after 48 hours at 60C, which is long enough for significant in-diffusion of new monomer from outside the ~5mm diameter exposed region. The matrix counter-diffuses in response, partially "re-inflating" the grating.

Next, many other weak angle-multiplexed gratings are recorded in the same location. This polymerizes all the writing monomer within the 4mm region of exposure, causing more pronounced polymerization-induced shrinkage without otherwise affecting the original grating. The media layer is mechanically constrained from shrinkage at the glass/media interfaces,

whereas in the center of the media layer, the media is free to dimple inward, distorting the fringes. This leads to a broadened and asymmetric angular spectrum, Figure 8 (b).

Finally, the sample is held at 60C for 48 hours, to allow significant in-diffusion of new writing monomer from outside the 4mm exposed region. This in-diffusion of writing monomer leads to a corresponding expansion or counter-diffusion of the matrix over this 4mm scale. This expansion increases the fringe spacing, thus partially "re-inflating" the volume grating. At this point, shown in Figure 8 (c), the angular spectrum has narrowed, showing that the polymerization-induced shrinkage has been partially compensated by this "re-inflation". Finally, as in-diffusion continues, within the exposed region the matrix is eventually stretched/displaced outward relative to its initial state, as shown by the confocal Raman measurements above. Thus, the fringe spacing is greater than in the initial condition, and the grating might be said to be *over*-inflated (not shown in Figure 8).

This sequence explains an empirical finding[20] from the holographic data storage literature: that it is advantageous to prevent in-diffusion of new monomer from outside the exposed region. It can be seen that this in-diffusing monomer leads precisely to the "over-inflation" of matrix just discussed, and therefore the bending or outward dimpling of hologram fringes.

One way to prevent this in-diffusion is simply to uniformly post-cure the entire sample, including the unexposed regions, before diffusion can cause significant mass transport over the scale of the exposure region. This has the additional benefit of introducing recording-induced shrinkage uniformly throughout the sample, which further ameliorates fringe bending. However, it also means that only a single session of recording is possible, which is undesirable for many applications including data storage. Therefore other approaches have been explored, including a

writing monomer that is initially tethered to the matrix, and then selectively mobilized only in the recorded regions.[156]

2.4: Formula limit concept

In the previous section, we used standard refractive index measurements to establish an analytical relationship between index and writing polymer concentration. From this relationship we can now calculate the "formula limit", defined as the maximum achievable holographic index modulation Δn, only reached if 100% of the consumed writing monomer is patterned with perfect fidelity. For a series of sufficiently many weak angle-multiplexed holographic exposures to consume all available writing monomer, this can readily be calculated from Equation 2 as:

$$\Delta n_{formula} = (n_{writing\ polymer} - n_{matrix})\ \varphi_{writing\ polymer}$$

where Δn is defined, following the Kogelnik equation, as the peak-to-mean sinusoidal amplitude of the index modulation.

For exposure schemes other than a series of weak angle-multiplexed holograms, the maximum achievable index contrast may be given by some other expression. For example, a single strong sinusoidal exposure can only consume writing monomer in the bright fringes, and thus can achieve at most half of the formula limit defined above. But for any such exposure scheme, it is possible to write a similarly straightforward equation for the maximum index contrast.

For this model material, we find $\Delta n_{formula} = 5.1 \times 10^{-3}$. The usable Δn, measured via the standard technique of weak multiplexed Bragg gratings[106], is only a fraction of this limit, as shown in Figure 9. The wasted remainder must correspond to the fraction of polymerized writing monomer that is not patterned at the holographic spatial frequency. Instead, it must be uniformly distributed, since patterning at higher spatial frequencies can be ruled out in the limit of weak gratings.[78]

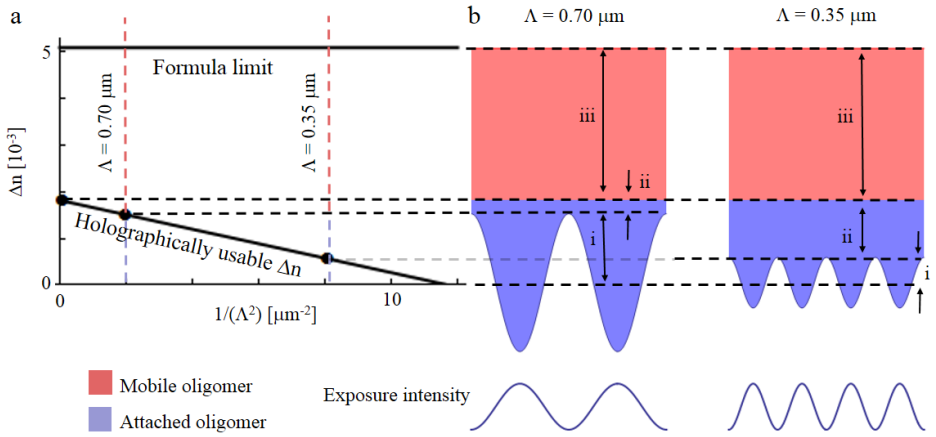

Figure 9. (a) Holographically usable peak-to-mean refractive index modulation Δn, as a function of grating pitch Λ, compared to the ideal "formula limit" calculated from Fig. 1. For multiple weak exposures, this formula limit is simply $\Delta n = n(6\%\ \text{TBPA}) - n(0\%\ \text{TBPA})$, where 6% is the initial uniform TBPA concentration. (b) Distribution of polymerized TBPA at $\Lambda = 0.7$ μm and 0.35 μm, drawn to match the Δn scale in (a). For any exposure dose, three categories of writing oligomer are generated, in a ratio determined by Λ: (i) attached oligomer that is holographically patterned, (ii) attached oligomer that is spatially uniform, and (iii) mobile oligomer, which diffuses to become spatially uniform.

The magnitude and resolution of this usable index response will be shown to depend crucially on the processes of immobilization and re-mobilization of radicals. Immobilization is typically attributed to reduced diffusivity of long chains; however, this is inconsistent with theory. The writing monomer forms non-branching chains, since typical monomers including TBPA are mono-functional to minimize shrinkage-inducing functional groups per high-index group.[20] Diffusivity of linear chains in a matrix is predicted to decrease, at the most extreme, only as the

square of chain length,[113] resulting in a predicted hologram lifetime of only hours for chains up to 100 monomer units long. We observe lifetimes of at least 6 months, and lifetimes of decades have been reported;[114] thus, immobility must be due to bonding to the host matrix and not to the reduced diffusivity of long-chained oligomers.

However, even though the final hologram is composed entirely of matrix-attached species, this must be preceded by significant diffusion of mobile radicals before they attach to the matrix, since the usable holographic Δn (Figure 9, quantity i) exhibits the $1/\Lambda^2$ scaling that is characteristic of diffusional blurring. This blurring leads to a uniform component in the attached oligomer profile (quantity ii). This is surprising, because reaction/diffusion models typically[115] assume that mobile live chains grow so quickly and become entangled so promptly that their diffusion can be neglected (although some models are exceptions[91]).

This blurring causes a fundamental media resolution limit, readily found by extrapolating the $1/\Lambda^2$ scaling to the point at which the holographic component of the material response goes to zero. At this scale, diffusion of radicals results in a uniform polymer distribution and thus no measurable holographic response. This is noteworthy because no consensus exists in the literature on what causes media resolution limits in general (compare, for instance, refs [84] and [116]). In the model material, this extrapolation from a few readily accessible Λ yields a resolution limit of Λ = ~300 nm, consistent with our observation that the material does not support reflection holograms, even at exposure wavelengths up to 532 nm, corresponding to Λ ~ 180 nm .

Extrapolating instead to large feature size ($1/\Lambda^2 \rightarrow 0$) where this diffusional blurring effect vanishes, we find (in Figure 9) that holographically patterned Δn still corresponds to at best only

~35% of the polymerized TBPA. The remaining ~65% (quantity iii) of polymerized TBPA must instead be uniformly distributed (higher spatial frequencies can be ruled out in the weak grating limit). This is only possible if it comprises terminated but still mobile oligomer chains, which diffuse into a uniform distribution, as observed in other media[117]. This uniform distribution of dead mobile oligomer is invisible to Bragg diffraction, but still visible to the prism coupler measurements of Figure 3.

As a more direct confirmation that quantity iii corresponds to mobile oligomer, a solvent extraction is performed on one of the confocal Raman calibration samples, to remove whatever fraction of the writing monomer comprises mobile chains. Then the confocal Raman measurement is repeated, showing that 56% of the writing monomer has been extracted, in reasonably good agreement with the 65% mobile fraction shown as quantity iii.

This large fraction of mobile oligomer is consistent with the existence of attached oligomer (Figure 9, quantities i and ii), for the following reason. The attachment of radicals to the host matrix most plausibly occurs via hydrogen abstraction, a process which terminates the short live oligomer chain but leaves it still mobile. Accounting for this mobile dead oligomer allows us to correctly predict the usable Δn, and in particular the previous phase imaging result at $\Lambda = 500$ μm (Figure 5 c).

Finally, on a much longer timescale, re-mobilization and spatial equilibration of attached radicals causes the eventual cessation of hologram growth. In more typical materials, this cessation is ascribed instead to radical termination; however, we find in this material that unconsumed monomer (measured as above) continues to be depleted according to the polymerization rate constant, long after the growth of the sinusoidal index structure revealed by Bragg diffraction has

ceased. We conclude, therefore, that radicals are still present after cessation of growth, but are blurred by diffusion into a uniform distribution so that the continued polymerization is invisible to Bragg detection.

As further evidence for diffusional blurring over long time scales, we note that timescale of this cessation of growth is itself dependent on the hologram pitch, with larger pitches corresponding to slower cessation of growth. This is not consistent with typical termination mechanisms (e.g. bimolecular termination, or termination by fast-moving oxygen), but it is consistent with the diffusional blurring proposed above.

This blurring cannot be due to reaction-diffusion of the radicals tips of immobile chains, since the distances involved are as large as $\Lambda = 5$ μm, not consistent with the stoichiometrically expected average writing polymer chain lengths of < 10 units. This blurring also cannot be due to the effect already discussed by which the initial photogenerated mobile radicals freely diffuse for a brief time before becoming matrix-attached, since, as will be shown below, cessation of grating growth takes place over a much longer timescale. Instead, we must postulate a reaction path by which matrix-attached radicals are converted back to freely-diffusing radicals. The most plausible mechanism is a chain transfer reaction that terminates a propagating oligomer chain, resulting in a terminated matrix-attached chain and a new mobile radical.

Thus, reaction/diffusion kinetics not only cause the usable Δn to fall short of the formula limit, but the fraction of monomer not used in reaching this limit undergoes unwanted reactions that restrict both resolution (attached oligomer) and, potentially, environmental stability (mobile oligomer). In the next chapter, we will extract rate coefficients for each of these reaction/diffusion processes independently.

CHAPTER 3

REACTION/DIFFUSION MODEL

3.1 Set of reaction paths

3.1.1 Introduction

As shown in the preceding section, the set of reaction paths (Figure 10) must include not only polymerization, but also immobilization and re-mobilization of radicals. These most plausibly occur via hydrogen abstraction and chain transfer respectively, but for the sake of generality we give only a phenomenological description in terms of species balance.

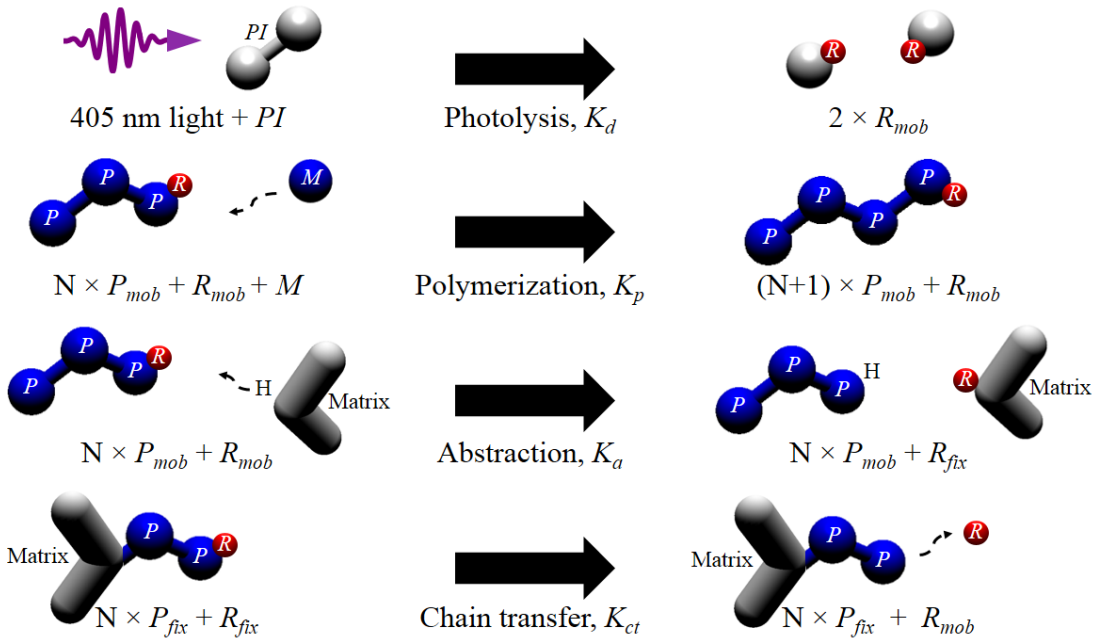

Figure 10. Species balance description of the set of reaction paths. As shown above, this set must be extended to separately track all of the following species: unconsumed photoinitiator *PI*; unreacted monomer *M*; mobile radicals R_{mob} and matrix-attached radicals R_{fix} (attached to chains of any length); and polymerized chain units P_{mob} and P_{fix}, belonging respectively to mobile or matrix-attached chains of any length.

In order to describe this set of reaction paths with a tractably small set of coupled reaction/diffusion equations (Table 2), the following simplifying approximations are made.

Photoinitiator, PI	$\frac{d}{dt}[PI] = -K_d I[PI]$
Monomer, M	$\frac{d}{dt}[M] = -K_p([R_{fix}] + [R_{mob}])\,[M] + D\nabla^2[M]$
Mobile radical, R_{mob}	$\frac{d}{dt}[R_{mob}] = 2\varepsilon K_d I[PI] - K_a[R_{mob}] + K_{ct}[R_{fix}] + D\nabla^2[R_{mob}]$
Attached radical, R_{fix}	$\frac{d}{dt}[R_{fix}] = K_a[R_{mob}] - K_{ct}[R_{fix}]$
Mobile chain unit, P_{mob}	$\frac{d}{dt}[P_{mob}] = K_p[M][R_{mob}] + D\nabla^2[P_{mob}]$
Attached chain unit, P_{fix}	$\frac{d}{dt}[P_{fix}] = K_p[M][R_{fix}]$

Table 2: Reaction/diffusion equations based on the reaction paths in Figure 10. I is the exposure intensity and 2ε is the radical quantum yield of the photoinitiator. For generality, both hydrogen abstraction and chain transfer are treated as first-order processes, rather than explicitly tracking the concentrations of matrix abstraction sites and of chain transfer agents.

3.1.2 Simplifying approximations

First, all rate constants are treated as independent of the local concentration of writing polymer, in contrast to single-chemistry systems in which material properties are highly conversion-dependent.[81] This is justified by dynamic mechanical analysis showing that even polymerization of 100% of the writing monomer leads to only a ~4°C change in T_G (Figure 1), and is attributed to the fact that writing polymer comprises only short, non-crosslinked linear chains.

Similarly, we neglect any local heating due to the exotherm of the polymerization reaction. The concentration of writing monomer is so low that even its complete and instantaneous polymerization would only heat the sample by several ºC, based on a typical reported heat of reaction for acrylate polymerization of 20.6 kcal/mol.[118]

Next, we assume that oligomers of all chain lengths can be described by a single set of molecular-weight-averaged rate constants. This neglects, for instance, chain-length-dependent diffusivity, which is reasonable since the average chain length is expected to be less than10 units strictly from stoichiometric considerations, and even shorter once chain transfer processes are taken into account. This is corroborated by solvent extraction of unattached oligomer, followed by direct measurement of its molecular weight distribution via gel permeation chromatography (Figure 11). This measured distribution of molecular weight suggests that most unattached oligomers have a chain length of only 1 or 2. (Figure 12 below provides indirect evidence that

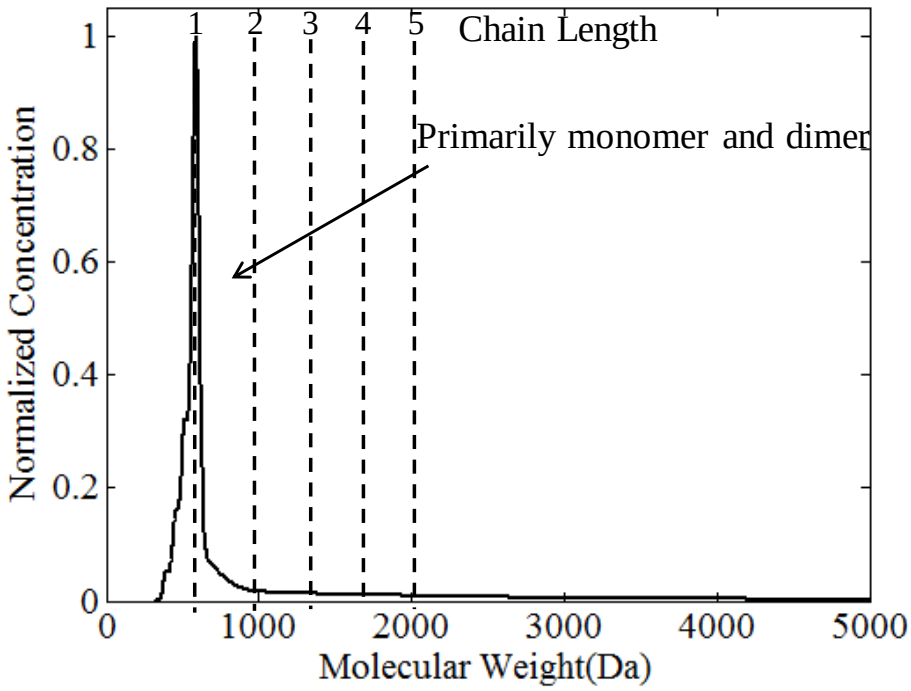

Figure 11. Gel permeation chromatography shows the molecular weight distribution of unattached oligomer, as extracted from a photocured sample of the polymer. Concentration is normalized to the peak value; dashed lines show multiples of the molecular weight of the writing monomer. Extraction of oligomer is performed by soaking the 500 μm thick sample in tetrahydrofluorine for 1 week at 50 ºC. (Image courtesy of Adam Urness)

attached oligomers are similarly short.) This further supports the use of a single set of molecular-weight-averaged rate constants to describe all unattached oligomers.

Next we assume that, even though primary radicals are more reactive than propagating chains, nevertheless both primary initiation and continued propagation can described by a single propagation rate constant K_p, on the grounds that both processes are transport-limited rather than reaction-limited, with similar diffusivities for both species. The value of K_p measured below is found to be five orders of magnitude smaller than the reaction-limited K_p for typical acrylate polymerizations,[119] confirming that propagation is well into the diffusion-limited regime in this media. Similarly, it has been shown elsewhere[120] that initiation of acrylate polymerizations by TPO primary radicals is diffusion-limited rather than reaction-limited, even in significantly less viscous media of only ~200 cP.

Finally, we explicitly neglect bimolecular termination. This is in contrast to most radical polymerizations, for which bimolecular termination in fact dominates, leading to an index response that has a half-power dependence on intensity. However, the model material demonstrates an index response that is linear in intensity and dose, showing that bimolecular termination must be negligible on the timescale of these experiments.

This linear response is demonstrated by the standard media characterization technique of writing a series of weak overlapping angle-multiplexed holograms (Figure 12). Successive identical exposures generate successively fewer primary radicals, due to depletion of photoinitiator. This depletion is calculated using the rate coefficient for photo-dissociation K_d obtained in section

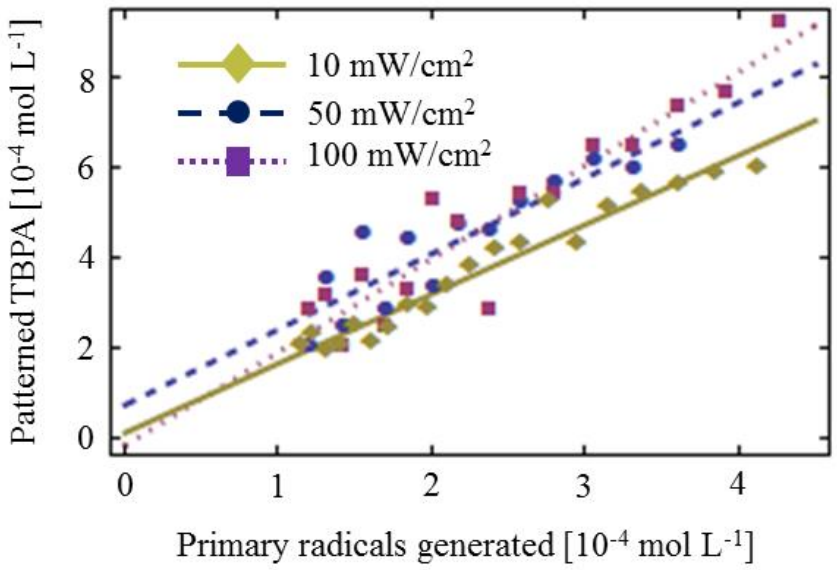

Figure 12. Index response is nearly linear in the number of primary radicals generated, which is only possible if bimolecular termination is negligible. For each of the three intensities used, each data point corresponds to one of a series of weak multiplexed gratings with different photoinitiator concentrations. Concentration of generated radicals is calculated from exposure dose using previously measured values of K_d and quantum yield.

3.2.1 below. Monomer is not depleted between successive exposures, due to the unusually slow polymerization in this media. Rather, the entire series of exposures is completed before any of the gratings has grown significantly (< 30 sec) and all the holograms grow effectively simultaneously, and are affected equally by monomer depletion.

Finally, the gratings are read out with a Bragg-matched probe beam; their diffraction efficiencies are converted to grating strengths, Δn, and then to concentrations of patterned writing polymer, as described in section 3.2.3 below. The results of this experiment, repeated at a range of

exposure intensities, confirm that material response is linear in the number of radicals generated, thereby ruling out significant bimolecular termination.

This is further corroborated by measurements of polymerization rate (Figure 17 b, below) showing that it is linearly proportional to writing intensity over fully two orders of magnitude.

Physically, this is attributed to the fact that mobile radicals quickly become immobilized by attachment to the matrix, and thus cannot reach each other. Bimolecular termination predominantly occurs via the mechanism of reaction diffusion, in which the radical tips of growing chains can eventually meet. This mechanism is much slower, and, as will be argued in section 3.3.1 below, negligible on the timescale of grating growth.

The observed linearity of index response is, however, consistent with the presence of a unimolecular termination mechanism, perhaps radical trapping or less-than-unity efficiency of chain transfer re-initiation. But this unimolecular termination, if present, is sufficiently weak that its effect cannot be distinguished over the ~10^3 second timescale of these experiments. With these simplifications, the model is characterized by five rate constants, each independently measured and verified as described next.

3.2 Independent measurements of rate coefficients

3.2.1 Rate coefficient for photolysis K_d

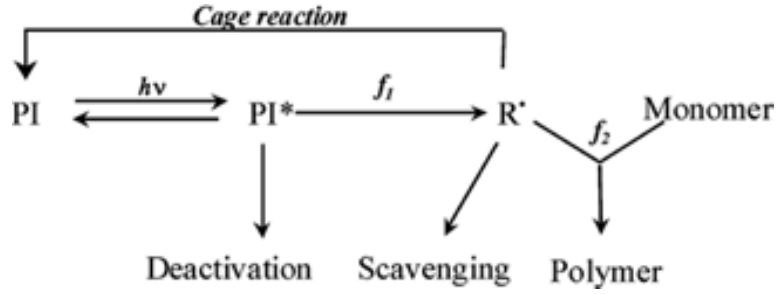

Figure 13. Photoinitiation schema, showing the sequence of absorption, photolysis, and finally initiation of chain growth. From Decker, 2002 (ref. 115).

The rate coefficient for photo-dissociation of the photoinitiator, $K_d = 1.1\times10^{-3}$ cm^2 mJ^{-1}, is calculated *ab initio* from the reported molar absorptivity[121] of TPO. First, the intensity absorbed by the photoinitiator, I_a, can be expressed in terms of the incident intensity I_0, the photoinitiator concentration [PI], and its molar absorptivity a:

$$I_a = I_0 \times (1 - 10^{-[PI]\,a})$$

Then, excited-state photoinitiator PI* will be generated at the same rate at which photons are absorbed:

$$\frac{d[PI*]}{dt} = I_a/h\nu$$

where $h\nu$ is the photon energy. Next, the rate of actual initiation events can be calculated from the reported quantum efficiency.[122] Following the notation of the scheme in Figure 13, some fraction f_1 of excited-state photoinitiators successfully dissociate (and the remainder undergo e.g. vibrational relaxation). Each dissociation event produces on average some number of radicals f_2 that react with monomer and initiate polymerization. The maximum possible value of f_2 is 2 since two free radicals are generated per molecule of TPO; the actual value will fall short of this

since some radicals are lost to e.g. scavenging or geminate recombination yielding an inert photoproduct.[123] This yields the following expression for the rate of chain initiation: [115]

$$ri = \frac{d[PI*]}{dt} \times f_1 \times f_2$$

Then the overall initiation efficiency $f_1 \times f_2 = 2\varepsilon$ just the number of initiating radicals produced per molecule of PI destroyed. The reported value of 1.3 is rather close to the maximum possible value of 2; this good performance is attributed to the fact that geminate recombination from the triplet excited state is spin-forbidden.

However, it should be noted that this value for initiation efficiency was measured in a liquid resin, and there is a possibility that when we go to a nearly-glassy matrix instead, caging effects mean that newly-generated radical pairs are more susceptible to geminate recombination instead of reaction with writing monomer (i.e. f_2 is lower). Worse, this effect may not lead to a measurable difference in the exposure dose needed to overcome oxygen inhibition, since oxygen quenching possibly can occur even before geminate pairs escape their solvent cage, due to oxygen's low molecular weight and high mobility.

Going forward we assume that f_2 is the same in our matrix as in Decker's resin. If f_2 is in fact lower in our densely crosslinked matrix, then our subsequent calculations will overestimate the number of radicals present, and in turn underestimate polymerization rates by the same factor, with no net effect on the calculated values for any measurables such as Δn.

For verification, the calculated value is used to predict the exposure dose needed to overcome oxygen inhibition (i.e. the induction dose), using the equilibrium oxygen concentrations reported for similar polymers.[124] The calculated induction dose of 70 mJ cm^{-2} (at $\lambda = 405$ nm) is found to

be within 10% of measured values. This is also in reasonably good agreement with induction doses reported elsewhere, e.g. 20 mJ cm^{-2} for mercury lamp illumination with a $\lambda > 380$ nm step filter.[125]

3.2.2 Diffusivity *D*

The small-molecule diffusivity, $D = 1.5\times10^{-3}$ μm^2/sec, is directly observed (Figure 14) through fluorescence recovery after photobleaching (FRAP).[126] The mobile fluorescent dye used, coumarin 6, has similar molecular weight to TBPA monomer (491 and 385, respectively) and should therefore have similar diffusivity.

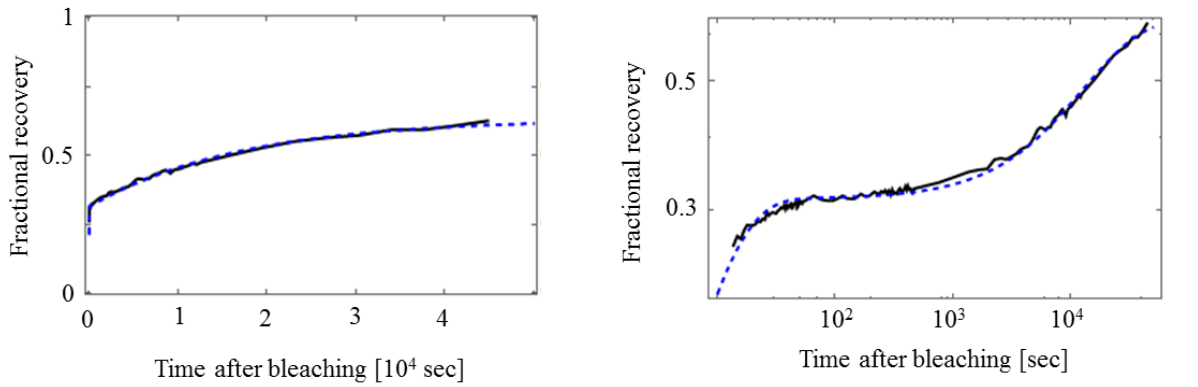

Figure 14. (a) Diffusivity measured by fluorescence recovery after photobleaching (FRAP) using coumarin 6 dye. "Fractional recovery" is defined as the fluorescence signal over the photobleached region of interest, normalized to a nearby non-bleached region to compensate for any additional bleaching induced by repeated measurement scans. At very short times, a faster non-diffusive recovery mechanism is apparent, as is typical in FRAP. Dashed line is a fit to a Fickian diffusion model, yielding $D = 1.5 \times 10^{-3}$ μm^2/sec, with an added exponential term to account for fast non-diffusive recovery. (b) Log-log plot of the same data to emphasize these two distinct recovery processes. Note that recovery does not approach unity even at long times; this is attributed to some fraction of the dye molecules becoming immobilized by attachment to the matrix during the matrix-forming thermoset step.

This value is corroborated by recording a large (>500 μm) feature and using phase-sensitive imaging[127] to monitor the in-diffusion of new TBPA monomer (Figure 15). Fitting this data to a simple Fickian diffusion model yields $D = 1.6 \times 10^{-3}$ μm^2/sec.

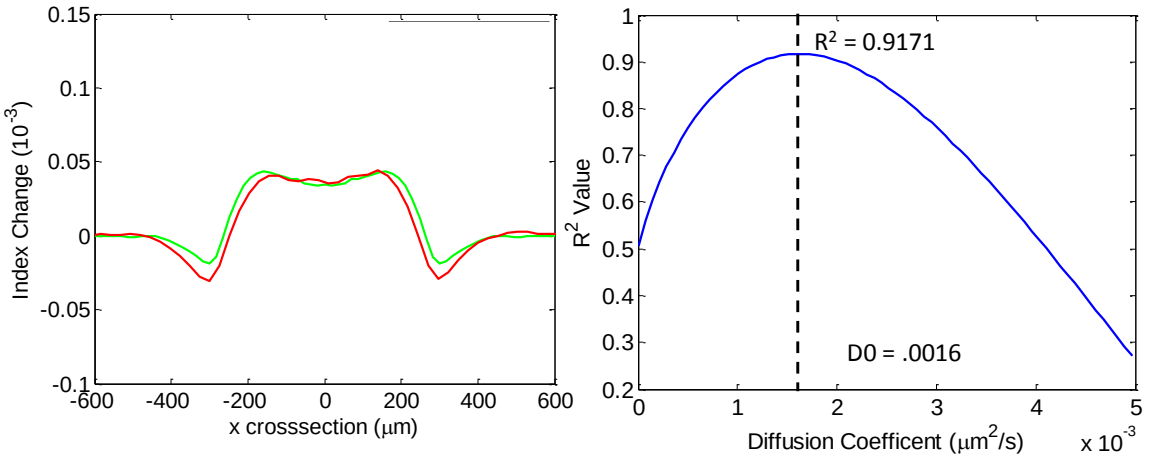

Figure 15. Diffusivity measured by phase imaging of a large developing feature. (a) Measured (red) and simulated (green) refractive index profile show partial in-diffusion of new writing monomer from the unexposed regions. Simulation uses a simple Fickian diffusion model, with diffusivity as an adjustable fit parameter. The initial exposure profile, not shown, is simply a Gaussian. (b) Best-fit value of diffusivity. Image courtesy of Adam Urness.

3.2.3 Polymerization rate coefficient K_p

The polymerization rate coefficient, $K_p = 0.21$ M^{-1} sec^{-1}, is measured by monitoring the diffraction of a Bragg hologram that is slowly polymerizing in the dark after a brief initial exposure. The probe beam is aligned to the external half-angle θ_{Bragg} that satisfies the Bragg condition, as shown in Figure 16. Under this condition, the diffraction efficiency η_{Bragg} is related to the grating index modulation Δn via the standard Kogelnik equation:[128]

$$\eta_{Bragg} = \sin^2\left(\frac{\pi \, \Delta n \, D}{\lambda \cos \theta_{Bragg}}\right)$$

where λ is the vacuum wavelength of the probe beam and *D* is the sample thickness. Using the simple Kogelnik equation rather than rigorous coupled-wave analysis (RCWA) is equivalent to

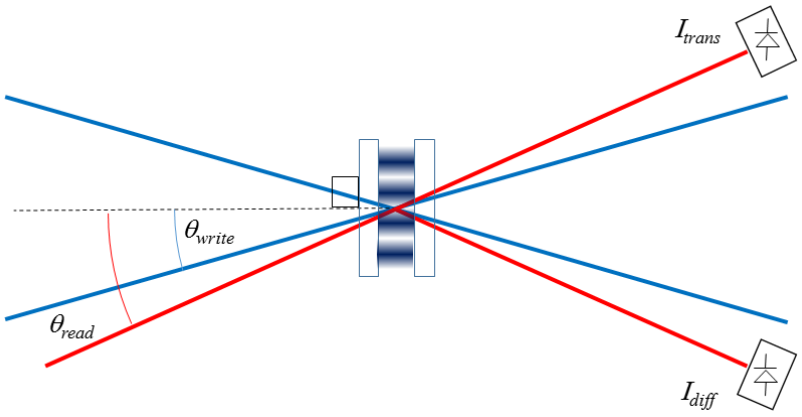

Figure 16. Geometry of Bragg monitoring layout. The writing beam is provided by a wavelength-stabilized 405 nm laser diode (Ondax, 40mW collimated TO-can mounted). After the writing beam is spatially filtered and collimated to a (1/e) diameter of ~4mm, the maximum available intensity is ~100 mW cm^{-2}. The readout beam, from a 633 nm He-Ne laser (JDS Uniphase) is spatially filtered and passed through a ~1mm diameter aperture.

assuming that no higher diffracted orders are present, an assumption that is justified for these thick (~200 μm) and weakly modulated (Δn of, at most, order 10^{-4}) gratings. Diffraction efficiency is defined in terms of the diffracted and zero-order transmitted intensities: $\eta = I_{diff} / (I_{diff} + I_{trans})$; this corrects for power lost to Fresnel back-reflections from the sample faces, and for power drift in the readout laser. Having obtained the index modulation Δn, it is then converted via Equation 2 to a modulation of writing polymer concentration.

To ensure independent measurement of K_p, it is crucial that the time scales of exposure, diffusion, polymerization and apparent termination are all separated. We consider each of these in turn. First, moderately weak gratings require exposure doses of 10 to 100 mJ cm^{-2}. Using the available recording intensity of ~100 mW cm^{-2}, exposure times are as short as 1 sec or less, well below the timescale of grating development, as required.

Next, diffusion time is also short compared to the timescale of grating development. For a typical grating pitch Λ = 0.7 μm, and assuming Fickian diffusion with D as measured above, the characteristic diffusion time from a dark fringe to a bright fringe (a distance of $\Lambda/2$) is only ~10 sec. For comparison, the grating continues to grow at a nearly constant rate for order 100 sec before gradual cessation of growth occurs (Figure 17).

K_p is extracted as follows. This period of nearly steady growth is driven by the growth of matrix-attached oligomer chains (since unattached chains diffuse relatively quickly into a uniform distribution that is invisible to Bragg detection). The rate of growth is then, from Table 2, simply:

$$\frac{d}{dt}[P_{fix}] = K_p[M][R_{fix}]$$

where [M] is simply the initial monomer concentration as calculated from the material formulation, since depletion is negligibly small, and [R_{fix}] is simply the radical concentration

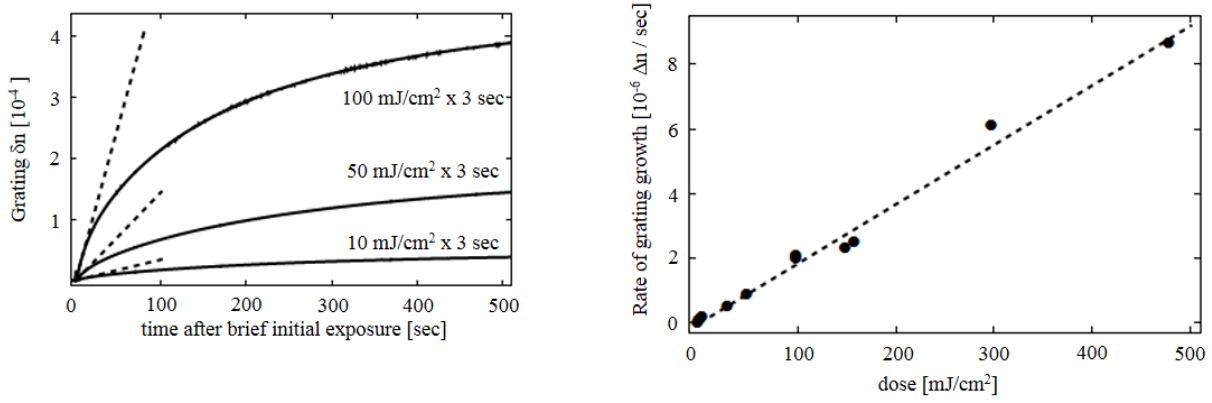

Figure 17. K_p as measured via Bragg monitoring. (a) Grating growth curves and their initial slopes, as extracted from linear fits. Exposure intensities are 10, 50, and 100 mJ cm^{-2}, all exposure times are 3 sec. (b) Rate of grating growth is linearly proportional to dose, over three decades of dose, 0.5 to 500 mJ cm^{-2}. The slope of the dashed line (least-squares fit) yields a rate coefficient K_p = 0.21 M^{-1} sec^{-1}. In all cases grating pitch Λ = 0.7 μm and sample thickness is ~200 μm.

produced by the exposure, as calculated using the value for K_d obtained above. Thus, a value for K_p is fully determined.

This experiment is repeated for a range of exposure intensities and total doses. We expect, based on the proposed reactions structure (Table 2), that the polymerization rate is proportional to dose, and the extracted K_p is constant regardless of dose. Measured values of K_p are indeed found to be nearly constant (with fit quality $R^2 = 0.994$) for exposure doses ranging over three orders of magnitude, ~1 to ~10^3 mJ cm^{-2}, reached by varying exposure intensity from 5 mW cm^{-2} to 100 mW cm^{-2}, and concurrently varying exposure time from 200 msec to 10 sec. Thus, the proposed reaction structure is corroborated.

The extracted K_p in this system is much less than the reaction rate for typical neat acrylate polymerizations, as expected since polymerization in this system is transport-limited rather than reaction-limited. As a further validation of this measurement technique (discussed in more detail below), the experiment is repeated in a different matrix with lower crosslink density, in which diffusion is so fast that polymerization is expected to be reaction-limited rather than transport-limited. The extracted K_p then becomes comparable to reported values for acrylate polymerizations.

Finally, FTIR spectroscopy provides an independent measurement technique that corroborates the unusually low K_p in this media, giving a value of 0.15 M^{-1} sec^{-1} (Figure 18). It should be emphasized that, due to this slow polymerization, the usual steady-state condition does not obtain here. Instead, within the first few minutes of exposure, almost all the photoinitiator has been consumed, so that nearly no additional radicals will be generated. By this point only negligible polymerization has taken place. Then, over the next 30 minutes, this initial population of radicals will slowly consume writing monomer.

This measurement requires a thick sample (here 3 mm) in order to compensate for the low concentration of acrylate groups. Furthermore, the ~3080 cm^{-1} absorption peak associated with the alkene =C-H stretch mode is overwhelmed by spurious absorption from the urethane matrix, so we instead monitor its first overtone.

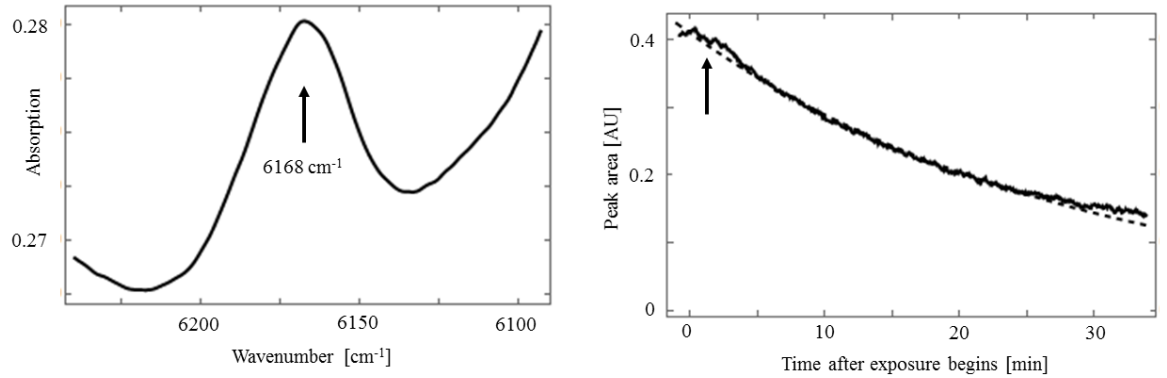

Figure 18. K_p as measured via FT/IR spectroscopy. (a) The monitored absorption peak, corresponding to unreacted acrylate groups. The first overtone of the alkene =C-H stretch peak is chosen in order to avoid spurious absorption by the matrix. Sample thickness is 3mm. (b) Conversion of acrylate bonds under continuous illumination of 8 mW cm^{-2}, starting at t = 0. At the time indicated by the arrow, the photoinitiator is mostly depleted (1/e of the initial concentration of 0.2 wt% TPO). Dashed line shows an exponential decay of the polymerization rate, as expected simply due to the depletion of free writing monomer. From this fit, the initial polymerization rate is calculated to be 1.3e-4 M/sec. Assuming that effectively all of the photoinitiator has been consumed, producing radicals with the report quantum yield of 0.8, the polymerization rate coefficient can be calculated to be 0.15 M^{-1} sec^{-1}, in rather good agreement with the value of 0.21 M^{-1} sec^{-1} calculated from grating growth curves.

A promising area for future work is the use of confocal Raman spectroscopy for spatially and temporally resolved monitoring of both reaction and diffusion. This technique was used above to monitor the concentration of writing monomer molecules, without distinguishing between the monomeric and polymerized states. However, it has been demonstrated[129] that this technique can also distinguish between monomeric and polymerized forms of a methacrylate writing monomer.

3.2.4 Rate coefficient of matrix attachment, K_{abs}

The rate coefficient of hydrogen abstraction from the matrix (the process by which mobile radicals are terminated and new matrix-tethered radicals are created) is found to be K_{abs} = 0.12 sec^{-1} by observing the effect of diffusional blurring of mobile radicals, as follows. First, the half-life of mobile radicals before they are terminated by hydrogen abstraction can be approximated by:

$$\tau_{lifetime} = \frac{1}{K_{abs}}$$

where K_{abs} is a pseudo-unimolecular rate coefficient, since the concentration of abstractible hydrogens is not known precisely, but can safely be assumed to be in large stoichiometric excess compared to mobile radicals. This characteristic lifetime can then be compared to the characteristic time for a mobile radical to diffuse a distance $\Lambda/2$ (from a bright fringe to a dark null). Assuming 1-D Fickian diffusion, the characteristic (1/*e*) time for diffusion from a bright fringe to a dark null is simply:

$$\tau_{diffusion} = \frac{(\Lambda/_2)^2}{2\,D}$$

Then the loss in fringe visibility (1-*V*), due to diffusional blurring of mobile radicals, is proportional simply to the ratio of these two characteristic times

$$(1 - V) = \frac{\tau_{lifetime}}{\tau_{diffusion}}$$

This yields

$$(1 - V) = 8\,D/K_{abs}\frac{1}{\Lambda^2}$$

Or, rearranging of the desired quantity K_{abs}:

$$K_{abs} = 8\,D/(\Lambda^2(1-V))$$

Since the diffusivity *D* was already measured above, knowledge of the fringe visibility *V* at one particular grating pitch Λ is sufficient to determine K_{abs}. So, for example, using the linear fit in Figure 9, we see that the visibility falls to zero at Λ ~ 320 μm, yielding an estimated value for K_{abs} = 0.12 sec^{-1}.

We will return several times to this fundamental concept that recording fidelity is governed by a unitless ratio, analogous to the Zhao and Mouroulis parameter *R*, between two characteristic timescales: the mobile radical lifetime and the time to diffuse across a grating fringe. This remains true whether mobile radical lifetime is limited by hydrogen abstraction reactions, as here, or by reactions with other matrix sites, as will be explored below in other material formulations.

So far, for the sake of a simple phenomenological description, we have not considered the concentration of abstractible hydrogens on the matrix, instead lumping this into the first-order rate coefficient K_{abs} = 0.12 sec^{-1}. However, by estimating this concentration, we can obtain an approximate value for the true second-order rate coefficient. Each arm of a polyol molecule (eq wt ~550) contains, at a very conservative estimate, order 10 abstractible hydrogens, and the concentration of polyol arms is 2.6 M from stoichiometric calculations. This yields a second-order rate coefficient K_a of order 10^{-4} M^{-1} sec^{-1} or lower. This is comparable to reported values of hydrogen abstraction for other systems, as measured by laser flash photolysis: order 10^{-4} M^{-1} sec^{-1} for *tert*-butoxy radicals[130] and order 10^{-5} to 10^{-4} M^{-1} sec^{-1} for benzophenone radicals.[131]

A crucial implication of this small K_{abs} is that hydrogen abstraction is a reaction-limited process, unlike polymerization which is transport-limited. This means that the two processes scale differently as diffusivity is varied, as discussed further below.

3.2.5 Rate coefficient of remobilization of attached radicals via chain transfer, K_{ct}

The rate coefficient of chain transfer from a matrix-attached chain, $K_{ct} = 3.5\times10^{-3}$ sec^{-1}, is found as a single fit parameter to the long-term shape of grating growth curves, because, as discussed above, this chain transfer process is responsible for the eventual cessation of grating growth. This occurs as radicals equilibrate to a uniform distribution, via a process of chain-transfer to a mobile state, diffusion, and then reattachment to the matrix. Deceleration occurs on a timescale of order 10^3 sec, long enough to be well separated from both diffusion and polymerization.

One consequence of this diffusion-mediated grating deceleration mechanism is the continued uniform polymerization of writing monomer even after cessation of grating growth, mentioned previously. Another unusual consequence is that the deceleration of grating growth is slower for larger Λ. As shown next, the model accurately predicts this slowing with the single set of rate constants derived through the independent experiments described above.

The efficiency of a chain transfer process is, in general, expected to fall short of 100% efficiency, since some radicals undergo side reactions rather than initiate new polymer chains. Phenomenologically, this appears as a unimolecular termination mechanism. But the fact that little termination is observed on the timescale of these experiments allows us at least to place a lower bound on this efficiency.

3.3 Validating completed model

3.3.1 Is the observed lack of bimolecular termination consistent with measured rate coefficients?

Having obtained independent measurements of all rate coefficients, we now validate the model as a whole. An obvious first question is whether the linearity of index response with dose (implying negligible bimolecular termination) is consistent with the rest of the physics described in the model.

First we consider the situation immediately after a moderately weak exposure, when initially mobile radicals have been generated (with concentration [rad] on the order of 10^{-3} M) but before they have transferred to the matrix. Bimolecular termination is diffusion-limited, and thus can be assumed to have roughly the same rate constant as diffusion-limited polymerization, 0.21 M^{-1} sec^{-1}. This yields a bimolecular termination rate of $-d[rad]/dt = 10^{-5}$ M sec^{-1}. Thus, a negligible amount of bimolecular termination is expected within the first handful of seconds after exposure.

After this, most radicals are immobilized via transfer to the matrix, at which point bimolecular termination occurs predominantly through reaction-diffusion. In general, reaction-diffusion-mediated termination has a rate coefficient $k_t = R\,k_p$ [m] where $R \sim 3$ M^{-1} is characteristic of acrylate polymerizations.[132] Given our measured $k_p = 0.21$ M^{-1} sec^{-1} and [m] = 0.17 M as calculated from the formulation, this yields $k_t \sim 0.04$ M^{-1} sec^{-1}. Moderately weak exposures generate radical concentrations [rad] of order 10^{-3} M, so radicals should be lost to reaction-diffusion-mediated bimolecular termination at an initial rate $-d[rad]/dt = k_t [rad]^2$ of order 10^{-7} M^{-1} sec^{-1}. Thus, based on previously measured rate coefficients, this termination mechanism is expected to have only a small effect over the experimental timescales of hundreds of seconds.

This is in contrast to neat acrylate polymerizations, in which bimolecular termination is dominant. However, bimolecular termination must be minima in some commercial two-chemistry holographic media, since they are observed to have a linear index response with dose.[20] The one-half-power response with dose that is characteristic of bimolecular termination would be undesirable here, since it would lead to wasted dynamic range due to lack of recording fidelity, and possibly coupling effects between multiple exposures in quick succession. Thus, in short, the termination behavior measured in the model material is internally consistent with the other measured rate coefficients, and is plausible in light of similar two-chemistry media.

3.3.2 Further evidence of long dark polymerization in model material

Similarly, the low termination rates, and correspondingly long-lived radical populations, predicted by the model are not observed in neat acrylate polymerizations. However, it should be emphasized that crosslink densities in this two-chemistry media are significantly higher than those achieved in neat acrylate polymerizations, which typically reach only ~80% conversion. In highly crosslinked media, radical lifetimes of as long as days have been observed.[133] Several experiments provide further evidence that the steady continued growth of holograms in the model material must be due to continued dark polymerization from a long-lived radical population, as opposed to, for instance, unexpectedly slow diffusion of writing monomer from unexposed into exposed regions.

First, a polymerization retarder is added to the model material formulation. If grating growth is driven by slow dark polymerization, as predicted by the model, the addition of retarder should produce earlier, sharper cessation of grating growth. But if instead polymerization is relatively fast and grating growth is limited by slow diffusion of monomer from unexposed to exposed regions, then the addition of retarder should only reduce the strength of the grating, without

affecting the shape of the grating growth curve. As shown in Figure 19, the shape of the growth curve is in fact markedly changed by the addition of retarder, as predicted by the model.

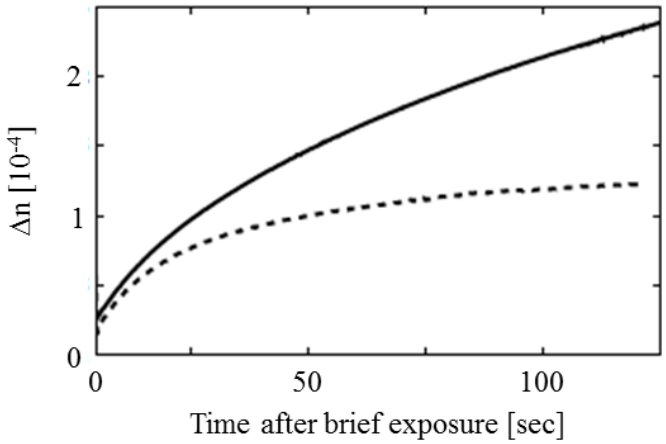

Figure 19. Identical exposures into media with (dashed line) and without (solid line) polymerization retarder (0.8 wt% benzhydrol). The growth curves are different not only in magnitude but also in shape, showing that the rate-limiting step for grating growth is indeed continued dark polymerization rather than diffusion across fringes. (Grating pitch $\Lambda = 0.7$ mm, exposure intensity I = 100 mW cm^{-2} and time t = 5 sec)

Second, Figure 20 compares two gratings with markedly different pitch ($\Lambda = 0.35$ μm and $\Lambda = 5$ μm) but otherwise identical exposure conditions. The diffusion time from a dark null to a bright fringe differs by a factor of more than 10^2 between these two cases. The initial growth rate, however, is rather similar: thus it must be limited by slow dark polymerization rather than by monomer diffusion across fringes.

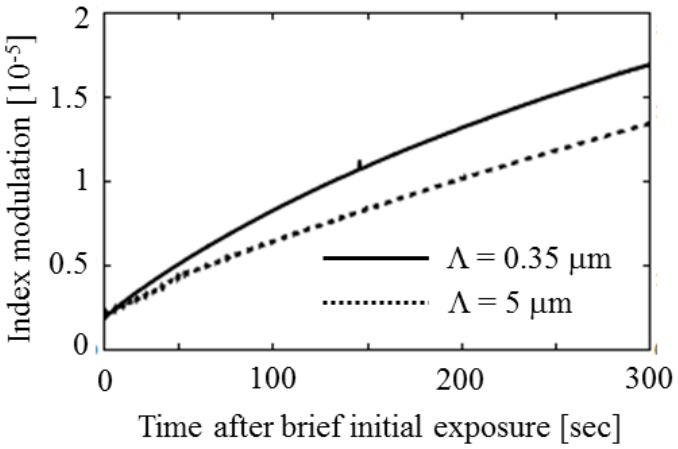

Figure 20. Gratings with two markedly different pitches, but otherwise identical exposure conditions, exhibit nearly identical initial growth rates. This confirms that growth rate must be limited by slow dark polymerization rather than diffusion across fringes. Exposure conditions: I = 60 mW cm^{-2}, exposure time t = 3 sec.

3.3.3 Predictions of index response

Having addressed the physical plausibility of the measured rate coefficients, we next turn to quantitative validation of the model as a whole. The model accurately predicts material response, using only the rate coefficients measured above and no additional adjustable

parameters (Figure 21). These predictions are valid over a wide range of exposure conditions, spanning a range of 10^2 in index and thus 10^4 in diffraction efficiency.

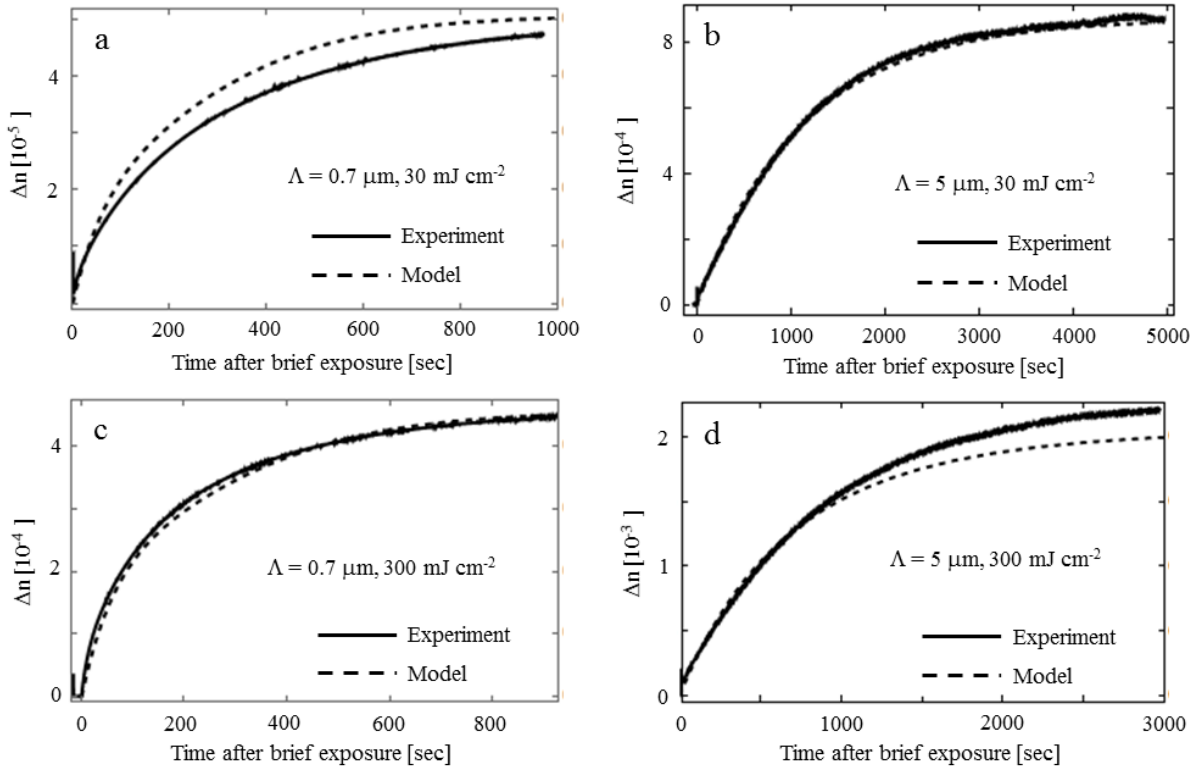

Figure 21. Grating growth curves measured by Bragg diffraction, compared to predictions from the reaction/diffusion model with no additional adjustable fit parameters. Exposure conditions: (a) Λ = 0.7 μm, I = 10 mW cm^{-2}, (b) Λ = 0.7 μm, I = 100 mW cm^{-2}, (c) Λ = 5 μm, I = 10 mW cm^{-2}, (d) Λ = 5 μm, I = 100 mW cm^{-2}. In all cases, exposure time is 3 sec, media layer thickness is 200 μm and precure dose is 200 mJ cm^{-2}.

Furthermore, the model also predicts the pitch-dependent cessation of grating growth (due to the unusual diffusion-mediated mechanism discussed above). As shown in more detail in Figure 22, this pitch-dependence cannot be attributed merely to longer monomer diffusion times, since not only the development time but also the eventual grating strength is pitch-dependent. With the inclusion of the model predictions shown in Figure 5 (c) above, the model's validity is demonstrated over a range of ~10^3 in spatial scale.

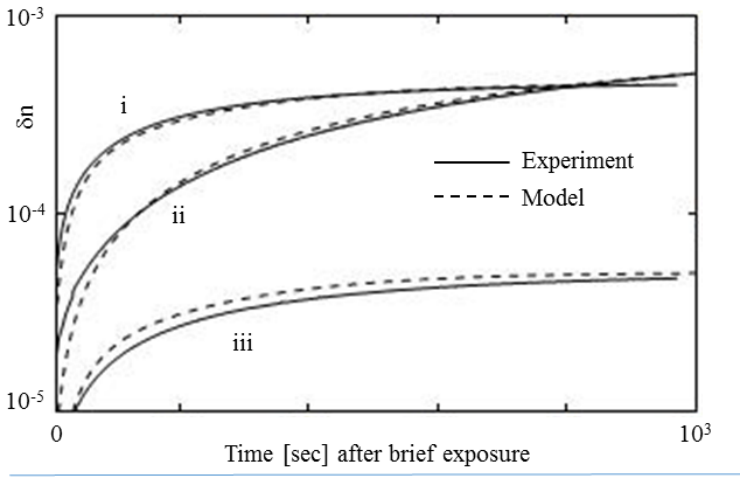

Figure 22. Log plot of grating growth curves measured by Bragg diffraction, compared to predictions from the reaction/diffusion model with no additional adjustable fit parameters. Note that the apparent termination rate varies with Λ, since grating termination is actually governed by diffusional mechanisms that are successfully captured by the model. (i) Λ = 0.7 μm, exposure intensity I = 100 mW cm^{-2}, exposure time t = 3 sec , ii) Λ = 5 μm, I = 100 mW cm^{-2}, t = 1 sec, (iii) Λ = 0.7 μm, I = 10 mW cm^{-2}, t = 3 sec.

Finally, an even more rigorous test of such a model is to predict the loss of recording fidelity that arises when reaction/diffusion coupling becomes strong[78]. This coupling occurs at large grating pitch (Λ = 5 μm) so that the timescales of reaction and diffusion are mixed, and large exposure dose (600 mJ cm^{-2}) so there is significant writing monomer depletion. To quantify fidelity, we monitor diffraction from the weak second harmonic of the grating caused by material nonlinearity[134]. This technique requires an optically thick grating (i.e. one in the Bragg diffraction regime); in the case of a thin grating, unwanted higher diffracted orders from the fundamental grating would be present, overlapping with the signal of interest from the second spatial harmonic. This thick-grating condition is satisfied if the Nath parameter ρ exceeds unity;

[135] here the sample thickness is 200 μm and $\Delta n < 4\times10^{-4}$, so $\rho > 10$ and this requirement is satisfied.

The model successfully predicts the growth curves of both the fundamental and second-harmonic components, as shown in Figure 23. This accurate prediction of nonlinear material response due to coupled dynamics validates the individual rate constants as extracted in uncoupled experiments. Even more importantly, it confirms that the proposed reaction structure (Table 2) fully captures the relevant underlying physics.

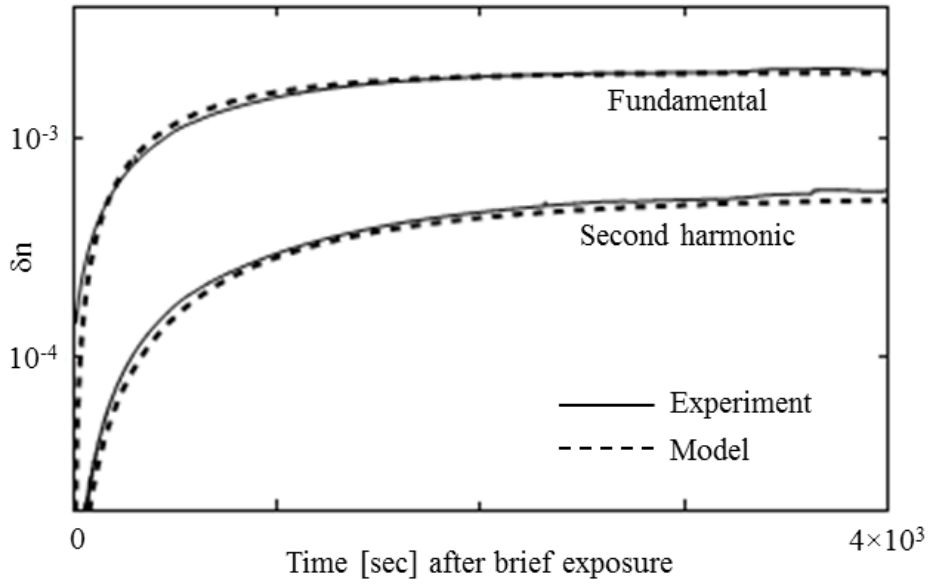

Figure 23. Model successfully predicts growth of both fundamental and second spatial harmonics. To ensure strong reaction/diffusion coupling leading to a pronounced second spatial harmonic, the pitch is large (Λ = 5 μm) and the exposure is strong (I = 60 mW cm^{-2}, t = 10 sec).

CHAPTER 4

RATIONAL DESIGN OF MEDIA

4.1 Introduction

The insights obtained from analyzing this particular model material more broadly enable guided exploration of the design space of two-chemistry media. While the clearly separated timescales of the model material are particularly convenient for a detailed kinetic study, the basic insights into the underlying physics still apply to other materials with coupled timescales.

First, a crucial part of the materials design process is predicting and experimentally surveying the performance of candidate chemistries, and the formula limit concept enables additional information about underlying kinetics to be extracted from these quick surveys. It now becomes possible to readily distinguish between two distinct and possibly competing effects: changes in index contrast (revealed by the formula limit) and recording fidelity (revealed by the usable fraction, and crucial because imperfect fidelity is not just wasteful, but actively exacerbates problems like shrinkage, environmental stability, etc). Furthermore, the $1/\Lambda^2$ scaling of usable fraction is also readily obtained from a quick survey of a few readily accessible grating pitches. This reveals the spatial resolution limit of the material and gives information about the rate of radical attachment to the matrix relative to the rate of radical diffusion across a fringe.

Armed with these concepts, and using the model material as a starting point, we next consider a range of design modifications, starting with the writing monomer, and then turning to the matrix. Finally, informed by the physical insights obtained from the model material, we propose and then characterize a range of new chemical strategies to improve performance.

4.2 Varying the writing monomer

4.2.1 Different loadings of original writing monomer

First the formula concentration of writing monomer is varied, while leaving the matrix unchanged from the original model material. The reaction/diffusion model obtained above predicts that the achievable dynamic range should be linearly proportional to this writing monomer loading. This is confirmed experimentally, over a range of loadings from ~4% to ~8%, as shown in Figure 24.

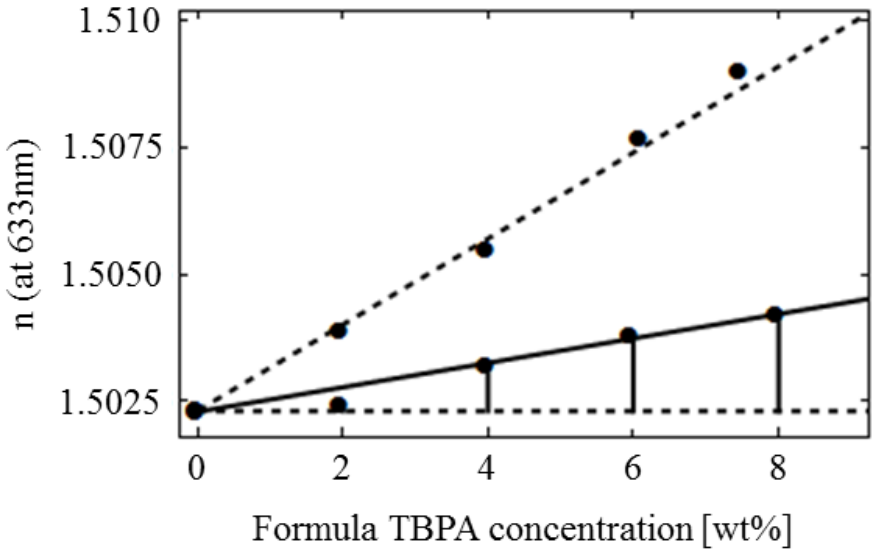

Figure 24. Usable dynamic range scales linearly with formula concentration of writing monomer, as predicted by reaction/diffusion model. Top dashed line: prism coupler measurements, showing formula limit. Solid line: usable dynamic range, as measured from many weak angle-multiplexed holograms at $\Lambda = 0.7$ μm.

When the TBPA loading is decreased to 2%, the dynamic range is somewhat lower than expected. This effect is reproducible and has also been observed in commercial media, but the explanation is not immediately obvious.

When the TBPA loading is increased to 10 wt% or above, the dynamic range again falls below the expected value, and measurements become much less reproducible. This is attributed to the

fact that 10 wt% is approaching the solubility limit, so that phase separation of the writing monomer from the matrix is beginning to be observed. This phase separation is expected to increase the optical scatter of the media and degrade optical performance.

4.2.2 Difunctional writing monomer

Next, a new writing monomer is substituted for the original monofunctional writing monomer. In order to explore the design space as fully as possible with a limited number of candidates, a difunctional monomer is chosen: bisphenol-A ethoxylate diacrylate (eq. wt. 344).

This new material formulation is characterized using the same divide-and-conquer strategy. First, the analytical relation between index and monomer concentration is established using the prism coupler procedure described above. From this the formula limit is readily calculated. In order to make a relevant comparison to the original formulation with tribromophenyl acrylate, we calculate the formula limit at an equivalent molar concentration of acrylate functional groups (since it is this concentration that governs design tradeoffs such as recording-induced volume shrinkage). This yields a formula limit of 2.7×10^{-3} for bisphenol-A diacrylate, moderately smaller than the formula limit of 5.1×10^{-3} for tribromophenyl acrylate, as expected due to the former's lack of heavy atoms.

As before, the usable dynamic range is then compared to this formula limit (Figure 25 a). The ratio of usable dynamic range to formula limit is roughly the same as in the original TBPA formulation; in other words, these two writing monomers can be patterned with comparable fidelity, even though they offer different matrix/monomer index contrast. The ability to distinguish these two effects illustrates the usefulness of the formula limit concept, and offers important guidance for materials design.

Next, rate coefficients can be measured independently as before. Constructing a complete predictive model for this second material formulation is outside the scope of this work, but we will go into enough detail to show the generality of this approach and derive some interesting results.

In particular, K_p can be independently measured just as before. Grating growth curves are measured for various exposure doses, and the initial rates of polymerization are extracted. These are again found to be proportional to exposure dose (Figure 25 b). From these, a value for K_p is calculated, just as before except that the concentration of reactive acrylate groups is now twice the concentration of (difunctional) monomer molecules.

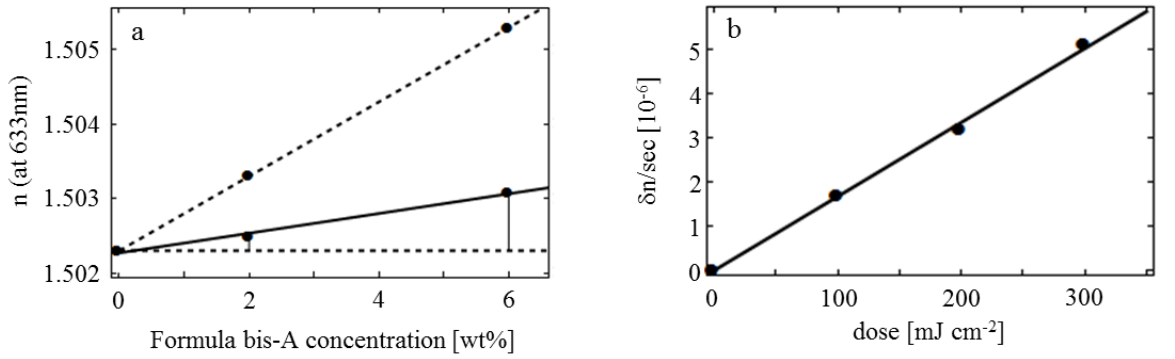

Figure 25. Characterization of a new difunctional writing monomer, bisphenol-A ethoxylate diacrylate (Mn ~ 688), used as received from Sigma-Aldrich. (a) Top dashed line: formula limit as shown by prism coupler measurements. Solid line: usable dynamic range, from measurements of weak angle-multiplexed holograms at $\Lambda = 0.7$ μm. (b) Initial polymerization rate as a function of exposure dose, as extracted from Bragg growth curves. Slope of solid line (least-squares fit) yields a polymerization rate coefficient of $K_p = 0.21$ M^{-1} sec^{-1}, almost identical to that measured for the previous monofunctional acrylate writing monomer.

Strikingly, even though the measured index changes and absolute polymerization rates are different, the extracted K_p value, 0.21 M^{-1} sec^{-1}, is in quite good agreement with that obtained from TBPA. This provides further proof that acrylate polymerizations in this matrix are transport-limited. Also, it further confirms that the rate-limiting process in grating growth is

polymerization. If diffusional transport across grating fringes were the rate-limiting process, then switching to a writing monomer with moderately different polarizability and diffusivity would be expected to yield a different apparent K_p.

4.3 Changing matrix T_G

4.3.1 Matrix Tg is a critical design parameter

Having briefly explored the possibilities of changing writing monomer, we next turn to the host matrix itself. It is well understood that the crosslink density, and therefore the glass transition temperature T_G, represents a crucial design parameter that must be tuned to optimize over a large set of design tradeoffs. A high T_G yields desirable bulk mechanical properties. These include high stiffness (especially important when the media cannot conveniently be encased within a hard package, but must be exposed to the environment) and low coefficient of thermal expansion (especially critical for holographic applications, which generally demand that Bragg matching be maintained over a range of operating temperatures). But at the same time, a high T_G leads to an unwanted reduction in the sensitivity[97] (i.e. the index change produced from a given exposure dose). This is attributed to the higher T_G matrix slowing diffusion and therefore hindering transport-limited polymerization reactions.

An additional design consideration is the effect on formula limit. Changing the matrix composition will of course change the matrix bulk refractive index. For the model chemistry above, a lower T_G can most readily be achieved by using longer polyol chains, leading to a lower bulk refractive index. This is desirable since it modestly enhances the contrast to the high-index writing monomer, which, as we have seen, increases the formula limit.

Finally, the crosslink density has been empirically shown to affect the optical clarity and scatter. Here we consider only the inherent scatter of unexposed media; the recording process introduces its own additional scatter which is highly dependent on exposure conditions and will be treated in detail below. The inherent scatter of unexposed media is dominated by unwanted phase separation of the imperfectly-soluble writing monomer. Increasing the crosslink density reduces the maximum possible size of these microdomains of aggregated writing monomer, and thus reduces scatter.[136]

4.3.2 New matrix formulations

It is well understood that the media glass transition temperature is a crucial design parameter that can readily be tuned by substituting polyols of different molecular weights into the urethane matrix formulation, while keeping the same nearly stoichiometric ratio between polyol and isocyanate groups. Here we explore two such new formulations (Table 3 and Table 4) in order to sample a range of glass transition temperatures that span typical values for commercial formulations (Figure 26).

As expected, a lower T_G corresponds to a lower refractive index of the matrix, and thus an increased formula limit. However, the usable fraction decreases dramatically (Figure 27 and Figure 28), for reasons that will be explored in the following section.

Component	Name	Source	wt%
Urethane matrix			
1. Polyol	Glycerol propoxylate mn ~1500	Bayer	68.81
2. Isocyanate	Desmodur 3900 (eq wt 179)	Bayer	21.89
3. Plasticizer	Dibutyl phthalate	Aldrich	3.0
4. Catalyst	Dibutyltin dilaurate	Aldrich	0.1
Writing chemistry			
5. Photoinitiator	TPO: (2,4,6-trimethylbenzoyl)diphenylphosphine oxide	Aldrich	0.20
6. Writing monomer	TBPA: (2,4,6) tribromophenyl acrylate	Huyang Puicheng	6.00

Table 3: New formulation with moderately lower T_G (-20ºC), As before, components are used as received, except TBPA which is purified by dissolving in methylene dichloride and filtering with a Millipore 0.5 micron pore membrane filter. Components 3-6 are mixed into the polyol at 60ºC, degassed, then mixed with isocyanate and cast between glass slides

Component	Name	Source	wt%
Urethane matrix			
1. Polyol	Multranol (functionality 3, mn ~4800)	Bayer	85.1
2. Isocyanate	Desmodur 3900 (eq wt 179)	Bayer	8.46
3. Plasticizer	Dibutyl phthalate	Aldrich	0.50
4. Catalyst	Dibutyltin dilaurate	Aldrich	0.01
Writing chemistry			
5. Photoinitiator	TPO: (2,4,6-trimethylbenzoyl)diphenylphosphine oxide	Aldrich	0.04
6. Writing monomer	TBPA: (2,4,6) tribromophenyl acrylate	Huyang Puicheng	6.00

Table 4: Formulation with low T_G (-60ºC); prepared as in Table 3.

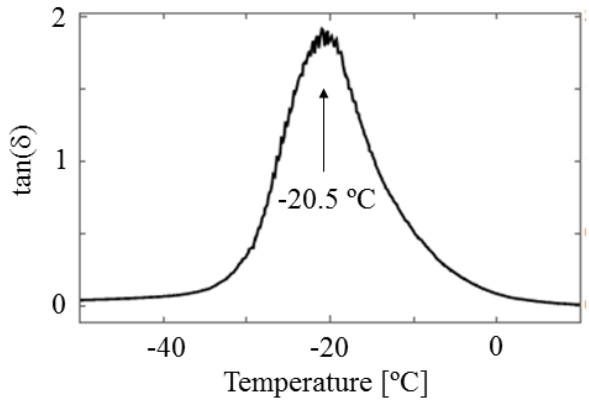

Figure 26. Dynamic mechanical analysis of new model material with T_G -20C. (1 Hz, flood-cured)

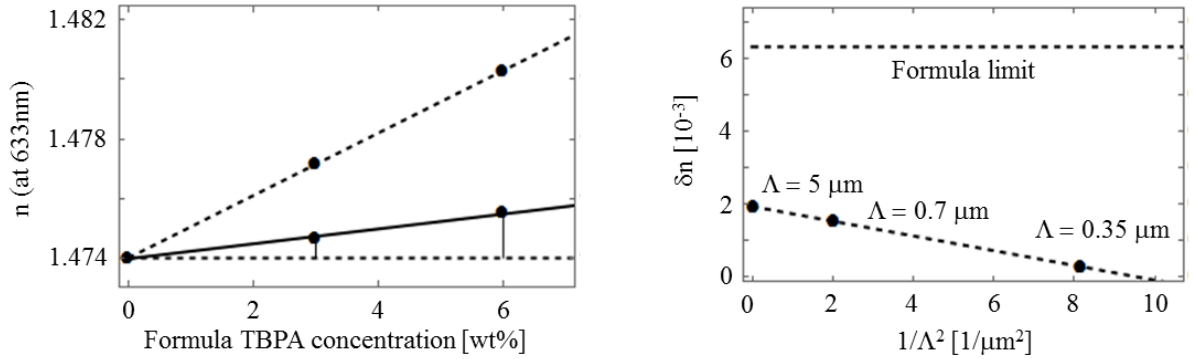

Figure 28. Modified matrix with T_G -20C. (a) Formula limit (upper dashed line, via prism coupler) and usable dynamic range (solid line, via weak multiplexed grating technique) as a function of writing monomer loading. Note that the formula limit is greater, but the usable fraction is smaller, than in the original T_G ~ 20C material. (b) Usable dynamic range as a function of grating pitch, showing media resolution limit of Λ ~ 0.32 μm.

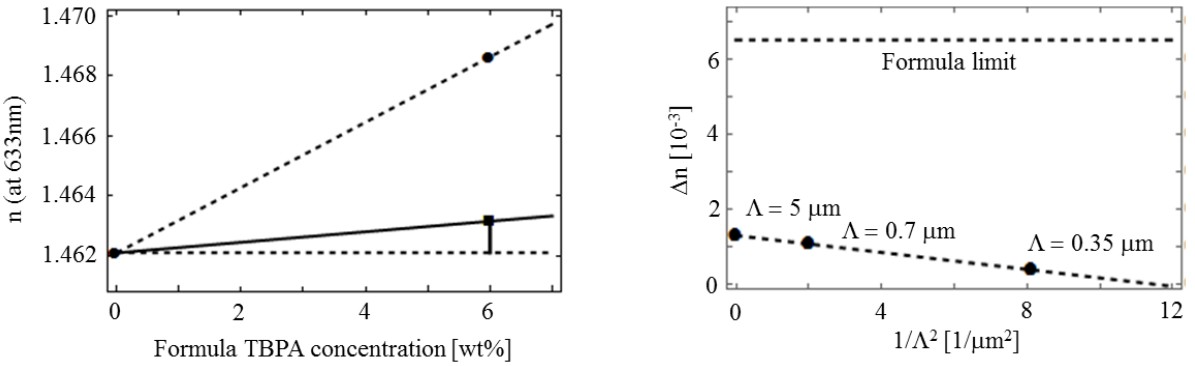

Figure 27. Modified matrix with ~60ºC T_G. (a) Formula limit (upper dashed line, via prism coupler) and usable dynamic range (solid line, via weak multiplexed grating technique) as a function of writing monomer loading. Note that the formula limit is greater, but the usable fraction is smaller, than in the original ~20ºC T_G material. (b) Usable dynamic range as a function of grating pitch, showing media resolution limit of Λ ~ 0.29 μm.

4.3.3 How kinetics change with T and T_G

Until this point, the various rate coefficients for a particular model material have been treated as independent, phenomenological quantities. But from a materials design perspective, these rate coefficients cannot be adjusted independently. Rather, they are jointly determined by more physically fundamental quantities, such as matrix T_G and sample temperature during the recording process T. Understanding how rate coefficients scale with these more fundamental quantities provides crucial design guidance in optimizing T_G and T to meet the demands of a particular application. For example, a high T_G, corresponding to a rugged optical article at room temperature, can be combined with a high recording temperature T for fast index development.

To understand how rate coefficients depend on temperature, we first recall that reactions in general can be either reaction-limited or diffusion-limited; in the transport-limited case, the reaction rate coefficient should be straightforwardly determined by the diffusivity according to the Smoluchowski relation:[137]

$$K_{Smol} = 4\pi\,(D_A + D_B)\,r$$

where D_A and D_B are the diffusivities of the two reacting species and r is the radius of interaction.

However, measured polymerization rates surprisingly do not obey this Smoluchowski relationship to measured translational diffusion rates. Rather, as the temperature decreases toward T_G, and as translational diffusivity D slows with the expected Arrhenius scaling, polymerization instead slows much more abruptly. This suggests that some other, possibly steric, effect must be further hindering polymerization. By the point T approaches T_G, as in the case of the model material at room temperature, this divergence has become so pronounced that

the measured K_p is fully five orders of magnitude smaller than the transport-limited K_p as calculated from the Smoluchowski relation. It should be emphasized that these are the conditions under which both K_p and D have been most thoroughly characterized, with multiple independent measurement techniques confirming their values. These results are summarized in Figure 29 for the case of the original 20ºC T_G model material, heated to temperatures ranging up to 60ºC.

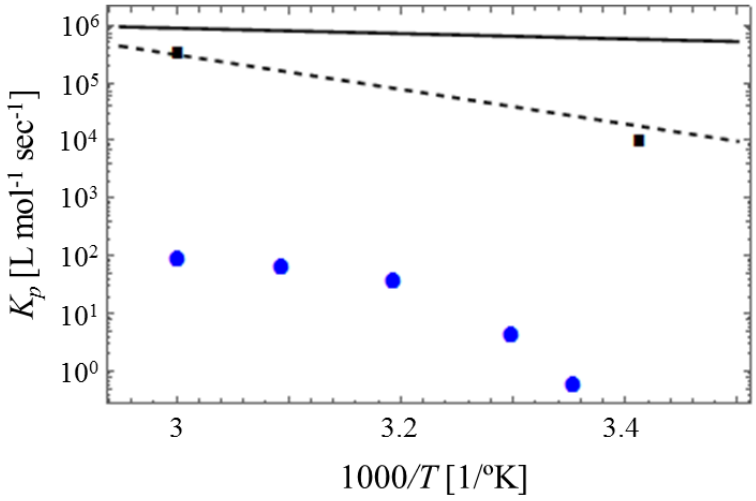

Figure 29. As temperature is reduced toward T_G, measured polymerization rates diverge from Smoluchowski predictions, suggesting that polymerization is further hindered by some other effect. All data is in original ~20ºC T_G material, in a chamber with closed-loop heat control. Lower data points (●) are directly measured K_p. Dashed line is the Smoluchowski prediction for transport-limited K_p, based on directly measured diffusivities (■). For reference, the top (solid) line is reaction-limited K_p as reported elsewhere.

It should be emphasized that there is not merely a discrepancy in all cases between measured K_P and measured diffusivity. Rather, there is good agreement when T is well above T_G. Indeed, for the case T = 25 ºC and T_G = -60 ºC, polymerization should be reaction-limited rather than transport-limited according to the Smoluchowski relation, and indeed the measured $K_p = 2 \times 10^5$ M^{-1} sec^{-1} matches the expected rate coefficient for reaction-limited acrylate polymerizations, with other reported values[138] ranging from 2 to 6×10^5 M^{-1} sec^{-1}.

It is only when temperatures decrease toward T_G that a decoupling is observed between measured rates of diffusion and measured rates of transport-limited polymerization – in other words, the two processes exhibit different temperature dependencies. This is more clearly seen in Figure 30, which combines results for matrices with differing T_G into a master curve using the normalized Arrhenius variable T_G/T.

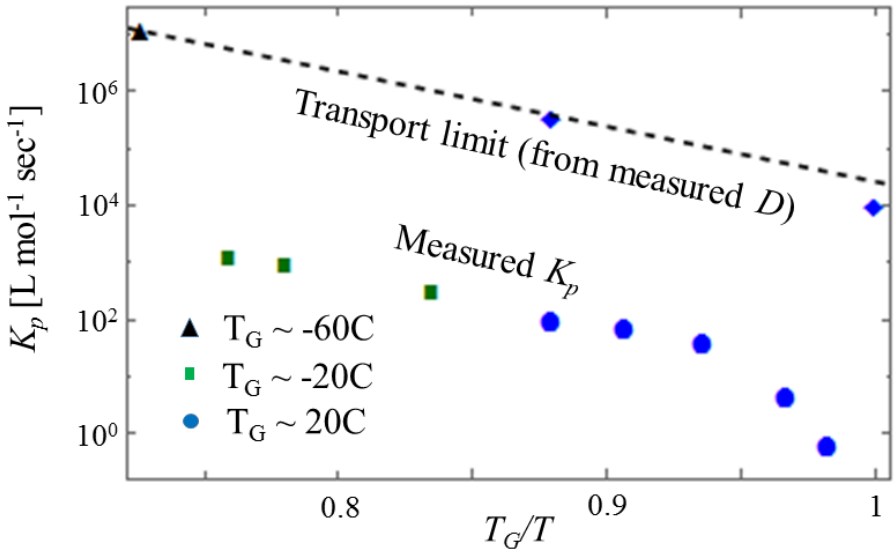

Figure 30. Master curve incorporating data from formulations with -20ºC T_G and -60ºC T_G. In order to show all data on the same plot, x-axis is normalized units of T_G/T. As in Fig. 29, lower data points (●) are directly measured K_p and dashed line is the Smoluchowski prediction for transport-limited K_p, based on directly measured diffusivities.

We will speculate below on the underlying physics of this discrepancy, but even this phenomenological observation yields important insights. First of all, we can recognize that this discrepancy, with polymerization abnormally slow relative to diffusion, is what made it possible, in the study of the model material above, to separate the timescales of polymerization and diffusion. Second, Figure 30 reveals that, at temperatures near T_G, small changes in sample temperature lead to drastic changes in polymerization rate, thereby suggesting a facile mechanism for "gating" index development in order to, for example, achieve quasi-latent recording.

4.3.4 Segmental vs chain relaxation

Finally, we consider the underlying cause of this discrepancy. It is suggestive to introduce here the fundamental polymer physics concept of segmental versus chain relaxation modes. Macroscopic mechanical properties of the matrix are determined by relaxations of long polymer chains, involving the coordinated motion of many chain units. Diffusion of small probe molecules (including writing monomer) within the matrix depends on smaller segmental relaxations or α-relaxations, involving the coordinated motion of only tens of chain units.[139]

The classical assumption (in e.g. Rouse or reptation models) is that all of these relaxation modes, regardless of the number of chain units involved, can be described by the same effective friction coefficient. This assumption is the foundation of the time-temperature superposition principle. [140] On this assumption, the macroviscosity and microviscosity should be the same even for temperatures approaching T_G, as is indeed observed in some bulk polymers.[141]

However, it has long been understood that, in many other bulk polymers, as the temperature approaches T_G, the micro- and macro-viscosity diverge by as much as orders of magnitude (e.g. Plazek 1965 in polystyrene,[142] Nishijima 1970 in polyethylene[143]). This divergence is observed even when the micro-viscosity is probed on the micron scale rather than the molecular scale. For further review of this body of experimental work, see [144] and [145]. The critical temperature below which this divergence occurs, $T_C \sim 1.3\ T_G$, is associated with the onset of intermolecular cooperative motion as predicted by mode coupling theory.[146]

4.3.5 Chain vs segmental effects in our model materials

We look for this divergence in the model material as follows. Segmental relaxations are probed by monitoring the diffusion of small probe molecules. The small-molecule diffusivity D was

measured above using fluorescence recovery imaging or gravimetry; that diffusivity is then converted to an effective microviscosity via the Stokes-Einstein relation:

$$D = \frac{k_B\, T}{4\, \pi\, \eta\, r}$$

where η is the microviscosity, r is the radius of interaction, and the factor of 4 rather than 6 is the Sutherland correction for a solute comprising large molecules.[147] The radius of interaction r is estimated to be ~0.4 nm based on the molar volume of TBPA, which in turn is estimated to be 0.18 M^{-1} from the component van der Waals radii.[148]

Larger chain relaxations (corresponding to the terminal relaxation time, or equivalently the macroviscosity) are probed by using dynamic mechanical analysis (DMA) to measure the loss modulus E''. Then the macroviscosity η is straightforwardly given as $\eta = E'' / \omega$, where ω is the angular frequency of measurement.

Thus, both segmental and chain relaxation can be characterized as a function of temperature, for each of our matrices of varying T_G. This raises the question of whether results in different matrices can be compiled into some single master curve. Somewhat surprisingly, it was shown by Ding and Sokolov[149] that such a master curve can be constructed, at least for the chain relaxation, by using the normalized Arrhenius variable T_G / T. This master curve was shown to be valid for six widely different polymers. Segmental relaxation behavior was found to be much less universal. Ding and Sokolov's result was later verified for an even broader set of polymers, and extended to include both the Arrhenius regime ($T > 1.3\ T_G$) and WLF regime ($1.3T_G > T > T_G$), in [150].

This normalization approach is followed in Figure 31, comparing macro- and micro-viscosity for the -20ºC T_G and 20ºC T_G model materials. First we note a breakdown of time-temperature superposition similar to that described above, with a discrepancy of fully five orders of magnitude between macroviscosity and microviscosity. Furthermore, there are suggestive relationships between the macroviscosity and the measured polymerization rate. Both have the same temperature dependence (and indeed, even the absolute values of the measured K_p are in surprisingly good agreement with predictions made simply by applying the Stokes-Einstein relation to the measured macroviscosity).

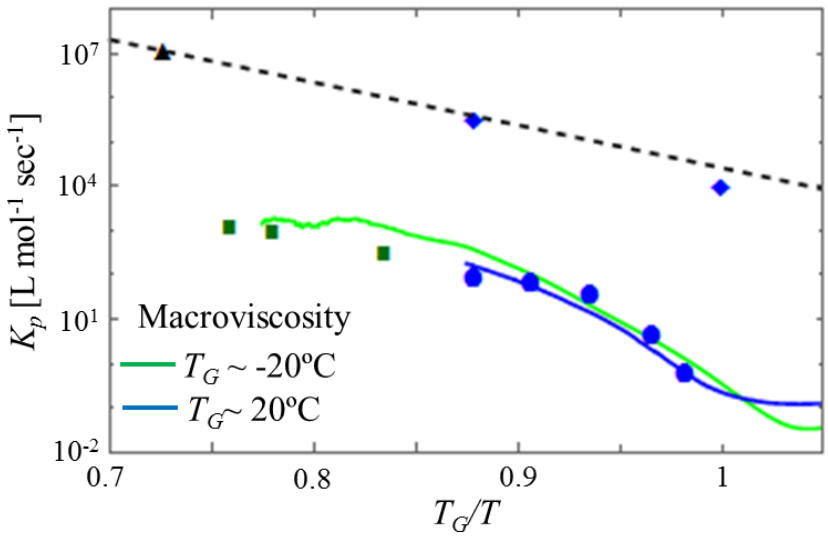

Figure 31. Macroviscosity exhibits the same temperature scaling as directly measured K_p. In order to plot all data with the same units, macroviscosities as measured by DMA are converted to diffusivities via the Einstein-Stokes equation, and then to predicted K_p via the Smoluchowski relation.

Finally, we consider the nanometer-scale behavior that gives rise to this evident breakdown of time-temperature superposition. It is understood from general thermodynamic arguments[151,152] that, as the material is cooled toward T_G, the onset of cooperative matrix motions leads to dynamic heterogeneity of the material (or, equivalently, motional or relaxational heterogeneity),

with a spatial scale on the order of a few nanometers. This is confirmed by single-molecule probe techniques.[153]

This dynamic effect is to be distinguished from static, compositional heterogeneity. While our materials might plausibly develop compositional heterogeneity during the thermosetting process, in the form of poorly crosslinked regions or "pools", such an effect would be expected to be visible in DMA measurements, in the form of a broadened glass transition or a splitting into multiple glass transitions.[154] But neither of these symptoms is observed, so instead the breakdown of time-temperature superposition must indeed be attributed to dynamic heterogeneity.

Finally, the question remains why the rate of photopolymerization should be so closely correlated to the rate of chain relaxation. We speculate that any given temporary matrix configuration will occlude some matrix-tethered radicals. These occluded radicals will be unable to participate in polymerization until matrix reconfiguration occurs. This reconfiguration, on the timescale of chain (rather than segmental) relaxation, will thus be the rate-limiting process for polymerization.

4.4 Other design strategies

4.4.1 Overview

So far, the formula limit concept has allowed us to quantify how much dynamic range is being wasted due to various mechanisms (diffusional blurring of blurring, dead unattached oligomers, etc). Next we will show how this new understanding of the underlying reaction/diffusion kinetics can suggest a range of strategies to improve the usable dynamic range. A range of these

strategies are implemented in new material formulations, and their performance is quantitatively evaluated using the same divide-and-conquer approach as before.

4.4.2 Immobilizing writing oligomer via topological entanglement

One obvious strategy to increase the rate of immobilization of radicals is to use multifunctional writing monomers. Branched oligomers are expected to be much more effectively entangled in the matrix, compared to linear oligomers of similar molecular weight.[113] This effect has already been exploited in Bayer media[21] to improve the spatial resolution by tuning the ratio of monofuctional to multifunctional writing monomer.

In order to study this effect independent of other paths for immobilization (in particular, radical transfer to the matrix via hydrogen abstraction, as in the model material) we move to a wholly different matrix in which these effects are absent. This new matrix is a commercial crosslinked matrix designed for intraocular lenses (Rayacryl®, lens blanks provided by Rayner and used as received). This matrix comprises 2-hydroxy ethyl methacrylate (HEMA), methyl methacrylate (PMMA), and ethylene glycol dimethacrylate (EGDMA). None of these components are expected to contain readily abstractible hydrogens. In particular, they lack the ether groups which were present in the model material, and which were particularly favorable for hydrogen abstraction because the lone pair electrons of an oxygen atom could exert a stabilizing effect on an adjacent carbon-centered radical. Thus, in this new matrix the effect of multifunctional writing monomers can be explored in isolation from the effect of hydrogen abstraction.

Additionally, these experiments provide an important proof-of-concept showing that our photopatterning can be implemented in commercially existing lens materials after the lenses have

already been formed; this is an important milestone toward realizing arbitrary custom photopatterned aberration corrections.

In order to introduce the writing chemistry into a sample of already-formed matrix, the sample is submerged in a solvent bath, into which a low concentration of photoinitiator and writing monomer, as described below, have been dissolved. The solvent gradually infiltrates the matrix, causing the matrix to swell. (If the solvent is too aggressive, mechanical stresses between the swelled and non-swelled sections of the matrix can cause cracks and tears. A moderately aggressive solvent composed of equal parts by weight of toluene and methanol is used here.) Once the sample is saturated, it is removed from the solvent bath, laminated against a microscope slide to ensure optical flatness, and dried under vacuum. The solvent evaporates, leaving behind the writing chemistry, now dissolved within the matrix.

Three different writing chemistry formulations are explored (Figure 32). In the first, the writing monomer is monofunctional (N-vinyl-2-pyrollidone, NVP, chosen to have a high refractive index). Upon recording, a grating forms, but promptly decays as the linear writing oligomer chains diffuse (Figure 32). In the second case, the writing monomer is multifunctional so that it can act as a crosslinker (glycerol propoxylate triacrylate, GPTA). In this case, the recorded grating is permanent, since the writing oligomer is crosslinked and thus entangled with the matrix and cannot diffuse. (Similar results were demonstrated as early as 1978 in porous glasses.[155])

However the grating is rather weak due to the low index contrast of GTPA to the matrix. Finally, in the last case, a blend of these two writing monomers is used. Since both have acrylate functionality, they copolymerize, and the resulting writing oligomer chains contain sufficiently many crosslinks to be immobilized, but also sufficiently many high-index groups to yield a greater overall dynamic range.

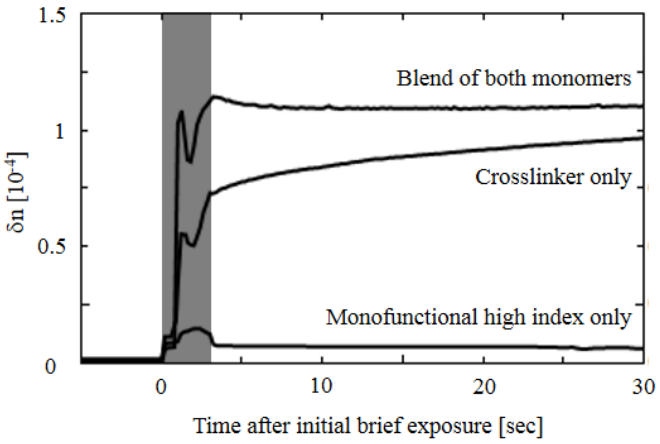

Figure 32. Introduction of crosslinking writing monomer, to create topological entanglements, enables recording of permanent structures even in a matrix without hydrogen abstraction sites. Matrix is Rayacryl (proprietary PMMA/HEMA blend).

The formula limit is not calculated for these systems, since the samples are too rigid to be laminated against the face of the prism coupler, making measurements of absolute index impractical. But even without knowing the formula limit, the spatial resolution limit is readily calculated. As before, the usable dynamic range is measured using the standard technique of many weak angle-multiplexed gratings. When this measurement is repeated at a handful of readily accessible grating pitches Λ, the expected $1/\Lambda^2$ scaling is observed (Figure 33), and an extrapolation of this scaling yields a resolution limit of ~300 nm.

Even though performance has not been optimized for this system, it demonstrates that writing chemistry can be infiltrated into already-formed commercial lens materials, and can be used to record arbitrary 3D index patterns that have good environmental stability. Submicron spatial resolution is readily achieved, and while this is not necessary for conventional lenses, it enables diffractive elements such as Fresnel zoneplates, which can achieve relatively high optical powers with a small overall dynamic range.

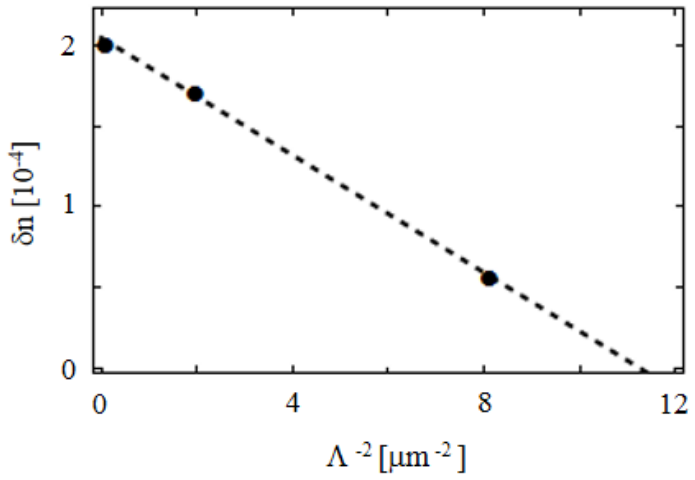

Figure 33. $1/\Lambda^2$ scaling of usable dynamic range in the Rayacryl matrix, showing diffusional blurring of active radicals. Extrapolating this scaling to small spatial frequencies yields a resolution limit of $\Lambda \sim 300$ nm. Blend of writing monomers is the same as shown in Fig. 32.

Having demonstrated the usefulness of adding a small amount of crosslinking writing monomer, in a system that is devoid of radical transfer to matrix, we now turn back to the original model material and apply the same approach. Again, we use a blend of two writing monomers that copolymerize, one of which is high-index and one of which is multifunctional – in this case, these are the two writing monomers already explored, TBPA and bisphenol-A diacrylate. As shown in Figure 34, this blend has much better sensitivity, per molar fraction of reactive groups, than either writing monomer alone. This improvement is attributed to the following mechanism: before, the short dead chains of writing polymer were wasted because they quickly escaped into

a uniform distribution via reptative diffusion. But now, with the addition of a crosslinker, those short chains of writing polymer are no longer linear, but star-shaped, drastically hindering reptative diffusion, or perhaps even forming rotaxanes, as proposed in [156].

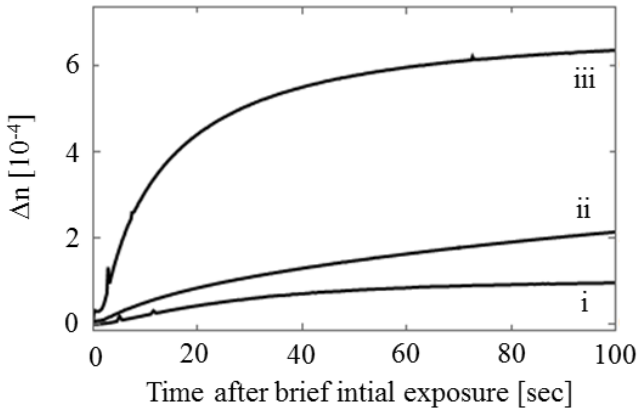

Figure 34. A blend of difunctional and high-index monofunctional writing monomers yields better performance than either writing monomer alone. In all three cases, exposure intensity is 100 mW cm^{-2} and dose is 300 mJ cm^{-2}. (i) bisphenol-A diacrylate only, 6 wt%. (ii) tribromophenyl acrylate only, 6 wt%. (iii) blend with 2 wt% bisphenol-A diacrylate and 4 wt% tribromophenyl acrylate. Since these two monomers have similar equivalent weights, the total molar concentration of monomer reactive groups is roughly equivalent in all three cases.

Furthermore, any entanglement or diffusive slowing of live (radical-tipped) chains will tend to improve the spatial resolution. Recall that the spatial resolution is limited by diffusional blurring of these live chains, an effect which is proportional to the ratio of two characteristic times: the lifetime of the live chain before undergoing hydrogen abstraction, and the time for a live chain to diffuse from a bright fringe to a dark null, as follows (from section 3.2.4 above):

$$(1 - V) = \frac{\tau_{lifetime}}{\tau_{diffusion}}$$

where V is the fringe visibility. If the diffusion of live chains is hindered by their branched topology, but the rate of hydrogen abstraction is roughly unchanged, this pushes the lifetime ratio in the favorable direction of increased fringe visibility and improved spatial resolution.

However, this higher degree of crosslinking carries a penalty: polymerization of writing monomer now has a non-negligible effect on the mechanical properties of the media. One consequence is that not only is a resolution limit on high spatial frequencies observed, but also a low spatial frequency cut-off (Figure 35). At these low spatial frequencies, the vitrification of the developing regions can interrupt the slow in-diffusion of new writing monomer from unexposed regions. This same effect is observed in other systems with crosslinking writing monomer[21] and is to be distinguished from the Zhao and Mouroulis "rabbit-ears" effect, which can be ruled out in the case of weak multiplexed gratings.

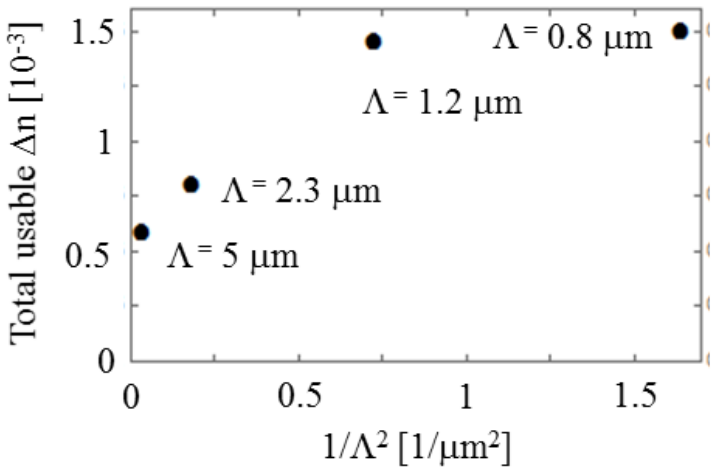

Figure 35. A low spatial frequency cutoff is observed once a significant fraction of crosslinking writing monomer is introduced into the model formulation (2 wt% bisphenol-A diacrylate and 4 wt% tribromophenyl acrylate), due to non-negligible vitrification when writing monomer is polymerized.

Here we have evaluated only a single value of the ratio of monofunctional to difunctional writing monomer: that is, only a single point in what is clearly a large design space, weighted by constraints that are specific to particular applications. The formula limit concept enables quantitative understanding and evaluation of these design choices.

4.4.3 Enhancing matrix attachment by adding reactive sites to matrix

Increasing the rate at which mobile radicals transfer to the matrix via hydrogen abstraction would desirable for two reasons. First, as we saw above, the spatial resolution of the media is fundamentally limited by the diffusional blurring of radicals, an effect which is governed by the ratio of two characteristic times:

$$(1 - V) = \frac{\tau_{lifetime}}{\tau_{diffusion}}$$

where V is the fringe visibility, $\tau_{lifetime}$ is the average lifetime of a mobile radical before being terminated by (in this case) hydrogen abstraction, and $\tau_{diffusion}$ is the characteristic time for a mobile radical to diffuse from a bright fringe to a dark null. The lifetime of mobile radicals was expressed above in terms of the effective (pseudo-unimolecular) rate coefficient for hydrogen abstraction:

$$\tau_{lifetime} = \frac{1}{K_{abs}}$$

but increasing the concentration and/or reactivity of hydrogen abstraction sites on the matrix will increase this effective K_{abs}, and therefore decrease the lifetime ratio, which in turn corresponds to decreased diffusional blurring and improved spatial resolution.

Second, a large part of the wasted dynamic range is due to polymerization that takes place before hydrogen abstraction occurs. Upon hydrogen abstraction, the mobile chain that has been built up so far is terminated and diffuses to equilibrium. Therefore both resolution and usable dynamic range should be improved by increasing the rate of hydrogen abstraction.

To this end, we test a matrix formulation in which the off-the-shelf diol is replaced by a synthesized diol (eq. wt. 381) containing thioester and thioether groups. These new groups are expected to contain more readily abstractible hydrogens; however, they also produce an unwanted increase in matrix refractive index (and thus reduced contrast to the high-index writing monomer). Crucially, the formula limit concept now allows us to quantitatively evaluate the improvement in recording fidelity, independent of the simultaneous penalty in index contrast.

As shown in Figure 36, the measured recording fidelity and usable fraction of dynamic range are in fact worse than in the standard model material. Nor is any improvement observed in spatial resolution (as inferred from measurements at three grating pitches, as in Figure 9). This suggests

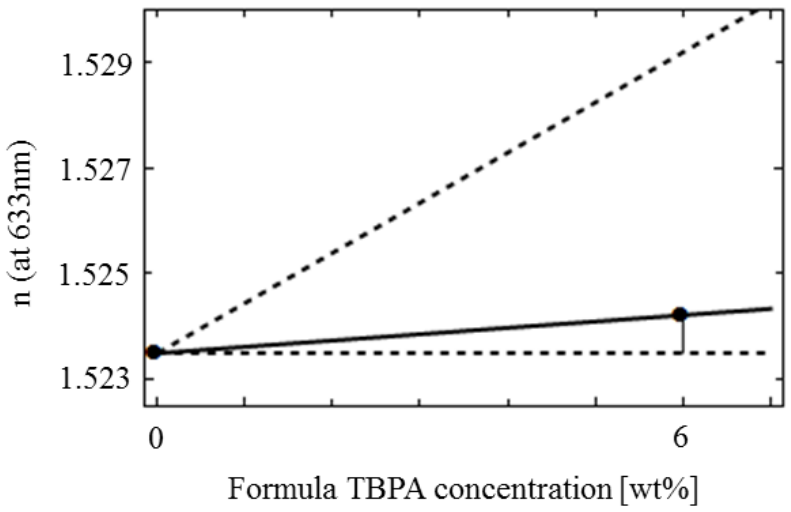

Figure 36. Novel thioether/ester matrix with more readily abstractible hydrogens. Top dashed line: formula limit, using previously obtained value for molar refractivity of writing monomer. Solid line: usable dynamic range, measured via standard technique of many weak angle-multiplexed holograms.

that the thioester and thioether groups are not, as hoped, more susceptible to hydrogen abstraction, but rather less susceptible. While disappointing, this unambiguously negative result illustrates the utility of our approach for quick experimental surveys of candidate formulations.

Other implementations of this general enhanced-attachment concept remain a promising area for future work.

4.4.4 Reducing chain transfer

Chain transfer from matrix-attached growing chains is, as shown above, a crucial limiting factor in the development of recorded features. The mobile radicals produced from chain transfer diffuse some distance before reattaching; over repeated iterations of this process, the radical distribution gradually blurs into a uniform distribution. For submicron features, as in holographic gratings, this leads to significant unwanted polymerization in the dark regions, and thus significant wasted dynamic range (Figure 9).

So far, this chain transfer process has been treated in strictly phenomenological terms, but now we consider the chemical pathway by which it occurs. The most plausible candidate for a chain transfer agent is the photoinitiator (or some photoproduct formed by its geminate recombination), following the reaction path in Figure 37 (from [157]). This is supported

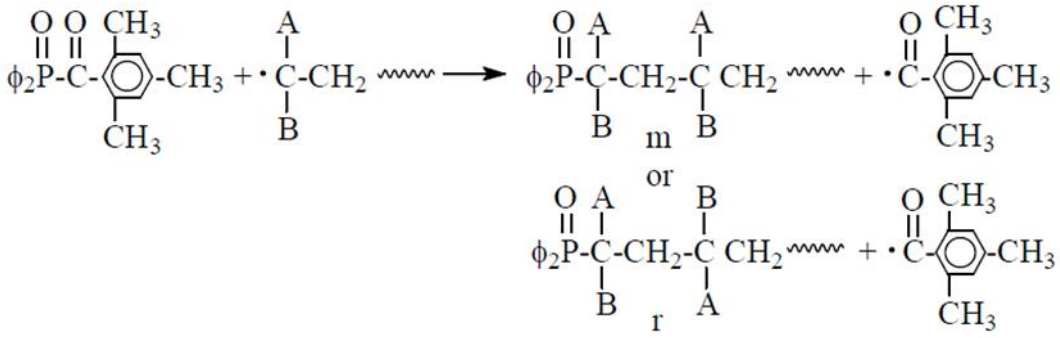

Figure 37. Photoinitiator TPO acts as a chain transfer agent, from Medsker et al.[157]

experimentally by measuring grating growth curves for a formulation identical to the model material except for a reduced TPO concentration. We observe (in addition to the expected loss of sensitivity) a longer time until cessation of patterned grating growth, as shown in Figure 38.

When TPO is replaced with another acyl phosphine derivative photoinitiator (Irgacure 819), a similar timescale for grating growth cessation is observed, indicating similar chain transfer behavior.

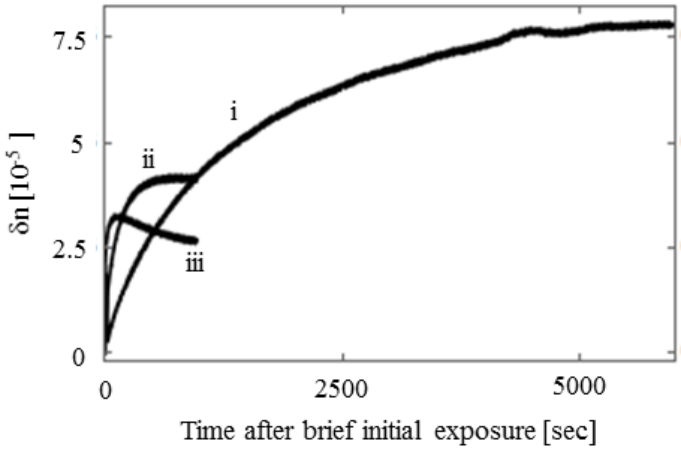

Figure 38. As the photoinitiator concentration is increased, cessation of grating growth happens more quickly. This is evidence that the photoinitiator is acting as a chain transfer agent, facilitating the re-mobilization of matrix-tethered radicals which is responsible for the cessation of grating growth. (i) 0.07 wt% TPO, (ii) 0.4 wt% TPO, (iii) 2 wt% TPO. Exposure doses are adjusted to yield gratings of comparable strength: (i) 3000 mJ cm^{-2}, (ii) 100 mJ cm^{-2}, (iii) 15 mJ cm^{-2}. Grating pitch is 0.7 μm in all three cases.

These observations motivate the exploration of macro-photoinitiators that can be tethered to the matrix. This should reduce their ability to participate in chain transfer reactions; an additional benefit of this scheme is that it should reduce eliminate the diffusional blurring of initially mobile primary radicals. It has been demonstrated that a range of commercial photoinitiators can be tethered, by their aliphatic hydroxyl groups on one or both ends, to the isocyanate groups in the matrix.[158] This has been shown to sharply reduce the volatility of photoproducts; exploring the effects on hologram fidelity is a promising area for future research.

4.4.5 Matrix-attached protected radical groups

Having considered several strategies to reduce diffusional blurring effects, we next turn our attention to another, and in these materials much more significant, cause of wasted dynamic range. We saw that a large fraction of the wasted dynamic range in the original model material was due to mobile oligomer chains that are terminated but left mobile when the radical transfers to the matrix (and therefore do not remain in a patterned distribution). One strategy to reduce this waste is to incorporate into the matrix a different reactive site, one that will tether the entire growing oligomer chain to the matrix, rather than just transferring a radical to the matrix as in hydrogen abstraction.

An appealing candidate is a protected radical capable of undergoing bimolecular termination with a growing mobile oligomer chain. Attachment of such protected radicals to the matrix has already been shown to yield remarkable improvements in usable dynamic range;[159] now, with the formula limit concept, we are in a position to quantify the potentially achievable improvement and understand what kinetic conditions are favorable to achieving it. As shown in Figure 39 and Figure 40, we achieve dramatic improvements, as much as threefold, in usable dynamic range by adding these protected radical groups to the matrix, in the case of two different matrices.

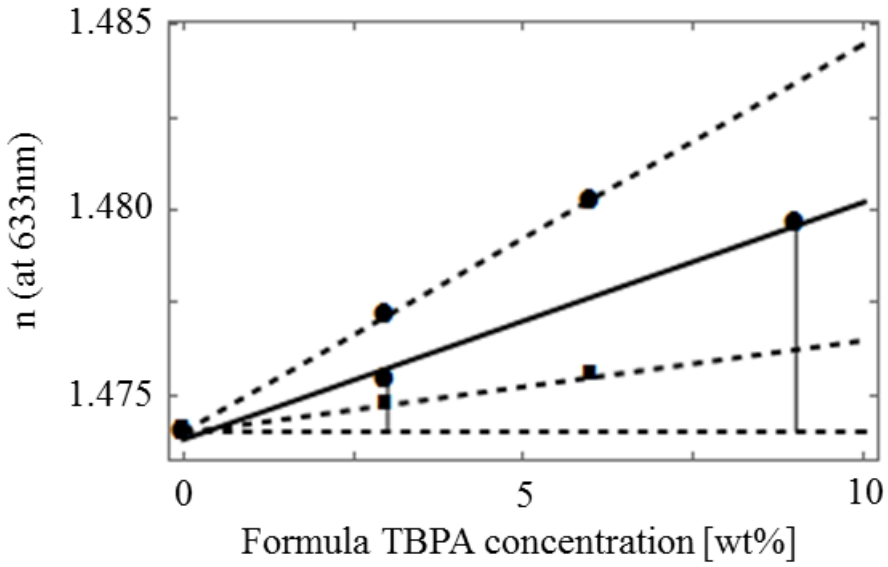

Figure 39. Incorporating protected-radical groups into the -20ºC T_G matrix leads to improved performance (solid line) compared to previous results (bottom dashed line), although the formula limit has not yet been reached (top dashed line). 0.04 wt% 4-hydroxy-TEMPO is reacted with the isocyanate, catalyzed by 0.002 wt% dibutyltin dilaurate, prior to mixing with the other components. In all other respects the formulation is as described above, including 0.4 wt% TPO photoinitiator.

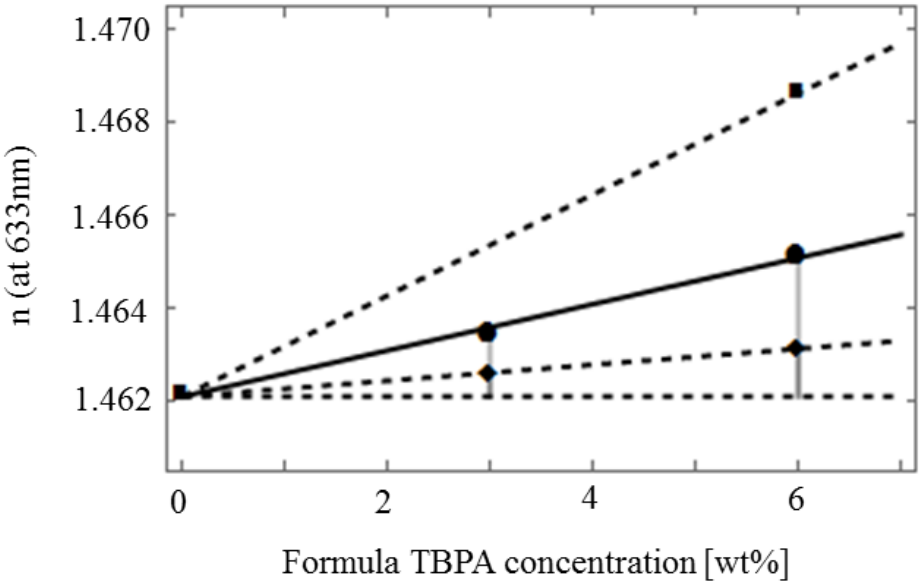

Figure 40. Incorporating protected-radical groups into the -60ºC T_G matrix leads to improved performance (solid line) compared to previous results (bottom dashed line), although the formula limit has not yet been reached (top dashed line). 0.04 wt% 4-hydroxy-TEMPO is incorporated into the matrix, using the same procedure as in the previous figure.

As a corroboration of this proposed mechanism for enhancement of usable dynamic range, we note that the amount of newly usable dynamic range roughly matches the amount of previously wasted dynamic range that was attributed to dead mobile oligomer (that is, quantity i in Figure 9). (This could be further tested by repeating, in these new formulations, the solvent extraction/confocal Raman experiments described above, in which this quantity i was found to correspond closely to the fraction of writing polymer that could be removed by solvent extraction.)

However, this new formulation still falls measurably short of converting all of this previously wasted dynamic range into usable dynamic range. This is attributed to the fact that some mobile radical chains still react with the matrix at a hydrogen abstraction site, rather than a protected-radical site as desired. Further optimization of the concentration of protected-radical groups is expected to lead to further performance improvement.

Based on our simple set of proposed reaction paths, the rate of immobilization should increase linearly with concentration of protected-radical sites, leading to a linear improvement in lifetime ratio. Eventually, a threshold is reached at which this rate of immobilization is so fast that it overtakes the rate of polymerization. Since this immobilization process now terminates the radicals (unlike hydrogen abstraction, which left matrix-attached radicals capable of continued dark polymerization), this means that the radical population is depleted before all the writing monomer is able to be consumed, corresponding to a sharp drop in usable dynamic range.

Finally, the $1/\Lambda^2$ plots for these formulations (Figure 27 and Figure 28) quickly rule out a superficially plausible alternative explanation for the improvements in usable dynamic range:

that instead the protected-radical groups selectively terminate polymerization in the dark fringes. This mechanism would improve the fringe visibility of the attached oligomer profile (i.e. improve the media spatial resolution), and thus would lead to a reduction only in quantity ii above. But, at typical grating pitches $\Lambda \geq 0.7$ μm, this quantity ii represents only a small portion of the wasted dynamic range, for any of these model materials. For the -20ºC T_G material, this improvement in usable Δn is as much as as 2.3×10^{-3}, but quantity ii is less than 1×10^{-4}. Similarly, for the -60ºC T_G material, the improvement in usable Δn is $2. \times 10^{-3}$, but quantity ii is only 2×10^{-4}. So this alternative explanation cannot account for the observed improvements in usable dynamic range.

4.4.6 Reducing recording-induced scatter by slowing development

Next we turn to the problem of recording-induced scatter. This is to be distinguished from the inherent scatter of unexposed media, which is typically due primarily to unwanted phase separation between writing monomer and matrix.[160] As such, the inherent scatter can generally be made quite small by engineering the solubility of the writing monomer in the matrix of choice; some strategies for this are given in [161].

A much more serious problem is the additional scatter induced by recording. This effect is attributed to a feedback process, loosely analogous to filamentation in photorefractive media.[162,163] A manifold of weak "parasitic" or noise gratings are formed by the interference of the coherent writing beams and scattered light. If these parasitic gratings begin to develop while the writing beams are still on, they diffract more and more of the writing beams, preferentially amplifying the manifold of noise gratings at the expense of the intended grating.

Since this feedback process only takes place if the timescales of exposure and index development overlap, it can be ameliorated by delaying the index development (or by shortening the exposure time, but this is typically already constrained by the available laser power and the required doses). In other words, slow dark polymerization is actually favorable for scatter reduction, in contradiction to claims made elsewhere.[20]

This can be accomplished by modifying the chemistry, including fully latent recording schemes where no index development occurs until well after photoexposure.[164] Alternatively, a similar effect can be achieved without modifying the chemistry, simply by tuning the sample temperature. For example, a sample is formulated using a high T_G matrix (T_G ~ 60ºC) then heated so that it is near its T_G during recording. (The exact choice of recording temperature involves balancing the opposing requirements of good sensitivity and slow index development). Then, after the exposure, the sample is heated even further, to speed up index development in a quasi-latent way. Finally the sample is cooled back down to room temperature. Since it is now well below its T_G, it has desirable material properties including good stiffness and low coefficient of thermal expansion.

This approach is potentially advantageous in another way. We saw in the original model material that most of the wasted dynamic range was due to oligomer chains that formed prior to the transfer of radicals to the matrix (and therefore did not remain in a patterned distribution). This waste is thus minimized if radical transfer to the matrix is fast relative to polymerization. And the relative rates of these two processes can in fact be adjusted by tuning the recording temperature and therefore the diffusivity, since under typical conditions one process is transport-limited (polymerization) and the other is reaction-limited even near T_G (radical transfer to the matrix, via hydrogen abstraction). Thus, not only scatter, but also wasted dynamic range will be

minimized by choosing a recording temperature near T_G, and then raising the temperature to complete the development process.

4.5 Conclusion

The proposed "divide-and-conquer" strategy not only yielded a quantitative model of index development in the original model material; it also, even more importantly, afforded insights into the various underlying reaction/diffusion processes responsible for wasted dynamic range. These insights, in turn, suggested new materials design strategies. A range of these strategies were implemented and demonstrated to yield performance improvements. Crucially, the "formula limit" concept enabled quantitatively meaningful comparisons of performance based on relatively fast experimental surveys. Many more suggested strategies remain to be surveyed, including unreactive low-index counterdiffusants and matrix-tethered photoinitiators. Finally, the formula limit concept also facilitates quantitative understanding of the complicated design tradeoffs involved in application-specific material optimization.

REFERENCES

[1] L. Dhar, A. Hale, H. E. Katz, M. L. Schilling, M. G. Schnoes and F. C. Schilling, "Recording media that exhibit high dynamic range for digital holographic data storage," *Opt. Lett.* 24, 7 (1999): 487-489.

[2] Ye, Chunfang, Keith T. Kamysiak, Amy C. Sullivan, and Robert R. McLeod. "Mode profile imaging and loss measurement for uniform and tapered single-mode 3D waveguides in diffusive photopolymer." *Opt. Expr.* 20, no. 6 (2012): 6575-6583.

[3] Bernal, M-P., P. M. Lundquist, C. Poga, H. Coufal, R. K. Grygier, R. G. DeVoe, Y. Jia et al. "Holographic digital data storage in a photorefractive polymer." *Opt. Lett.* 21, no. 12 (1996): 890-892.

[4] Günter, Peter, and Jean-Pierre Huignard, eds. *Photorefractive materials and their applications*. Berlin: Springer-Verlag, 1989.

[5] W. E. Moerner, S. M. Silence, F. Hache, and G. C. Bjorklund. "Orientationally enhanced photorefractive effect in polymers." *JOSA B* 11, no. 2 (1994): 320-330.

[6] C. Erben, E. P. Boden, K. L. Longley, X. Shi, B. L. Lawrence. "Ortho-Nitrostilbenes in Polycarbonate for Holographic Data Storage." *Adv. Func. Mat.* 17, no. 15 (2007): 2659-2666.

[7] A. Khan, G. D. Stucky, and C. J. Hawker. "High-Performance, Nondiffusive Crosslinked Polymers for Holographic Data Storage." *Adv. Mat.* 20, no. 20 (2008): 3937-3941.

[8] V. Cimrova, D. Neher, S. Kostromine, and T. Bieringer. "Optical anisotropy in films of photoaddressable polymers." *Macromol.* 32, no. 25 (1999): 8496-8503.

[9] A. Zakery, and S. R. Elliott. "Optical properties and applications of chalcogenide glasses: a review." *J. Non-Crystalline Solids* 330, no. 1 (2003): 1-12.

[10] Teteris, Janis. "Holographic recording in amorphous chalcogenide thin films."*Current Opinion in Solid State and Materials Science* 7, no. 2 (2003): 127-134.

[11] B. J. Chang, "Dichromated gelatin holograms and their applications." *Opt. Eng.* 19, no. 5 (1980): 195642-195642.

[12] J. M. Kim, B. S. Choi, S. I. Kim, J. M. Kim, H. I. Bjelkhagen, and N. J. Phillips. "Holographic optical elements recorded in silver halide sensitized gelatin emulsions. Part I. Transmission holographic optical elements." *Appl. Opt.* 40, no. 5 (2001): 622-632.

[13] G. J. Steckman, I. Solomatine, G. Zhou, and D. Psaltis. "Characterization of phenanthrenequinone-doped poly (methyl methacrylate) for holographic memory." *Opt. Lett.* 23, no. 16 (1998): 1310-1312.

[14] Y. Gritsai, L. M. Goldenberg, and J. Stumpe. "Phase holographic material with diffusion enhancement based on 1, 2-naphthoquinone." *J. Opt.* 12, no. 1 (2010): 015107.

[15] G. J. Steckman, V. Shelkovnikov, V. Berezhnaya, T. Gerasimova, I. Solomatine, and D. Psaltis, "Holographic recording in a photopolymer by optically induced detachment of chromophores," *Opt. Lett.*, vol. 25, no. 9, p. 607, 2000.

[16] D. A. Waldman, R. T. Ingwall, P. K. Dhal, M. G. Horner, E. S. Kolb, H-Y. S. Li, R. A. Minns, H. G. Schild, "Cationic ring-opening photopolymerization methods for volume hologram recording." *Proc. SPIE* Vol. 2689 (1996).

[17] Monroe, B. M., W. K. Smothers, D. E. Keys, R. R. Krebs, D. J. Mickish, A. F. Harrington, S. R. Schicker, M. K. Armstrong, D. M. T. Chan, and C. I. Weathers. "Improved photopolymers for holographic recording. I, Imaging properties." *J. Imaging Sci.* 35, no. 1 (1991): 19-25.

[18] R. T. Ingwall and M. Troll. "Mechanism of hologram formation in DMP-128 photopolymer." *Opt. Eng.* 28, no. 6 (1989): 286586-286586.

[19] R. T. Ingwall, A. Stuck, and W. T. Vetterling. "Diffraction properties of holograms recorded in DMP-128." In *OE/LASE'86 Symp (January 1986, Los Angeles)*, pp. 81-87. International Society for Optics and Photonics, 1986.

[20] *Holographic Data Storage: From Theory to Practical Systems*. K. Curtis, L. Dhar, A. Hill, W. Wilson, M. Ayres. Wiley (2011)

[21] H. Berneth, F-K. Bruder, T. Fäcke, R. Hagen, D. Hönel, D. Jurbergs, T. Rölle, and M-S. Weiser. "Holographic recording aspects of high-resolution Bayfol® HX photopolymer." In *Proc. SPIE*, vol. 7957 (2011).

[22] M. Ayres, K. Anderson, F. Askham, and B. Sissom. "Progress in second-generation holographic data storage." In *SPIE Optical Engineering+ Applications*, pp. 92010V-92010V. International Society for Optics and Photonics, 2014.

[23] M. G. Schnoes, L. Dhar, M. L. Schilling, S. S. Patel, and P. Wiltzius. "Photopolymer-filled nanoporous glass as a dimensionally stable holographic recording medium." *Opt. Lett.* 24, no. 10 (1999): 658-660.

[24] M. L. Calvo and P. Cheben. "Photopolymerizable sol–gel nanocomposites for holographic recording." *J. Opt. A: Pure Appl. Opt.* 11, no. 2 (2009): 024009.

[25] A. Khan, A. E. Daugaard, A. Bayles, S. Koga, Y. Miki, K. Sato, J. Enda, S. Hvilsted, G. D. Stucky, and C. J. Hawker. "Dendronized macromonomers for three-dimensional data storage." *Chem. Commun.* 4 (2009): 425-427.

[26] Waldman, D. A., H. Li, and M. G. Horner. "Volume shrinkage in slant fringe gratings of a cationic ring-opening holographic recording material." *Journal of Imaging Science and Technology* 41, no. 5 (1997): 497-514.

[27] K. Choi, J. W. M. Chon, M. Gu, N. Malic, and R. A. Evans. "Low-Distortion Holographic Data Storage Media Using Free-Radical Ring-Opening Polymerization." *Adv. Func.Mat.* 19, no. 22 (2009): 3560-3566.

[28] A. Fimia, N. Lopez, F. Mateos, R. Sastre, J. Pineda, and F. Amat-Guerri. "Elimination of oxygen inhibition in photopolymer systems used as holographic recording materials." *J. Mod. Opt.* 40, no. 4 (1993): 699-706.

[29] N. S. Allen, "Photoinitiators for UV and visible curing of coatings: mechanisms and properties." *Journal of Photochemistry and Photobiology A: Chemistry* 100, no. 1 (1996): 101-107.

[30] V. Castelvetro, M. Molesti, and P. Rolla. "UV-curing of acrylic formulations by means of polymeric photoinitiators with the active 2, 6-dimethylbenzoylphosphine oxide moieties pendant from a tetramethylene side chain." *Macromol. Chem. Phys.* 203, no. 10-11 (2002): 1486-1496.

[31] K. J. Schafer, J. M. Hales, M. Balu, K. D. Belfield, E. W. Van Stryland, and D. J. Hagan. "Two-photon absorption cross-sections of common photoinitiators." *Journal of Photochemistry and Photobiology A: Chemistry* 162, no. 2 (2004): 497-502.

[32] M. C. Cole, F. R. Askham, and W. L. Wilson. "Holographic recording medium with control of photopolymerization and dark reactions." U.S. Patent Application 13/365,304, filed February 3, 2012.

[33] A. Beléndez, A. Fimia, L. Carretero, and F. Mateos. "Self-induced phase gratings due to the inhomogeneous structure of acrylamide photopolymer systems used as holographic recording materials." *Appl. Phys. Lett.* 67, no. 26 (1995): 3856-3858.

[34] K. Anderson, M. Ayres, B. Sissom, and F. Askham. "Holographic data storage: rebirthing a commercialization effort." In *SPIE OPTO*, pp. 90060C-90060C. International Society for Optics and Photonics, 2014.

[35] H. Peng, D. P. Nair, B. A. Kowalski, W. Xi, T. Gong, C. Wang, M. Cole et al. "High Performance Graded Rainbow Holograms via Two-Stage Sequential Orthogonal Thiol–Click Chemistry." *Macromol.* 47, no. 7 (2014): 2306-2315.

[36] M.-S. Weiser, F.-K. Bruder, T. Rölle, T.Fäcke, D. Hönel, and H. Berneth. "Chain transfer reagents in polyurethane-based photopolymer formulations." U.S. Patent Application 14/350,593, filed October 11, 2012.

[37] A. L. Mikaelian and V. A. Barachevsky. "Photopolymers for optical devices in the USSR." In *San Diego,'91, San Diego, CA*. International Society for Optics and Photonics, 1991.

[38] T. N. Smirnova and O. V. Sakhno. "PPC: self-developing photopolymers for holographic recording." In *Holography 2000*. International Society for Optics and Photonics, 2000.

[39] N. Suzuki, Y. Tomita, K.Ohmori, M. Hidaka, and K. Chikama. "Highly transparent ZrO_2 nanoparticle-dispersed acrylate photopolymers for volume holographic recording." *Opt. Expr.* 14, no. 26 (2006): 12712-12719.

[40] R. L. Sutherland, V. P. Tondiglia, L. V. Natarajan, T. J. Bunning, and W. W. Adams. "Electrically switchable volume gratings in polymer-dispersed liquid crystals." *Appl. Phys. Lett.* 64, no. 9 (1994): 1074-1076.

[41] A. Mertelj, Alenka, L. Spindler, M. Čopič. "Dynamic light scattering in polymer-dispersed liquid crystals." *Phys. Rev. E* 56, no 1 (1997): 549.

[42] C. C. Bowley, G. P. Crawford, "Diffusion kinetics of formation of holographic polymer-dispersed liquid crystal display materials," *Appl. Phys. Lett*. 76, no 16 (2000): 2235-2237.

[43] A. Hoskins, B. Ihas, K. Anderson, and K. Curtis. "Monocular architecture." *Japanese Journal of Applied Physics* 47, no. 7S1 (2008): 5912.

[44] R. R. McLeod, A. J. Daiber, M. E. McDonald, T. L. Robertson, T.Slagle, S. L. Sochava, L. Hesselink. "Microholographic multilayer optical disk data storage." *Appl. Opt.* 44, no. 16 (2005): 3197-3207.

[45] M. R. Ayres and R. R. McLeod. "Medium consumption in holographic memories." *Applied optics* 48, no. 19 (2009): 3626-3637.

[46] J. M. Tedesco, L. A. K. Brady, W. S. Colburn, "Holographic diffusers for LCD backlights and projection screens." *SID International Symposium Digest of Technical Papers* 24 (1993): 29-29.

[47] W. Chao and S. Chi, "Diffraction properties of windshield laminated photopolymer holograms" *J. Opt.* 29 (1998): 95.

[48] J. M. Castro, D. Zhang, B. Myer, and R. K. Kostuk. "Energy collection efficiency of holographic planar solar concentrators." *Appl. Opt.* 49, no. 5 (2010): 858-870.

[49] E. Mihaylova, I. Naydenova, S. Martin, and V. Toal, "Electronic speckle pattern shearing interferometer with a photopolymer holographic grating." *Appl. Opt*. 43 (2004): 2439-2442.

[50] D. Lanteigne, T. Hudson, and D. Gregory, "Matched spatial filtering using a new photopolymer," *Appl. Opt.* 26 (1987): 184-185.

[51] S. Yiou, F. Balembois, P. Georges, and J. Huignard, "Improvement of the spatial beam quality of laser sources with an intracavity Bragg grating," *Opt. Lett*. 28 (2003): 242-244.

[52] A. Heifetz, J. T. Shen, J-K. Lee, R. Tripathi, and M. S. Shahriar. "Translation-invariant object recognition system using an optical correlator and a super-parallel holographic random access memory." *Opt. Eng.* 45, no. 2 (2006): 025201-025201.

[53] U. Schellhorn, R. A. Rupp, S. Breer, and R. P. May. "The first neutron interferometer built of holographic gratings." *Phys. B: Condensed Matter* 234 (1997): 1068-1070.

[54] J. Klepp, C. Pruner, Y. Tomita, C. Plonka-Spehr, P. Geltenbort, S. Ivanov, G. Manzin et al. "Diffraction of slow neutrons by holographic SiO 2 nanoparticle-polymer composite gratings." *Phys. Rev. A* 84, no. 1 (2011): 013621.

[55] B. L. Booth and J. E. Marchegiano, "Waveguide properties and devices in photopolymer." In *Optical Communication, 1988.(ECOC 88). Fourteenth European Conference on* (Conf. Publ. No. 292), 589-590 (IET, 1988).

[56] A. C. Sullivan, M. W. Grabowski, and R. R. McLeod. "Three-dimensional direct-write lithography into photopolymer." *Appl. Opt.* 46, no. 3 (2007): 295-301.

[57] A. S. Kewitsch and A. Yariv, "Self-focusing and self-trapping of optical beams upon photopolymerization," *Opt. Lett.* 21, no. 1 (1996): 24-26.

[58] Q. Huang and P. Ashley, "Holographic Bragg grating input-output couplers for polymer waveguides at an 850-nm wavelength," *Appl. Opt.* 36 (1997): 1198-1203.

[59] J. M. Wang, L. Cheng, and A. A. Sawchuk. "Light-efficient two-dimensional perfect shuffles with DuPont photopolymer holograms." *Appl. Opt.* 32, no. 35 (1993): 7148-7154.

[60] E. D. Moore, A. C. Sullivan, and R. R. McLeod. "Three-dimensional waveguide arrays via projection lithography into a moving photopolymer." In *Photonic Devices+ Applications*, pp. 705309-705309. International Society for Optics and Photonics, 2008.

[61] D-D. Do, N. Kim, J-W. An, and K-Y. Lee. "Effects of apodization on a holographic demultiplexer based on a photopolymer grating."*Appl. Opt.* 43, no. 23 (2004): 4520-4526.

[62] I. P. Kaminow, H. P. Weber, and E. A. Chandross. "Poly (methyl methacrylate) dye laser with internal diffraction grating resonator." *Appl. Phys. Lett.* 18, no. 11 (2003): 497-499.

[63] V. KS. Hsiao, W. D. Kirkey, F. Chen, A. N. Cartwright, P. N. Prasad, and T. J. Bunning. "Organic solvent vapor detection using holographic photopolymer reflection gratings." *Adv. Mat.* 17, no. 18 (2005): 2211-2214.

[64] X. Yang, X. Pan, J. Blyth, C. R. Lowe, "Towards the real-time monitoring of glucose in tear fluid: Holographic glucose sensors with reduced interference from lactate and pH," *Biosensors and Bioelectronics* 23, no. 6 (2008): 899-905.

[65] M-E Baylor, B. W. Cerjan, C. R. Pfiefer, R. W. Boyne, C.L. Couch, N. B. Cramer, C. N. Bowman, and R.R. McLeod. "Monolithic integration of optical waveguide and fluidic channel structures in a thiol-ene/methacrylate photopolymer." *Opt. Mat. Expr.* 2, no 11 (2012): 1548-1555.

[66] A. C. Urness, E. D. Moore, K. K. Kamysiak, M. C. Cole, and R. R. McLeod. "Liquid deposition photolithography for submicrometer resolution three-dimensional index structuring with large throughput." *Light: Science & Applications* 2, no. 3 (2013): e56.

[67] R. Olson, N. Mamalis, and B. Haugen. "A light adjustable lens with injectable optics." *Current Opinion in Ophthalmology* 17, no. 1 (2006): 72-79.

[68] C. Carre, D. J. Lougnot, and J. P. Fouassier. "Holography as a tool for mechanistic and kinetic studies of photopolymerization reactions: a theoretical and experimental approach." *Macromol.* 22, no. 2 (1989): 791-799.

[69] D. H. Close, A. D. Jacobson, J. D. Margerum, R. G. Brault, and F. J. McClung. "Hologram recording on photopolymer materials." *Appl. Phys. Lett.* 14, no. 5 (1969): 159-160.

[70] R. H. Wopschall and T. R. Pampalone. "Dry photopolymer film for recording holograms." *Appl. Opt* 11, no. 9. (1972): 2096-2097.

[71] A. Bloom, Allen, R. A. Bartolini, and D. L. Ross. "Organic recording medium for volume-phase holography." *Appl. Phys. Lett.* 24, no. 12 (2003): 612-614.

[72] W. J. Tomlinson, I. P. Kaminow, E. A. Chandross, R. L. Fork, and W. T. Silfvast. "Photoinduced refractive index increase in poly (methylmethacrylate) and its applications." *Appl. Phys. Lett.* 16, no. 12. (1970): 486-489.

[73] J. M. Moran and I. P. Kaminow. "Properties of holographic gratings photoinduced in polymethyl methacrylate." *Appl. Opt.* 12, no. 8 (1973): 1964-1970.

[74] Bowden, M. J., E. A. Chandross, and I. P. Kaminow. "Mechanism of the photoinduced refractive index increase in polymethyl methacrylate." *Appl. Opt.* 13, no. 1 (1974): 112-117.

[75] W. J. Tomlinson, E. A. Chandross, H. P. Weber, and G. D. Aumiller. "Multicomponent photopolymer systems for volume phase holograms and grating devices." *Appl. Opt.* 15, no. 2 (1976): 534-541.

[76] M. L. Schilling, V. L. Colvin, L. Dhar, A. L. Harris, F. C. Schilling, H. E. Katz, T. Wysocki, A. Hale, L. L. Blyler, and C. Boyd. "Acrylate oligomer-based photopolymers for optical storage applications." *Chem. Mat.* 11, no. 2 (1999): 247-254.

[77] T. Todorov, P. Markovski, N. Tomova, V. Dragostinova, and K. Stoyanova. "Photopolymers—holographic investigations, mechanism of recording and applications." *Optical and Quantum Electronics* 16, no. 6 (1984): 471-476.

[78] G. Zhao, P. Mouroulis, "Diffusion Model of Hologram Formation in Dry Photopolymer Materials", *J. Mod. Opt.* 41, no. 10 (1994): 1929-1939.

[79] D. J. Lougnot, P. Jost, and L. Lavielle, “Polymers for holographic recording: VI. Some basic ideas for modelling the kinetics of the recording process,” *Pure Appl. Opt.* 6, no. 2 (1997): 225.

[80] E. S. Kovalenko, S. N. Sharangovich, T. E. Zelenskaya, "Dynamic model of hologram recording in photopolymer materials", *Proc. SPIE* 2851, Photopolymer Device Physics, Chemistry, and Applications III, 129 (1996).

[81] V. L. Colvin, R. G. Larson, A. L. Harris, and M.L. Schilling, "Quantitative model of volume hologram formation in photopolymers," *J. Appl. Phys.* 81, no. 9 (1997): 5913-23.

[82] M. L. Schilling, V. L. Colvin, L. Dhar, A. L. Harris, F. C. Schilling, H. E. Katz, T. Wysocki, A. Hale, L. L. Blyler, and C. Boyd. "Acrylate oligomer-based photopolymers for optical storage applications." *Chem. Mat.* 11, no. 2 (1999): 247-254.

[83] M. R. Gleeson and J. T. Sheridan. "A review of the modelling of free-radical photopolymerization in the formation of holographic gratings." *J. Opt. A: Pure Appl. Opt.* 11, no. 2 (2009): 024008.

[84] J. T. Sheridan and J. R. Lawrence. "Nonlocal-response diffusion model of holographic recording in photopolymer." *JOSA A* 17, no. 6 (2000): 1108-1114.

[85] J. R. Lawrence, F. T. O’Neill, and J. T. Sheridan. "Adjusted intensity nonlocal diffusion model of photopolymer grating formation." *JOSA B* 19, no. 4 (2002): 621-629.

[86] M. R. Gleeson, J. V. Kelly, C. E. Close, F. T. O'Neill, and J. T. Sheridan. "Effects of absorption and inhibition during grating formation in photopolymer materials." *JOSA B* 23, no. 10 (2006): 2079-2088.

[87] M. R. Gleeson, J. V. Kelly, D. Sabol, C. E. Close, S. Liu, and J. T. Sheridan. "Modeling the photochemical effects present during holographic grating formation in photopolymer materials." *J. Appl. Phys.* 102, no. 2 (2007): 023108.

[88] M. R. Gleeson, D. Sabol, S. Liu, C. E. Close, J. V. Kelly, and J. T. Sheridan. "Improvement of the spatial frequency response of photopolymer materials by modifying polymer chain length." *JOSA B* 25, no. 3 (2008): 396-406.

[89] J. V. Kelly, F. T. O'Neill, J. T. Sheridan, C. Neipp, S. Gallego, and M. Ortuno. "Holographic photopolymer materials: nonlocal polymerization-driven diffusion under nonideal kinetic conditions." *JOSA B* 22, no. 2 (2005): 407-416.

[90] S-D. Wu and E. N. Glytsis. "Holographic grating formation in photopolymers: analysis and experimental results based on a nonlocal diffusion model and rigorous coupled-wave analysis." *JOSA B* 20, no. 6 (2003): 1177-1188.

[91] S. Martin, C. A. Feely, and V. Toal. "Holographic recording characteristics of an acrylamide-based photopolymer." *Appl. Opt.* 36, no. 23 (1997): 5757-5768.

[92] T. Babeva, I. Naydenova, D. Mackey, S. Martin, and V. Toal. "Two-way diffusion model for short-exposure holographic grating formation in acrylamide-based photopolymer." *JOSA B* 27, no. 2 (2010): 197-203.

[93] S. Gallego, A. Márquez, D. Méndez, C. Neipp, M. Ortuño, A. Beléndez, E. Fernández, and I. Pascual. "Direct analysis of monomer diffusion times in polyvinyl/acrylamide materials." *Appl. Phys. Lett.* 92, no. 7 (2008): 073306.

[94] C. E. Close, M. R. Gleeson, and J. T. Sheridan. "Monomer diffusion rates in photopolymer material. Part I. Low spatial frequency holographic gratings." *JOSA B* 28, no. 4 (2011): 658-666.

[95] C. E. Close, M. R. Gleeson, D. A. Mooney, and J. T. Sheridan. "Monomer diffusion rates in photopolymer material. Part II. High-frequency gratings and bulk diffusion." *JOSA B* 28, no. 4 (2011): 842-850.

[96] S. Liu, M. R. Gleeson, and J. T. Sheridan. "Analysis of the photoabsorptive behavior of two different photosensitizers in a photopolymer material." *JOSA B* 26, no. 3 (2009): 528-536.

[97] T. J. Trentler, J. E. Boyd, and V. L. Colvin. "Epoxy resin-photopolymer composites for volume holography." *Chem. Mat.* 12, no. 5 (2000): 1431-1438.

[98] M. R. Gleeson, S. Liu, R. R. McLeod, and J.T. Sheridan. "Nonlocal photopolymerization kinetics including multiple termination mechanisms and dark reactions. Part II. Experimental validation." *JOSA B* 26, no. 9 (2009): 1746-1754.

[99] F-K. Bruder, F. Deuber, T. Fäcke, R. Hagen, D. Hönel, D. Jurbergs, T. Rölle, and M-S. Weiser. "Reaction-diffusion model applied to high resolution Bayfol HX photopolymer." In *OPTO*, pp. 76190I-76190I. International Society for Optics and Photonics, 2010.

[100] C. Barner-Kowollik, F. Bennet, M. Schneider-Baumann, D. Voll, T. Rölle, T. Fäcke, M-S. Weiser, F-K. Bruder, and T. Junkers. "Detailed investigation of the propagation rate of urethane acrylates." *Polym. Chem.*1, no. 4 (2010): 470-479.

[101] W. K. Smothers, B. M. Monroe, A. M. Weber, and D. E. Keys. "Photopolymers for holography." In *OE/LASE'90, 14-19 Jan., Los Angeles, CA*, pp. 20-29. International Society for Optics and Photonics, 1990.

[102] W. J. Tomlinson, E. A. Chandross, H. P. Weber, and G. D. Aumiller. "Multicomponent photopolymer systems for volume phase holograms and grating devices." *Appl. Opt.* 15, no. 2 (1976): 534-541.

[103] G.M. Karpov, V. V. Obukhovsky, T. N. Smirnova, and V. V. Lemeshko. "Spatial transfer of matter as a method of holographic recording in photoformers." *Opt. Comm.* 174, no. 5 (2000): 391-404.

[104] W. S. Colburn and K. A. Haines. "Volume hologram formation in photopolymer materials." *Appl. Opt.* 10, no. 7 (1971): 1636-1641.

[105] C. R. Kagan, T. D. Harris, A. L. Harris, and M. L. Schilling. "Submicron confocal Raman imaging of holograms in multicomponent photopolymers."*J. Chem. Phys.* 108 (1998): 6892-6896.

[106] F. H. Mok, G. W. Burr, and D. Psaltis. "System metric for holographic memory systems." *Opt. Lett.* 21, no. 12 (1996): 896-898.

[107] J. T. Gallo and C. M. Verber. "Model for the effects of material shrinkage on volume holograms." *Appl. Opt.* 33, no. 29 (1994): 6797-6804

[108] C. Ye and R. R. McLeod. "GRIN lens and lens array fabrication with diffusion-driven photopolymer." *Opt. Lett.* 33, no. 22 (2008): 2575-2577.

[109] W. Heller. "Remarks on refractive index mixture rules." *J. Phys. Chem.* 69, no. 4 (1965): 1123-1129.

[110] K. Kamysiak and R. R. McLeod, personal correspondence, 2012.

[111] J. E. Boyd, T. J. Trentler, R. K. Wahi, Y. I. Vega-Cantu, and V. L. Colvin. "Effect of film thickness on the performance of photopolymers as holographic recording materials." *Appl. Opt.* 39, no. 14 (2000): 2353-2358.

[112] T. Kubota. "The bending of interference fringes inside a hologram." *J. Mod. Opt.* 26, no. 6 (1979): 731-743.

[113] P-G. de Gennes, "Reptation of a polymer chain in the presence of fixed obstacles." *J. Chem. Phys.* 55, no. 2 (1971): 572-579.

[114] P. Wang, B. Ihas, M. Schnoes, S. Quirin, D. Beal, S. Setthachayanon, T. Trentler et al. "Photopolymer media for holographic storage at≈ 405 nm." In *Optical Data Storage Topical Meeting 2004*, pp. 283-288. International Society for Optics and Photonics, 2004.

[115] e.g. "Once monomer is converted to polymer, its diffusion is assumed to cease." In I. Aubrecht, M. Miler, and I. Koudela. "Recording of holographic diffraction gratings in photopolymers: theoretical modelling and real-time monitoring of grating growth." *J. Mod. Opt.* 45, no. 7 (1998): 1465-1477.

[116] I. Naydenova, R. Jallapuram, R. Howard, S. Martin, and V. Toal. "Investigation of the diffusion processes in a self-processing acrylamide-based photopolymer system." *Appl. Opt.* 43, no. 14 (2004): 2900-2905.

[117] I. Naydenova, E. Mihaylova, S. Martin, and V. Toal. "Holographic patterning of acrylamide-based photopolymer surface." *Opt. Expr.* 13, no. 13 (2005): 4878-4889.

[118] K. S. Anseth, C. M. Wang, and C. N. Bowman. "Kinetic evidence of reaction diffusion during the polymerization of multi (meth) acrylate monomers." *Macromol.* 27, no. 3 (1994): 650-655.

[119] J. M. Asua, S. Beuermann, M.Buback, P. Castignolles, B. Charleux, R. G. Gilbert, R. A. Hutchinson et al. "Critically Evaluated Rate Coefficients for Free-Radical Polymerization, 5." *Macromol. Chem. Phys.* 205, no. 16 (2004): 2151-2160.

[120] J. Lalevée, X. Allonas, S. Jradi, and J.-P. Fouassier. "Role of the medium on the reactivity of cleavable photoinitiators in photopolymerization reactions." *Macromol.* 39, no. 5 (2006): 1872-1879.

[121] M. G. Neumann, W. G. Miranda Jr, C. C. Schmitt, F. A. Rueggeberg, and I. C. Correa. "Molar extinction coefficients and the photon absorption efficiency of dental photoinitiators and light curing units." *J. Dent.* 33, no. 6 (2005): 525-532.

[122] C. Decker, "Kinetic study and new applications of UV radiation curing." *Macromol. Rapid Comm.* 23, no. 18 (2002): 1067-1093.

[123] G. W. Sluggett, C. Turro, M. W. George, I. V. Koptyug, and N. J. Turro. "(2,4,6-Trimethylbenzoyl)diphenylphosphine Oxide Photochemistry. A Direct Time-Resolved Spectroscopic Study of Both Radical Fragments." *J. Am. Chem. Soc*. 117 (1995): 5148-5153

[124] C. Decker and A. D. Jenkins. "Kinetic approach of oxygen inhibition in ultraviolet-and laser-induced polymerizations." *Macromol.* 18.6 (1985): 1241-1244.

[125] V. Castelvetro, M. Molesti, and P. Rolla. "UV-curing of acrylic formulations by means of polymeric photoinitiators with the active 2, 6-dimethylbenzoylphosphine oxide moieties pendant from a tetramethylene side chain." *Macromol. Chem. Phys.* 203, no. 10-11 (2002): 1486-1496.

[126] D. Axelrod, D. E. Koppel, J. Schlessinger, E. Elson, and W. W. Webb, "Mobility measurement by analysis of fluorescence photobleaching recovery kinetics." *Biophys. J.* 16, no. 9 (1976): 1055-1069.

[127] B. C. Platt, "History and principles of Shack-Hartmann wavefront sensing." *Journal of Refractive Surgery* 17.5 (2001): S573-S577.

[128] H. Kogelnik, "Coupled wave theory for thick hologram gratings." *Bell System Technical Journal* 48, no. 9 (1969): 2909-2947.

[129] Y. Cai, and J. Jessop. "Decreased oxygen inhibition in photopolymerized acrylate/epoxide hybrid polymer coatings as demonstrated by Raman spectroscopy." *Polymer* 47, no. 19 (2006): 6560-6566.

[130] H. Paul, R. D. Small Jr, and J. C. Scaiano, "Hydrogen abstraction by tert-butoxy radicals. A laser photolysis and electron spin resonance study." *J. Am. Chem. Soc.* 100, no. 14 (1978): 4520-4527.

[131] M. R. Topp, "Activation-controlled hydrogen abstraction by benzophenone triplet." *Chem. Phys. Lett.* 32, no. 1 (1975): 144-149.

[132] J. S. Young and C. N. Bowman. "Effect of polymerization temperature and cross-linker concentration on reaction diffusion controlled termination." *Macromol.* 32, no. 19 (1999): 6073-6081.

[133] K.S. Anseth, K. J. Anderson, and C. N. Bowman. "Radical concentrations, environments, and reactivities during crosslinking polymerizations." *Macromol. Chem. Phys.* 197, 833 (1996).

[134] G. Zhao and P. Mouroulis, "Second order grating formation in dry holographic photopolymers." *Opt. Comm.* 115, no. 5 (1995): 528-532.

[135] M. G. Moharam and L. Young, "Criterion for Bragg and Raman-Nath diffraction regimes." *Appl. Opt.* 17, no. 11 (1978): 1757-1759.

[136] C. B. Bucknall and I. K. Partridge. "Phase separation in crosslinked resins containing polymeric modifiers." *Polymer Engineering & Science* 26, no. 1 (1986): 54-62.

[137] J. Keizer, "Diffusion effects on rapid bimolecular chemical reactions." *Chem. Rev.* 87, no. 1 (1987): 167–180.

[138] F-D. Kuchta, A. M. van Herk, and A. L. German. "Propagation kinetics of acrylic and methacrylic acid in water and organic solvents studied by pulsed-laser polymerization." *Macromol.* 33, no. 10 (2000): 3641-3649.

[139] "Translational and rotational diffusion in supercooled orthoterphenyl close to the glass transition," F. Fujara, B. Geil, H. Sillescu, G. Fleischer, *Zeitschrift für Physik B Condensed Matter* 88, no. 2 (1992): 195-204

[140] Sokolov, A. P., and Y. Hayashi. "Breakdown of time–temperature superposition: From experiment to the coupling model and beyond." *Journal of Non-Crystalline Solids* 353, no. 41 (2007): 3838-3844.

[141] F. W. Bueche, M. P., W. M. Cashin, and P. Debye, "The Measurement of Self-Diffusion in Solid Polymers." *J. Chem. Phys.* 20, no. 12 (1956): 1956-1958.

[142] D. J. Plazek. "Temperature dependence of the viscoelastic behavior of polystyrene." *J. Phys. Chem.* 69, no. 10 (1965): 3480-3487.

[143] Y. Nishijima. "Studies on the structure change of polymer solids by the fluorescence methods." *Berichte der Bunsengesellschaft für physikalische Chemie* 74, no. 8-9 (1970): 778-784.

[144] C. Anandan, B. J. Basu, and K. S. Rajam. "Investigations of the effect of viscosity of resin on the diffusion of pyrene in silicone polymer coatings using steady state fluorescence technique." *Eur. Polym. J.* 40, no. 2 (2004): 335-342.

[145] K. L. Ngai and D. J. Plazek. "Identification of different modes of molecular motion in polymers that cause thermorheological complexity." *Rubber Chemistry and Technology* 68, no. 3 (1995): 376-434.

[146] D. Richter, R. Zorn, B. Farago, B. Frick, and L. J. Fetters. "Decoupling of time scales of motion in polybutadiene close to the glass transition." *Phys. Rev. Lett.* 68, no. 1 (1992): 71.

[147] W. Sutherland. "LXXV. A dynamical theory of diffusion for non-electrolytes and the molecular mass of albumin." *Phil. Mag.* 9, no. 54 (1905): 781-785.

[148] M. C. Cole, personal correspondence, 2012

[149] Y. Ding and A. P. Sokolov. "Breakdown of time-temperature superposition principle and universality of chain dynamics in polymers." *Macromol.* 39, no. 9 (2006): 3322-3326.

[150] C-Y. Liu, J. He, R. Keunings, and C. Bailly. "New linearized relation for the universal viscosity-temperature behavior of polymer melts." *Macromol.* 39, no. 25 (2006): 8867-8869.

[151] C. Bennemann, C. Donati, J. Baschnagel, and S. C. Glotzer. "Growing range of correlated motion in a polymer melt on cooling towards the glass transition." *Nature* 399, no. 6733 (1999): 246-249.

[152] C. M. Roland. "Characteristic relaxation times and their invariance to thermodynamic conditions." *Soft Matter* 4, no. 12 (2008): 2316-2322.

[153] L. A. Deschenes, and D. A. Vanden Bout. "Single-molecule studies of heterogeneous dynamics in polymer melts near the glass transition." *Science* 292, no. 5515 (2001): 255-258.

[154] A. R. Kannurpatti, J. W. Anseth, and C. N. Bowman. "A study of the evolution of mechanical properties and structural heterogeneity of polymer networks formed by photopolymerizations of multifunctional (meth) acrylates." *Polymer* 39, no. 12 (1998): 2507-2513.

[155] E. A. Chandross, W. J. Tomlinson, and G. D. Aumiller. "Latent-imaging photopolymer systems." *Appl. Opt.* 17, no. 4 (1978): 566-573.

[156] F. R. Askham. "Holographic storage medium and method for gated diffusion of photoactive monomer." U.S. Patent 8,232,028, issued July 31, 2012.

[157] R. E. Medsker, M. Chumacero, E. R. Santee, A. Sebenik, and H. J. Harwood. "^{31}P-NMR characterization of chain ends in polymers and copolymers prepared using LUCIRYN TPO as a photoinitiator."*Acta Chimica Slovenica* 45 (1998): 371-388.

[158] L. R. Boynton, I. V. Khudyakov, and K. W. Swiderski, "High-performance UV-curable urethane acrylate prepolymers." PCI Magazine (2010), http://www.pcimag.com/articles/print/high-performance-uv-curable-urethane-acrylate-prepolymers

[159] F. R. Askham, "Photopolymer media with enhanced dynamic range." U.S. Patent 8,658,332, issued February 25, 2014.

[160] T. Smirnova, O. Sakhno, and S. Lozenko. "The effect of structural-kinetic features of hologram formation on holographic properties of photopolymers." *Semiconductor Physics, Quantum Electronics & Optoelectronics* 7.3 (2004): 326-331.

[161] F.R. Askham, M. C. Cole, and T. J. Trentler. "Index Contrasting-Photoactive Polymerizable Materials, and Articles and Methods Using Same." U.S. Patent Application 11/738,394, filed April 20, 2007.

[162] Yakimovich, A. P. "Dynamic self-amplification of scattering noise in volume-hologram recording." *Opt. Spectrosc.* 49 (1980): 191-193.

[163] É. S. Gyul'Nazarov, T. N. Smirnova, D. V. Surovtsev, and E. A. Tikhonov. "Light scattering in holograms written on photopolymerizing compositions." *J. Appl. Spectrosc.* 51, no. 1 (1989): 728-733.

[164] M. R. Ayres and M. C. Cole. "Latent holographic media and method." U.S. Patent 7,678,507, issued March 16, 2010.